INFORMATION TO USERS

This manuscript has been reproduced from the microfilm master. UMI films the text directly from the original or copy submitted. Thus, some thesis and dissertation copies are in typewriter face, while others may be from any type of computer printer.

The quality of this reproduction is dependent upon the quality of the copy submitted. Broken or indistinct print, colored or poor quality illustrations and photographs, print bleedthrough, substandard margins, and improper alignment can adversely affect reproduction.

In the unlikely event that the author did not send UMI a complete manuscript and there are missing pages, these will be noted. Also, if unauthorized copyright material had to be removed, a note will indicate the deletion.

Oversize materials (e.g., maps, drawings, charts) are reproduced by sectioning the original, beginning at the upper left-hand corner and continuing from left to right in equal sections with small overlaps.

Photographs included in the original manuscript have been reproduced xerographically in this copy. Higher quality 6" x 9" black and white photographic prints are available for any photographs or illustrations appearing in this copy for an additional charge. Contact UMI directly to order.

Bell & Howell Information and Learning
300 North Zeeb Road, Ann Arbor, MI 48106-1346 USA
800-521-0600

UMI®

UNIVERSITY OF ALBERTA

PHASE BEHAVIOUR MODELLING AND COMPOSITIONAL SIMULATION OF ASPHALTENE DEPOSITION IN RESERVOIRS

by

LONG X. NGHIEM

A THESIS
SUBMITTED TO THE FACULTY OF GRADUATE STUDIES AND RESEARCH IN
PARTIAL FULFILLMENT OF THE REQUIREMENTS FOR THE DEGREE OF

DOCTOR OF PHILOSOPHY

in

PETROLEUM ENGINEERING

Department of Civil and Environmental Engineering

Edmonton, Alberta

Fall 1999

To Hanh, Sarah and Kristen

ACKNOWLEDGEMENTS

I wish to express my sincere thanks to:

- Dr. Farouq Ali, my supervisor, for motivating me to join the Ph.D. program at the University of Alberta and for his guidance during the course of this research;
- Dr. Quang Doan, my co-supervisor, for his assistance and valuable advices during my Ph.D. program;
- Computer Modelling Group (CMG) for providing me with a working environment that is conducive to creativity;
- My colleagues at CMG who have taught me a lot over the years; I am particularly thankful to Dr. Dennis Coombe, Dr. Bruce Kohse, Dr. Peter Sammon, Dr. Jim Grabenstetter, Mr. Mohamed Hassam for many useful discussions on the topics related to this research;
- And last but not least, to my lovely wife Hanh and my two charming daughters Sarah and Kristen, for their encouragement and support during the course of this study. This dissertation is dedicated to them.

ABSTRACT

Asphaltene are heavy hydrocarbon molecules that exist naturally in petroleum reservoir fluids. Asphaltene precipitation may occur during pressure depletion or during gas injection processes for Improved Oil Recovery (IOR). It is an important problem during oil production because it can result in formation damage and plugging of wellbore and surface facilities.

This dissertation describes methods for modelling (i) the phase behaviour of asphaltene precipitation, and (ii) the dynamic aspect of asphaltene deposition and plugging in reservoirs.

A thermodynamics approach is used for phase behaviour modelling. The precipitated asphaltene is represented by an improved solid model, while the oil and gas phases are modelled with an equation of state. A method for characterizing the asphaltene component in the oil phase is proposed. In this characterization method, the heaviest component is split into a non-precipitating and precipitating component. These components have identical properties and acentric factors, but different interaction coefficients with the light components. This approach is essential for the use of the solid model in predicting asphaltene precipitation. Laboratory asphaltene precipitation data for hydrocarbon gas injection, pressure depletion and for an asphaltene precipitation envelope are matched successfully with the proposed model.

Inside the reservoir, the precipitated asphaltene can deposit onto the rock surface or remain as a suspended solid in the oil phase. Adsorption and mechanical entrapment are the main deposition mechanisms. The deposited asphaltene may cause blocking of pore throats, which results in permeability reduction. Methods for modelling the above dynamics are proposed. To model the dynamic aspects, the thermodynamics model is implemented into an equation-of-state compositional simulator, which also incorporates the equations for multiphase multicomponent flow, adsorption, mechanical entrapment and formation plugging. Simulation results are in agreement with field observations in showing important phenomena associated with asphaltene precipitation in reservoirs.

TABLE OF CONTENTS

LIST OF TABLES

LIST OF FIGURES

NOMENCLATURE

a	=	parameter
a_i	=	EOS parameter
b	=	parameter
b_i	=	EOS parameter
C_{sf}	=	concentration of solid in the oil phase [ppm (μg/g)]
$\hat{C}_{sf}$	=	concentration of precipitated asphaltene in oil phase [m^3/m^3]
d_{ik}	=	interaction coefficients between component i and k
D	=	depth [m]
D_x^*	=	distance between Gibbs energy surface and tangent plane at **x**
e	=	adjustable parameter for interaction coefficients between hydrocarbons
f_{ij}	=	fugacity of component i in phase j with volume shift
f_{ij}^0	=	fugacity of component i in phase j without volume shift
f_s	=	solid fugacity [kPa]
f_s^*	=	reference solid fugacity [kPa]
F_j	=	mole fraction of phase j (j = o,g,s)
g	=	gravity acceleration [m/s^2]
G	=	Gibbs free energy
G^*	=	dimensionless Gibbs free energy
G_0	=	reference Gibbs free energy
$\mathbf{H}$	=	inverse of Jacobian matrix
$\mathbf{J}$	=	Jacobian matrix
k	=	permeability [md]
k^0	=	initial permeability [md]
k_{rj}	=	relative permeability of phase j (j = o,g,w)
K_a	=	ratio of rate constants of the adsorption/desorption reactions
K_{ij}	=	K-values of component i in phase j (j = g,s)
M_j	=	molecular weight of phase j

n_c = number of components in hydrocarbon phases

N_i = moles of component i per bulk volume

N_{ij} = moles of component i in phase j

N_s = moles of solid

N_{sa} = moles of adsorbed solid

N_{se} = moles of deposited solid through mechanical entrapment

N_{sf} = moles of solid in suspension in the oil

N_t = total moles in hydrocarbon phases

p = pressure [kPa]

p^* = reference pressure [kPa]

p_{ci} = critical pressure of component i [kPa]

p_f = melting-point pressure [kPa]

P_{cog} = oil-gas capillary pressure [kPa]

P_{cwo} = water-oil capillary pressure [kPa]

P_x^* = tangent plane to Gibbs free energy surface at $\mathbf{x}$

q_i = molar injection/production rate of component i [kmol/day]

$\hat{q}_i$ = molar injection/production rate of component i per unit volume [kmol/m^3 day]

R = gas constant [8.314 kPa m^3/kmol K]

R_f = permeability reduction factor

s_i = dimensionless volume shift for component i

S_j = saturation of phase j

T = temperature [K]

T_f = melting-point temperature [K]

T_{ci} = critical temperature of component i [K]

T_j = transmissibility of phase j [kmol/kPa·day]

u_o = oil Darcy velocity [m/s]

v_{ci} = critical volume of component i [m^3/kmol]

v_a = molar volume of asphaltene [m^3/kmol]

v_ℓ	=	liquid molar volume [m^3/kmol]
v_s	=	solid molar volume [m^3/kmol]
V	=	gridblock volume [m^3]
w_{sa}	=	mass of adsorbed asphaltene per mass of rock [mg/g]
$w_{sa,max}$	=	maximum adsorbed mass fraction [mg/g]
w_{sd}	=	mass of deposited asphaltene per mass of rock [g/g]
x_i	=	mole fraction of component i
y_i	=	mole fraction of component i
y_{ij}	=	mole fraction of component i in phase j (j = o,g,s)
y_{isf}	=	mole fraction of solid in suspension in oil phase
z_i	=	global mole fraction of component i
Z	=	compressibility factor
Z_c	=	critical compressibility factor
α	=	vector of ln K_i
α_0, α_1	=	parameters of mechanical entrapment equation [m^{-1}]
γ_j	=	$\tilde{\rho}_j$ g ; gradient of phase j (j = o,g,w) [kPa/m]
Γ	=	Gamma function
δ	=	constant value for interaction coefficients
$\bar{\delta}$,	=	solubility parameter of oil/solvent mixture
$\bar{\delta}_a$	=	solubility parameter of asphaltene
ΔC_p	=	heat capacity of fusion [cal/mol K]
ΔH_f	=	melting-point enthalpy of fusion [cal/mol]
ϕ	=	porosity
ϕ^0	=	initial porosity
$\hat{\phi}$	=	porosity not occupied by solid
φ_i	=	fugacity coefficient
$(\phi_a)_{max}$	=	maximum volume fraction of asphaltene soluble in oil
η	=	volume of asphaltene deposited per unit initial pore volume [m^3/m^3]
μ_j	=	viscosity of phase j [mPa·s]

ρ_j	=	molar density of phase j (j = o,g,w) [kmol/m^3]
$\tilde{\rho}_j$	=	mass density of phase j (j = o,g,w) [kg/m^3]
$\tilde{\rho}_R$	=	mass density of rock [kg/m^3]
σ	=	QNSS step
ω_i	=	acentric factor of component i
Ω_b	=	EOS parameter
ξ	=	vector of variables
Ψ	=	vector of functions

Superscripts

(k)	=	iteration level
n	=	old time level
n+1	=	new time level

Subscripts

c	=	critical
i	=	component
j	=	phase
g	=	gas
k	=	component
o	=	oil
s	=	solid

1. INTRODUCTION

Asphaltene precipitation from reservoir fluids during oil production is a serious problem because it can result in plugging of the formation, wellbore and production facilities. Field conditions conducive to asphaltene precipitation include normal depletion and gas injection for Improved Oil Recovery (IOR). A summary of the different field and laboratory observations associated with asphaltene precipitation is given in the following.

1.1 Asphaltene Precipitation During Primary Depletion

In normal pressure depletion, reservoirs that experience asphaltene precipitation usually have the following characteristics (de Boer et al., 1995):

- The fluid in place is light to medium oil with small asphaltene content.
- The initial reservoir pressure is much larger than the saturation pressure (the fluid is highly undersaturated).
- Maximum precipitation occurs around the saturation pressure.

Heavier crudes that contain a larger amount of asphaltene have very little asphaltene precipitation problems as they can dissolve more asphaltene. Leontaritis and Mansoori (1988) have compiled field cases with asphaltene precipitation problems during primary depletion. Extreme cases include the Venezuelan Boscan crude with 17 weight % asphaltene that was produced nearly trouble free, whereas the Venezuelan Mata-Acema crude with 0.4 to 9.8 weight % asphaltene, and the Algerian Hassi Messaoud crude with 0.062 weight % encountered serious precipitation problem during production.

1.2 Asphaltene Precipitation During IOR Gas Injection

The injection of hydrocarbon gases or CO_2 for IOR also promotes asphaltene precipitation. Numerous field reports and laboratory studies on this aspect have been published (Burke et al., 1990; Hirschberg et al., 1984; Monger and Trujillo, 1991; Novosad and Costain, 1990; Thomas et al. 1992; Srivastava et al., 1995; Turta et al. 1996). Precipitation can occur anywhere in the reservoir, although it manifests itself frequently at the production wellbore at solvent breakthrough.

Asphaltene precipitation may also occur during solvent injection into heavy oil reservoirs (Kokal et al.; 1992). Butler and Mokrys (1993) proposed an in situ solvent extraction process for heavy oils and tar sands called VAPEX. This process uses two horizontal wells (one injector and one producer). The injection of solvent (e.g. propane) creates a solvent chamber where oil is mobilized and drained toward the producer. In addition to the mobilization process, the solvent may also induce asphaltene precipitation, which provides an in situ upgrading of the oil.

1.3 Asphaltene Precipitation and Deposition

It has been accepted that asphaltenes are heavy hydrocarbon molecules that are in colloidal suspension in the oil, stabilized by resins adsorbed on their surface (Hirschberg et al., 1984; Leontaritis and Mansoori, 1987). Changes in pressure, temperature and composition may alter this thermodynamic equilibrium and cause asphaltene precipitation.

The Asphaltene Precipitation Envelope (APE) bounds the region where precipitation occurs. Figure 1.1 shows a typical pressure-composition APE and pressure-temperature APE (Leontaritis et al., 1994; Leontaritis, 1996). Leontaritis refers to the APE's as Asphaltene Deposition Envelopes (ADE). In this dissertation, the term "precipitation" refers to the formation of the asphaltene precipitate as a result of thermodynamic equilibrium, and "deposition" refers to the settling of the precipitated asphaltene onto the rock surface in a porous medium. The onset conditions correspond to points on the APE. Within the APE, the amount of precipitated asphaltene increases as pressure decreases from the upper onset pressure to the saturation pressure of the oil. The precipitation reaches a maximum value at the saturation pressure, and decreases as pressure decreases below the saturation pressure.

Inside the reservoir, after precipitation has occurred, the asphaltene precipitate can remain in suspension and flow within the oil phase, or can deposit onto the rock surface. The main deposition mechanisms are adsorption and mechanical entrapment. The deposited

asphaltene may cause plugging of the formation and alteration of rock wettability (from water-wet to oil-wet).

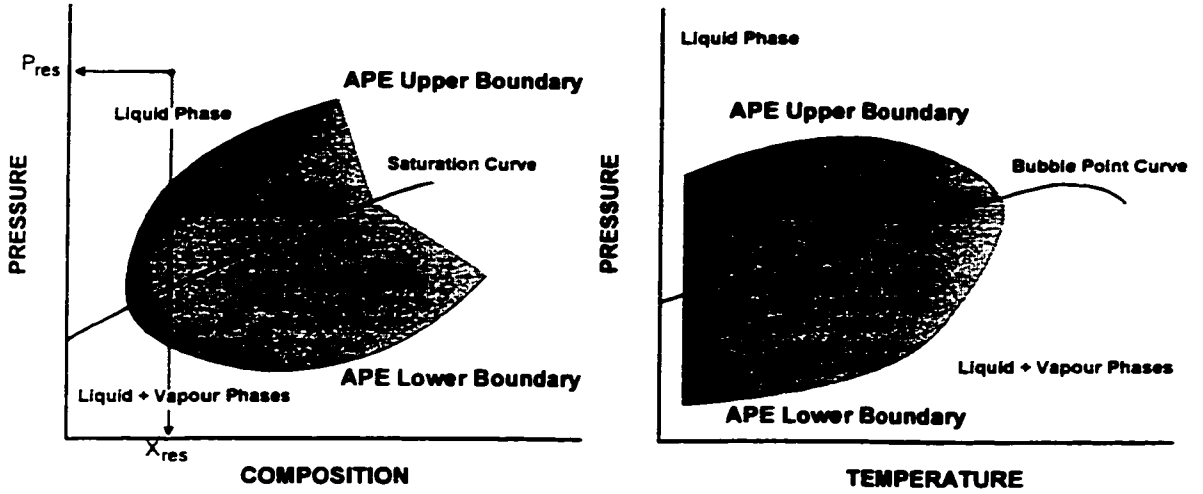

Figure 1.1: Pressure-composition and pressure-temperature Asphaltene Precipitation Envelopes (after Leontaritis et al. (1994) and Leontaritis (1996))

1.4 Scope of Research

The research in this dissertation addresses the modelling of (i) the phase behaviour of asphaltene precipitation, and of (ii) the dynamic aspect of asphaltene precipitation in porous media.

A thermodynamic model is proposed where the precipitated asphaltene is modelled as a pure solid, while the oil and gas phases are modelled with an equation of state (EOS). A method for characterizing the asphaltene component in the oil, which is crucial for obtaining proper predictions, is introduced. A multiphase flash calculation algorithm involving an oil phase, a gas phase and solid phase is developed. The thermodynamic model is validated with experimental precipitation data associated with gas injection and primary depletion processes under isothermal conditions. The extension of the thermodynamic model to include temperature effects is also described.

To model the dynamic aspect of asphaltene precipitation, the thermodynamic model is incorporated into a compositional simulator where the equations for multiphase multicomponent flow, the equations for thermodynamic equilibrium, and the equations for deposition and plugging are solved simultaneously. This allows the modelling of the precipitation with changes in pressure and composition as they occur in the reservoir. Gas injection and primary depletion processes are isothermal, and therefore the energy equations and the effect of temperature variations on asphaltene precipitation are not considered in the compositional simulation.

2. REVIEW OF THERMODYNAMIC MODELS FOR ASPHALTENE PRECIPITATION

2.1 Nature of Asphaltenes

Petroleum reservoir fluids are multicomponent mixtures, consisting primarily of hydrocarbons belonging to one of the following classes (McCain, 1990; Pedersen et al., 1989):

- Paraffins (or alkanes), that consist of chains of hydrocarbon segments ($-CH_2-$, $-CH_3$) that are connected by single bonds. Methane (CH_4) is the simplest and most common compound in petroleum reservoir fluids.
- Naphtenes, which are hydrocarbons similar to paraffins, but containing one or more cyclic structures.
- Aromatics, which contains one or more ring structures similar to benzene (C_6H_6). The atoms are connected by aromatic double bonds.
- Resins and asphaltenes, which are large molecules consisting primarily of hydrogen and carbon, with one to three sulfur, oxygen, or nitrogen atoms per molecule. The basic structure is composed of rings, mainly aromatics, with from three to ten or more rings per molecule.

In addition to hydrocarbons, non-hydrocarbon compounds such as nitrogen (N_2), carbon dioxide (CO_2), and hydrogen sulfide (H_2S) are often found in petroleum mixtures.

Asphaltenes do not dissolve in petroleum but are dispersed as colloids. Asphaltene micelles (aggregates) are kept in solution by a layer of resins adsorbed in their surface. Changes in pressure, temperature and composition alter the asphaltene/resin association and may cause precipitation. When petroleum is separated into fractions by distillation, the asphaltenes remain in the heaviest fraction, while the resins are distributed through the various fractions according to volatility.

A review of different models for asphaltene precipitation in the petroleum literature is given in the following.

2.2 *Solubility Model*

As asphaltenes are a solubility class that can be precipitated from petroleum by the addition of solvent, a thermodynamic solubility model can be used to describe their behaviour. Hirschberg et al. (1984) presented an approach that uses the Flory-Huggins solubility model (Prausnitz et al., 1986). Vapour-liquid equilibrium calculations with the Soave-Redlich-Kwong EOS (Soave, 1972) are first performed to split the petroleum mixture into a liquid phase and a vapour phase. The liquid phase is then divided into two components: a component that corresponds to the asphaltene and a component that represents the remaining oil (deasphalted oil). In the case solvent is added into the oil, the second component represents the mixture of deasphalted oil and solvent. These two components are for modelling asphaltene precipitation and do not correspond to any EOS components used in the vapour-liquid calculations. It is also assumed that asphaltene precipitation does not affect vapour-liquid equilibrium.

In this model, the maximum volume fraction, $(\phi_a)_{max}$, of asphaltene soluble in the oil follows the equation:

$$\ln(\phi_a)_{max} = \frac{v_a}{v_\ell}\left[1 - \frac{v_\ell}{v_a} - \frac{v_\ell}{RT}\left(\bar{\delta}_a - \bar{\delta}_\ell\right)^2\right] \tag{2.1}$$

where,

R	=	gas constant [8.314 kPa m^3/kmol K]
T	=	temperature [K]
v_a	=	molar volume of asphaltene [m^3/kmol]
v_ℓ	=	molar volume deasphalted oil/solvent mixture [m^3/kmol]
$\bar{\delta}_a$	=	solubility parameter of asphaltene [$kPa^{1/2}$]
$\bar{\delta}_\ell$	=	solubility parameter of oil/solvent mixture [$kPa^{1/2}$]

The molar volume, v_ℓ, and the solubility parameter, $\bar{\delta}_\ell$, of the deasphalted oil/solvent mixture are calculated from the composition of the liquid phase obtained from vapour-liquid calculations using the Soave-Redlich-Kwong EOS as described by Hirschberg et al. (1984). The other two parameters, the asphaltene molar volume, v_a, and the solubility

parameter, $\overline{\delta}_a$, of asphaltene are essential for the performance of this model. The molar volume is dependent on the molecular weight and density. Most methods for determinations of molecular weights give data that show a dependence on the aggregation effect (Andersen and Speight, 1999), and thus the maximum solubility in Equation (2.1) cannot be calculated accurately. The solubility parameter can be estimated by measuring the solubility of asphaltenes in different solvents of increasing solubility. The solubility parameter of asphaltene is taken to be that of the best solvent (Andersen and Speight, 1999).

It is found that the solubility parameter can be correlated as a linear equation with respect to temperature:

$$\overline{\delta} = a + b\,T \tag{2.2}$$

where a and b are constants. The parameter b is negative as the solubility parameter decreases with increasing temperature.

Hirschberg et al. (1984), Burke et al. (1990), and Novosad and Costain (1990) used this model with a limited degree of success. Hirschberg et al. (1984) pointed out that the Flory-Huggins model is not accurate for asphaltene and improvements are required. Kanakawa et al. (1991) extended this approach by considering asphaltenes to be heterogeneous polymers instead of homogeneous polymers as in Hirschberg et al. (1984). Although the fit improves with this model, the number of parameters also increases.

2.3 Thermodynamic Colloidal Model

Leontaritis and Mansoori (1987) proposed a more mechanistic approach based on the assumption that asphaltenes exist in the oil as solid particles in colloidal suspension, stabilized by resins adsorbed on their surface. As in Hirschberg et al. (1984), vapour-liquid equilibrium calculations were first performed with an EOS to establish a liquid phase from which asphaltene may precipitate. Based on experimental measurements of the onset of precipitation, a critical chemical potential for resins is estimated from Flory-Huggins polymer solution theory. This critical chemical potential is subsequently used to predict the onset of precipitation at other conditions.

2.4 Thermodynamic Micellization Model

Pan and Firoozabadi (1998) developed a thermodynamic framework based on the micellization process and direct minimization of the Gibbs free energy to describe asphaltene aggregation and precipitation in crude oils. The proposed model was able to reproduce experimentally observed trends. The computational effort is more demanding than for other models. Enhancements to the model are in progress.

2.5 Solid Model

The simplest model for precipitated asphaltene is the single-component solid model that was tried by Gupta (1986) and Thomas et al. (1992). The precipitated asphaltene is represented as a pure solid while the oil and gas phases are modelled with a cubic EOS. The fugacity of the pure solid is given by:

$$\ln f_s = \ln f_s^{\bullet} + \frac{v_s \left(p - p^{\bullet}\right)}{R\,T} \tag{2.3}$$

where,

f_s = solid fugacity [kPa]

$f_s^{\bullet}$ = reference solid fugacity [kPa]

p = pressure [kPa]

$p^{\bullet}$ = reference pressure [kPa]

R = gas constant [8.314 kPa m^3/kmol K]

v_s = solid molar volume [m^3/kmol]

T = temperature [K]

Thomas et al. (1992) did not obtain good results with Equation (2.3) and introduced an empirical model for ln f_s that is a function of pressure, temperature and global composition. This model has a large number of parameters that need to be tuned in order to match experimental data. The use of global composition creates conceptual difficulties as fluids with different global compositions may have the same liquid, vapour and solid compositions. Thomas et al. (1992) also investigated the representation of the precipitated asphaltene as a multicomponent solid. They used the liquid-solid model of Won (1986)

that was developed for wax. Thomas et al. (1992) reported some success with this model and identified areas for improvements, in particular the behaviour at increasing solvent concentration. Chung (1992) and MacMillan et al. (1995) also used this multicomponent solid model to match their experimental data. The drawback of using a multicomponent solid representation of the precipitate is the large number of parameters that must be specified.

2.6 *Model Selection*

The models reviewed in Sections 2.2 to 2.4 are based on activity coefficients (Prausnitz et al., 1986) whereas the solid model is based on fugacities. The solid model uses the same components that are used in the EOS for modelling the oil and gas phases. In the activity-coefficient approach, a two-phase oil-gas flash calculation is first performed to split the mixture into a oil phase and a gas phase. The oil phase is then divided into a different set of components for modelling asphaltene precipitation. In Hirschberg et al. (1984) approach, the oil phase is divided into two components: one component representing the asphaltene and one component representing the deasphalted oil. The thermodynamic colloidal model (Leontaritis and Mansoori, 1987) and the thermodynamic micellization model (Pan and Firoozabadi, 1998) use additional components to represent micelles and resins. Although the precipitation affects the equilibrium between the oil and gas systems, the activity-coefficient approach ignores this dependence, as there is no relationship between the EOS components for the oil and gas phases, and the activity-coefficient components. This assumption could introduce errors in the oil-gas phase behavior calculations, as heavy components such as asphaltenes have an important effect on the saturation pressures. Hirschberg et al. (1984) acknowledged that their solubility model based on Flory-Huggins polymer solution is not accurate, and that a method based on three-phase oil-gas-precipitated asphaltene calculation would be more advantageous. This is the approach taken in this dissertation.

The objective of the activity-coefficient approaches proposed in the literature is to model the phase behaviour of asphaltene precipitation only. There is no thought about their inclusion into a compositional simulator for modelling the dynamic aspect of asphaltene

precipitation. The use of the activity coefficients introduces conceptual difficulties in the implementation of asphaltene phase-behaviour calculations in a compositional simulator. Such a simulator solves for the multiphase multicomponent flow equations together with the phase equilibrium equations and the equations for solid deposition and plugging. It is essential that the same components be used in the flow equations, the equilibrium equations, the deposition and plugging equations, which is not the case if activity-coefficient models are used. The solid model is more advantageous in this respect, as it uses the same components as the EOS. Another important consideration of the solid model is seen in its computational efficiency. As vapour-liquid-solid equilibrium calculations are performed many times during a compositional simulation, the pure solid model is very attractive from a computational point of view.

The above discussion favors the solid model approach if the goal is to also incorporate the thermodynamic model into a compositional simulator. Attempts in modelling asphaltene precipitate as a pure solid have not been successful in the past (Thomas et al., 1992). One of the important contributions of this dissertation is the characterization of the asphaltene component, which is crucial for making the pure solid model work. This characterization enables the subsequent development of a compositional simulator for asphaltene precipitation. Without this first important step, the development of such compositional simulator would not have been feasible.

3. DYNAMIC ASPECTS OF ASPHALTENE PRECIPITATION

3.1 Outline

The dynamic aspect of asphaltene precipitation in petroleum reservoirs has been a topic of many recent investigations. This section reviews the investigations and laboratory observations of this aspect. In this dissertation, "precipitation" corresponds to the formation of a solid phase from thermodynamic equilibrium, whereas "deposition" means the settling of solid particles onto the rock surface.

Piro et al. (1996), Minssieux (1997), and Ali and Islam (1998) performed experiments on asphaltene deposition in sand packs and cores. Asphaltene precipitates were first induced by diluting crude oil with n-heptane. The diluted oil with precipitated asphaltenes is then injected into the core. Measurements of the outlet concentration of precipitated asphaltene determine the amount of asphaltene deposited in the porous rock. Measurements of the increase of pressure drop across the core give an indication of the plugging effect due to deposition.

3.2 Adsorption and Mechanical Entrapment

After asphaltene precipitates from the oil, it can deposit onto the rock and cause plugging and alteration of wettability. Recent investigations show that asphaltene deposition is due to adsorption followed by mechanical entrapment (Minssieux, 1997).

The first step in the deposition is the adsorption of asphaltene onto the rock surface. The adsorption of asphaltene onto different rocks has been extensively measured in laboratories. Collins and Melrose (1983), Dubey and Waxman (1991), and González and Travalloni-Louvisse (1993) showed that the asphaltene adsorption onto different rocks can be modelled with Langmuir isotherms. Figure 3.1 (from Dubey and Waxman, 1991) shows typical Langmuir isotherms for asphaltene adsorption on different rocks. The Langmuir isotherm equation is of the form:

$$w_{sa} = \frac{w_{sa,max} K_a C_{sf}}{K_a C_{sf} + 1} \tag{3.1}$$

where,

C_{sf}	=	concentration of suspended solid in the oil phase [ppm (μg/g)]
w_{sa}	=	mass of adsorbed asphaltene per mass of rock [mg/g]
$w_{sa,max}$	=	maximum adsorbed mass fraction (the plateau in Figure 3.1) [mg/g]
K_a	=	ratio of rate constants of the adsorption/desorption reactions

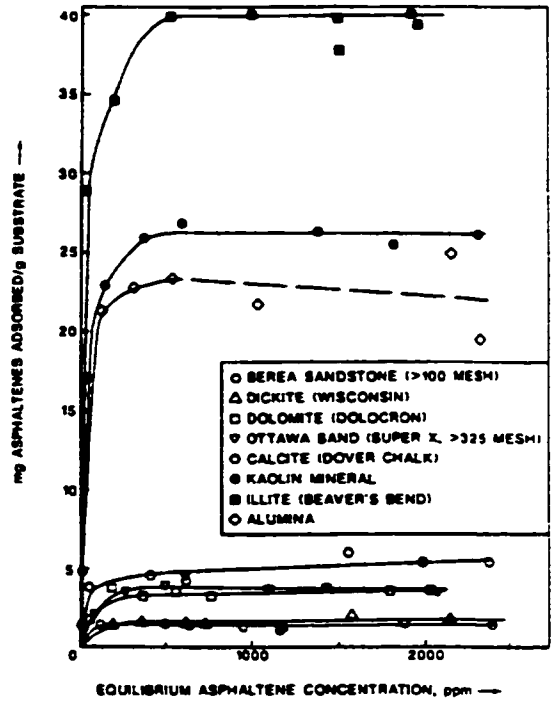

Figure 3.1: Langmuir isotherms for asphaltene adsorption (from Dubey and Waxman, 1991)

In addition to adsorption, Minssieux (1997) showed that the deposition also occurs because of mechanical entrapment. Piro et al. (1996), Turta et al. (1997), Ali and Islam (1998) have reported similar observations. This entrapment is similar to the deposition of fines in porous media.

The precipitated asphaltenes are fine particles that may form aggregates, which are large enough to be retained at small pore throats. A schematic of the process is shown in Figure 3.2. This deposition process through mechanical entrapment (also called plugging deposit as the deposition plugs the pore throat) is complex. An empirical model that has been

frequently used for mechanical entrapment is due to Gruesbeck and Collins (1982), who developed the equation for the deposition of fines in porous media. The deposition process follows an ordinary differential equation:

$$\frac{d\eta}{dt} = (\alpha_0 + \alpha_1 \eta)|u_o| \hat{C}_{sf} \tag{3.2}$$

where,

$\hat{C}_{sf}$ = volume ratio of precipitated asphaltene in oil phase [m^3/m^3]

u_o = oil Darcy velocity [m/s]

α_0, α_1 = empirical parameters [m^{-1}]

η = volume of asphaltene deposited per unit initial pore volume [m^3/m^3]

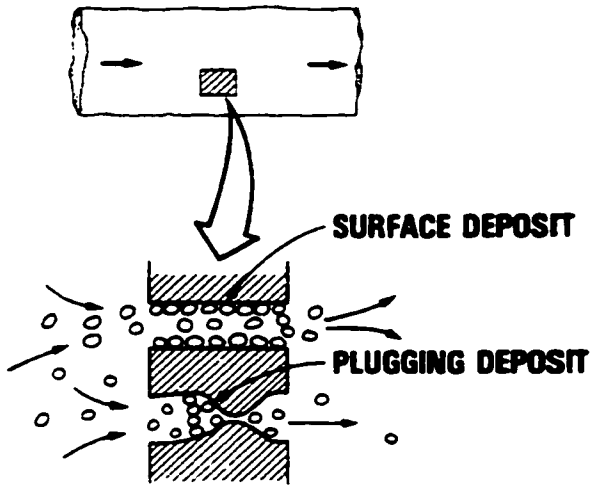

Figure 3.2: Mechanical entrapment of solids in porous media (from Gruesbeck and Collins, 1982)

In Equation (3.2), the term $|u_o| \hat{C}_{sf}$ is representive of the flux of suspended solids. Equation (3.2) implies that there is no deposit without fluid flow, and that the rate of deposition increases as the amount of deposit increases. Minssieux (1997) reports core permeability reduction of 20% to 90% depending on rock morphology, mineralogy and crude asphaltene content. In general, the permeability reduction is faster on low-permeability cores than in high-permeability cores. Turta et al. (1997) reported data on

permeability reduction for the injection of propane into cores containing oils from the Pembina Nisku pool and the Rainbow Keg River field. Effective permeability decreases as propane is injected and is reduced to almost zero after 30% pore volume injected.

Besides the plugging deposit, Gruesbeck and Collins (1982) also discussed mechanical deposition in non-pluggable pathways (surface deposit in Figure 3.2). Civan (1996) also presented a model that includes additional deposition processes. In this dissertation, the deposition process is focussed on adsorption and mechanical entrapment (or plugging deposition), which have been identified as the main deposition mechanisms (Minssieux, 1997). The adsorption process in Equation (3.1) is an equilibrium process, whereas the mechanical entrapment represented by Equation (3.2) is a rate process. These two processes occur simultaneously in the reservoir.

3.3 Permeability Reduction

Asphaltene deposition (or any solid particle deposition) leads to reduction of permeability or formation damage. Reduction of permeability is frequently related to the porosity reduction.

Kumar and Todd (1988) proposed the following approach based on the Kozeny-Carman equation:

$$k = \frac{\phi^3}{C(1-\phi)^2} \tag{3.3}$$

where,

C	=	Kozeny-Carman constant
k	=	actual permeability [md]
ϕ	=	actual porosity

From Equation (3.3), the actual permeability k is related to the initial permeability k^0 and initial porosity ϕ^0 through:

$$\frac{k}{k^0} = \left(\frac{\phi}{\phi^0}\right)^3 \left(\frac{1-\phi^0}{1-\phi}\right)^2 \tag{3.4}$$

where the actual porosity ϕ is calculated by subtracting the volume of deposited solids from the pore volume.

Civan (1992) suggested the following empirical equation:

$$\frac{k}{k_0} = \left(\frac{\phi}{\phi^0}\right)^a \tag{3.5}$$

where a is an empirical parameter. Chang and Civan (1997) and Civan (1996) discussed other models for formation plugging. These models are empirical and quite complex. In this dissertation, a generalized version of Equation (3.4) will be used to model the plugging process in Section 6.6. Another novel empirical model for permeability reduction will also be discussed.

3.4 Wettability Alteration

The alteration of formation wettability due to asphaltene deposition has been a subject of numerous investigations. Asphaltene adsorption onto the rock surface is the main factor for wettability alteration from water-wet to oil-wet. Collins and Melrose (1983), Kamath et al. (1993), Clementz (1982), Crocker and Marchin (1988) and Buckley et al. (1997) describe the change of formation wettability from water-wet to mixed-wet or oil-wet upon adsorption of asphaltene onto the rock surface. Clementz (1982) discussed the permanent alteration of core properties after asphaltene adsorption. Collins and Melrose (1983) showed that asphaltene adsorption is reduced but not eliminated by the presence of water films on water-wet rock. Crocker and Marchin (1988) and Buckley et al. (1997) studied asphaltene adsorption for different oil compositions and the corresponding degree of wettability alteration. Kamath et al. (1993) discussed the effect of asphaltene deposition on waterflood performance. Their results show that, while the increase in asphaltene deposition increased pore plugging and reduced permeability, the deposition may induce favorable changes in relative permeabilities and flow diversion that improve the displacement efficiency.

A review of the effect of wettability on oil recovery is given by Morrow (1990). Wettability has been shown to affect relative permeabilities, irreducible water saturation,

residual oil saturation, capillary pressures, dispersion and electrical properties. The alteration of relative permeabilities and the end points has the strongest influence on displacement processes. Morrow (1990) reviewed results for core waterfloods showing that the shift towards a less water-wet condition can range from being highly adverse to highly beneficial to oil recovery. Huang and Holm (1988), Lin and Huang (1990), and Yeh et al. (1992) presented results on the implication of wettability changes on Water-Alternating-Gas (WAG) processes. Typical results for CO_2 WAG processes (Huang and Holm, 1988) indicate that the amount of oil trapped in water-wet cores (45%) was much higher than that trapped in either mixed-wet (15% to 20%) or oil-wet cores (5%).

The modelling of wettability effects is itself a complex topic and is a subject of active research. Data and models that describe the alteration of wettability due to asphaltene deposition and its subsequent effects on the displacement efficiency are not currently available. The incorporation of wettability effects is beyond the scope of this dissertation and is not considered.

4. MODELLING ASPHALTENE PHASE BEHAVIOUR

4.1 Outline

This section describes a thermodynamic model for asphaltene precipitation, the characterization of the asphaltene component, and the numerical methods for performing flash calculation with a solid phase.

4.2 Solid Representation of Precipitated Asphaltene

The precipitate asphaltene is represented as a pure solid. It is shown in Appendix C that for a given temperature T and assuming that the solid is incompressible, the fugacity of the solid phase is:

$$\ln f_s = \ln f_s^{\bullet} + \frac{v_s (p - p^{\bullet})}{R\,T} \tag{4.1}$$

where,

f_s = solid fugacity [kPa]

$f_s^{\bullet}$ = reference solid fugacity [kPa]

p = pressure [kPa]

$p^{\bullet}$ = reference pressure [kPa]

R = gas constant [8.314 kPa m^3/kmol K]

v_s = solid molar volume [m^3/kmol]

T = temperature [K]

4.3 Oil and Gas Phases

The oil and gas phases are modelled with a cubic EOS with volume shift parameters (Penéloux et al., 1982; Jhaveri and Youngren, 1988). Appendix A describes the equations for the Soave-Redlich-Kwong EOS (Soave, 1972) and for the Peng-Robinson EOS (Peng and Robinson, 1976). The Peng-Robinson EOS is used for all calculations in this dissertation. The fugacity of component i in phase j (j = o,g) is:

$$\ln f_{ij} = \ln f_{ij}^{0} + \frac{s_i b_i p}{RT}; \quad i = 1,...,n_c; \quad j = o,g \tag{4.2}$$

where,

f_{ij} = fugacity of component i in phase j with volume shift [kPa]

f_{ij}^{0} = fugacity of component i in phase j without volume shift [kPa]

s_i = dimensionless volume shift

and b_i the EOS "b" parameter for component i, i.e.

$$b_i = \frac{\Omega_b R T_{ci}}{p_{ci}} \tag{4.3}$$

where

p_{ci} = critical pressure of component i [kPa]

T_{ci} = critical temperature of component i [K]

Ω_b = dimensionless EOS parameter (see Appendix A)

The molar volume of phase j with volume shift is:

$$v_j = v_j^{0} + \sum_{i=1}^{n_c} y_{ij} s_i b_i; \quad j = o,g \tag{4.4}$$

where v_j^{0} is the EOS molar volume without volume shift. The volume shift parameter was first introduced by Penéloux et al. (1982) to improve liquid density predictions. It was found that this parameter is also important in modelling the effect of pressure on asphaltene precipitation.

4.4 Representation of Asphaltene Component

In a mixture of n_c components, let the asphaltene component be the n_c-th component. When a gas phase, an oil phase and a solid phase coexist, the following thermodynamic equilibrium equations are satisfied:

$$\ln f_{ig} = \ln f_{io}; \quad i = 1,...,n_c \tag{4.5a}$$

$$\ln f_{n_c o} = \ln f_s \qquad (4.5b)$$

Characterization of components for oil/gas phase behaviour modelling is described in Appendix B. The crucial step in the modelling of asphaltene is the split of the heaviest component in the oil (e.g. C_{31+}) into a non-precipitating component (C_{31A+}) and a precipitating component (C_{31B+}). These two components have identical critical properties and acentric factors, but different interaction coefficients with the light components. The precipitating component has larger interaction coefficients with the light components. As discussed later (Chapter 5 and Chapter 8), with larger interaction coefficients, the precipitating component becomes more "incompatible" with the light components and tends to precipitate as the amount of light component in solution increases. Although C_{31B+} is called the precipitating component, the amount that precipitates is governed by Equation (4.5). Normally, only a portion of the total amount of C_{31B+} will precipitate during a calculation. Hirschberg et al. (1984) reported that the asphalt precipitate from a tank oil consist mainly (90%) of C_{30} to C_{60} compounds. For the purpose of modelling asphaltene precipitation, it is found a heaviest component in the vicinity of C_{30+} is adequate. For this example, C_{31+} is used.

Interaction coefficients between components are important parameters for phase behaviour predictions. In this work, the interaction coefficients between hydrocarbons are calculated from:

$$d_{ik} = 1 - \left(\frac{2 \cdot v_{ci}^{1/6} \cdot v_{ck}^{1/6}}{v_{ci}^{1/3} + v_{ck}^{1/3}} \right)^e \qquad (4.6)$$

where,

d_{ik} = interaction coefficients between component i and k [dimensionless]

e = adjustable parameter [dimensionless]

v_{ci} = critical volume of component i [m^3/kmol]

v_{ck} = critical volume of component k [m^3/kmol]

Equation (4.6) with e =1 was proposed by Chueh and Prausnitz (1967). Mehra (1981) showed that e = 1.2 provides a good fit of the methane interaction coefficients of Katz

and Firoozabadi (1978). Li et al. (1983) stated that a value of e = 1.2 also provides a good correlation for the paraffin-paraffin interaction coefficients of Oellrich et al. (1981). For pseudo components (components that encompass a range of carbon numbers), Li et al. (1983) treated e as an adjustable parameter.

Two approaches are used to calculate the interaction coefficients for the precipitating component. In the first approach, the interaction coefficients between the precipitating component (e.g. C_{31B-}) and the light components (e.g. C_1 to C_5) are set to a constant value, i.e.

$$d_{ik} = \delta, \tag{4.7}$$

while the interaction coefficients with the remaining heavier components are set equal to zero. In the second approach, Equation (4.6) is also used for the precipitating component. Different values for the parameter e is used for C_{31A-} and C_{31B-}, with $e(C_{31A-}) < e(C_{31B-})$. It is sometime necessary to use only Equation (4.6) for the interaction coefficients between the precipitating components and the light components, while the remaining interaction coefficients are zero. This is analogous to the case where Equation (4.7) is used for the interaction with the light components.

Equation (4.6) is used for interaction coefficients between hydrocarbon components. The interaction coefficients between hydrocarbons and non-hydrocarbons (e.g. CO_2, N_2,....) are specified directly.

4.5 Estimation of Model Parameters

At a given temperature T, the parameters associated with the asphaltene component are:

- The fugacity of pure asphaltene $\ln f^*$ at a reference pressure p^*.
- The volume shift parameter of the precipitating component.
- The molar volume of solid v_s.
- The interaction coefficients between the asphaltene components and other components.

The above parameters can be estimated from precipitation data as elaborated later. It is also shown that the volume shift parameter of the precipitating component and the solid molar volume play a similar role in modelling the effect of pressure on asphaltene precipitation and only one need to be considered.

4.6 Effect of Temperature

This dissertation is focussed at the modelling of asphaltene precipitation in reservoirs under pressure depletion or gas injection processes, which usually occur under isothermal conditions. Therefore the modelling of the effect of temperature is not necessary. However for other cases such as the modelling of asphaltene deposition in wellbores during production, the inclusion of temperature effects would be required. For completeness, the equations for modelling the effect of temperature are described in Appendix C and an example is given in Section 5.13.

4.7 Flash Calculations With a Solid Phase

4.7.1 Stability Test

Given a pressure p, a temperature T, and a mixture with global composition z_i (i = 1,..., n_c), flash calculations determine the phase molar fraction and composition by solving Equation (4.5). The complexity of multiphase flash calculations is due to the fact that the number of phases in equilibrium is not known a priori. Michelsen (1982a, 1982b) and Nghiem and Li (1984) developed a stagewise method for performing multiphase flash calculation with an EOS. The procedure is as follows:

1. The system is assumed to be single-phase at the outset.
2. A stability test based on an analysis of the Gibbs free energy is performed to see whether the system would be more stable by splitting into two phases.
3. Two-phase flash calculations are performed if the single-phase system is unstable.
4. A stability test is performed on one of the resulting phases in Step 3 to see whether the system would be more stable with the formation of a third phase.

5. Three-phase flash calculations are performed if the test in Step 4 indicates that the addition of a third phase would yield a more stable system;

6. Continue the process for additional liquid phases.

The above procedure was developed for calculations where all phases are modelled with an EOS. This procedure has been extended to the case where one of the phases is a solid phase represented by Equation (4.1). The additional complexity is in the number of combinations of solid and fluid phases in equilibrium. Figure 4.1 depicts the calculation procedure.

Appendix D provides details on the stability test of fluid phases represented by an EOS. To test the stability of a fluid phase (oil) with composition **x** at p and T, the following equation is solved for the variable Y_i:

$$g_i \equiv \ln Y_i + \ln \varphi_i(\mathbf{y},p,T) - \ln x_i - \ln \varphi_i(\mathbf{x},p,T) = 0; \quad i = 1,\ldots,n_c \tag{4.8}$$

with the fugacity coefficient given by

$$\varphi_i(\mathbf{y},p,T) = \frac{f_i(\mathbf{y},p,T)}{y_i\, p} \tag{4.9}$$

and

$$y_i = \frac{Y_i}{\sum_{k=1}^{n_c} Y_k} \tag{4.10}$$

The Y_i can be considered as unormalized composition. After convergence is achieved, the fluid phase is unstable if

$$\sum_{k=1}^{n_c} Y_k > 1. \tag{4.11}$$

To test the existence of a solid phase, the following test is performed.

The solid phase exists if

$$\ln f_{n_c o} \geq \ln f_s, \qquad \text{or} \tag{4.12a}$$

$$\ln f^{0}_{n_c o} + \frac{s_{n_c} b_{n_c} p}{RT} \geq \ln f^{*}_{s} + \frac{v_s (p - p^{*})}{RT}. \qquad (4.12b)$$

The solid phase does not exist if

$$\ln f_{n_c o} < \ln f_s, \qquad \text{or} \qquad (4.13a)$$

$$\ln f^{0}_{n_c o} + \frac{s_{n_c} b_{n_c} p}{RT} < \ln f^{*}_{s} + \frac{v_s (p - p^{*})}{RT}. \qquad (4.13b)$$

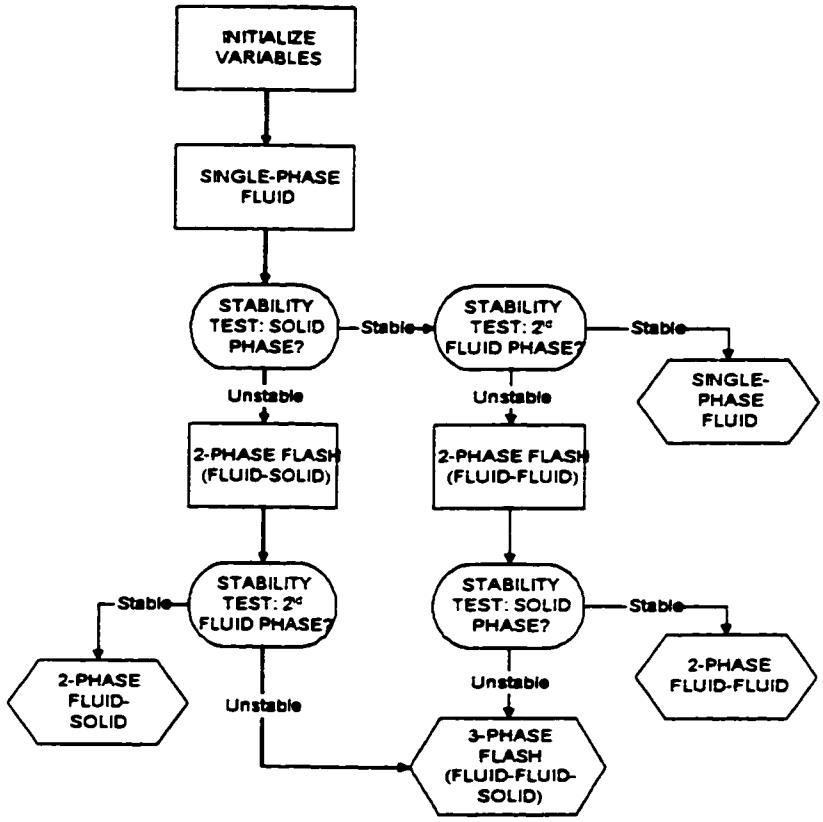

Figure 4.1: Three-phase vapour/liquid/solid flash calculation flow diagram

4.7.2 Flash calculations

Flash calculations consist of determining the phase splits and phase compositions for a feed with moles N_i, $i = 1,\ldots,n_c$, at a given p and T. Instead of N_i, the feed composition (global composition) can also specified. The following equations apply:

$$N_i = N_{io} + N_{ig}, \quad i = 1,...,n_c - 1 \tag{4.14a}$$

$$N_{n_c} = N_{n_c o} + N_{n_c g} + N_s \tag{4.14b}$$

$$N_t = \sum_{i=1}^{n_c} N_i \tag{4.15}$$

$$z_i = \frac{N_i}{N_t} \tag{4.16}$$

where,

N_{ij} = moles of component i in phase j

N_s = moles of solid

N_t = total moles in hydrocarbon phases

Equations (4.5) form a system of (n_c+1) equations that can be solved for N_{ig} $(i = 1,...,n_c)$ and N_s with Newton's method. Because of the existence of multiple solutions, a good initial guess of the solution is normally required to obtain convergence. Alternatively, the Quasi Newton Successive Substitution (QNSS) method discussed in the following, which does not require a good initial estimate of the solution, can be used to solve the equilibrium equations. Additional details regarding the QNSS method are given in Appendix E.

In flash calculations, the equilibrium equations are often written in terms of equilibrium ratios (K-values). The three-phase equilibrium Equations (4.5) can be rewritten as:

$$g_i \equiv \ln K_{ig} + \ln \varphi_{ig} - \ln \varphi_{io} = 0; \quad i = 1,...,n_c \tag{4.17}$$

$$g_{n_c+1} \equiv \ln K_{n_c s} + \ln \varphi_s - \ln \varphi_{n_c o} = 0 \tag{4.18}$$

with

$$K_{ig} = \frac{y_{ig}}{y_{io}} \tag{4.19}$$

$$K_{n_c s} = \frac{y_{n_c s}}{y_{n_c o}} = \frac{1}{y_{n_c o}} \tag{4.20}$$

$$\varphi_s = \frac{f_s}{p} \tag{4.21}$$

In Equation (4.20), $y_{n_c s} = 1$ because the solid phase is a pure solid. In conjunction with the above equations, the following material balance equations can be derived:

$$\sum_{i=1}^{n_c} \frac{(K_{ig} - 1) z_i}{1 + F_g (K_{ig} - 1) + F_s (K_{is} - 1)} = 0 \tag{4.22}$$

$$\sum_{i=1}^{n_c} \frac{(K_{is} - 1) z_i}{1 + F_g (K_{ig} - 1) + F_s (K_{is} - 1)} = 0 \tag{4.23}$$

where

F_g = mole fraction of gas phase

F_s = mole fraction of oil phase

Note that $K_{is} = 0$ for $i = 1,\ldots,n_c\text{-}1$. The oil and gas phase composition can be determined from K_{ig}, K_{is}, F_g, and F_s as follows:

$$y_{io} = \frac{z_i}{1 + F_g (K_{ig} - 1) + F_s (K_{is} - 1)} \tag{4.24}$$

$$y_{ig} = K_{ig}\, y_{io} \tag{4.25}$$

Let $\boldsymbol{\alpha}$ be the vector with elements $\ln K_i$, and let $\boldsymbol{\alpha}^{(k)}$ be the k-th iteration value for the vector $\boldsymbol{\alpha}$. The Quasi Newton Successive Substitution (QNSS) used by Nghiem and Li (1984) for multiphase flash calculation is as follows:

$$\Delta \boldsymbol{\alpha}^{(k)} = \boldsymbol{\alpha}^{(k+1)} - \boldsymbol{\alpha}^{(k)} \tag{4.26}$$

$$\boldsymbol{\alpha}^{(k+1)} = \boldsymbol{\alpha}^{(k)} - \sigma^{(k)}\, \mathbf{g}^{(k)} \tag{4.27}$$

$$\sigma^{(k)} = -\left(\frac{\Delta \boldsymbol{\alpha}^{(k-1)} \cdot \mathbf{g}^{(k-1)}}{\Delta \boldsymbol{\alpha}^{(k-1)} \cdot \Delta \mathbf{g}^{(k-1)}} \right) \sigma^{(k-1)} \tag{4.28}$$

$$\sigma^{(0)} = 1 \tag{4.29}$$

It was shown (Nghiem and Li, 1984) that the QNSS method is related to the gradient method and may not require a good initial estimate for convergence. However the convergence is only linear and not quadratic as in Newton's method. Hybrid methods have also been developed where the QNSS method is first applied and is replaced by Newton's method near the solution to obtain quadratic convergence.

5. PHASE BEHAVIOUR PREDICTIONS

5.1 Outline

In this section, the thermodynamic model is applied to predict the precipitation behaviour of petroleum reservoir fluid. A sensitivity analysis of the model prediction with changes in parameters is also given. The Peng-Robinson EOS (Peng and Robinson, 1976) is used to model the oil and gas phases.

The measurement of asphaltene precipitation under reservoir conditions is a difficult task. The onset of precipitation can be detected with changes in light intensity (Novosad and Costain, 1990), in optical fluorescence and electrical conductance (MacMillan et al., 1995), in viscosity (Escobedo and Mansoori, 1995; Turta et al., 1997), laser intensity (Hammami et al., 1999; Hammami and Raines, 1999), and acoustic resonance (Sivaraman et al. 1999). The measurement of the amount of precipitated asphaltene is a very challenging problem, as the harvesting of the precipitate from high pressure cells is complicated by deposits on equipment surfaces, residual oil in the precipitate, and precipitate entrained in the oil (Burke et al., 1990; MacMillan et al., 1995). These measurements take a long time and are subject to a high degree of experimental errors. Multiple tests are often performed to check the reproducibility of the measurements.

5.2 Burke et al. Oil 2

Table 5.1 reports the composition of two oils (Oil 1 and 2) and a solvent (HCG 2) from Burke et al. (1990). Pressure depletion experiments were performed on Oil 1, while Oil 2 was mixed with various amounts of solvent HCG 2. The matching of Oil 1 will be discussed later. Table 5.2 shows the precipitation and saturation pressure data for different concentrations of solvent in Oil 2. The weight % corresponds to the percentages with respect of the original mass of live oil. The last column in Table 5.2 shows the total amount of precipitates. These values show the existence of some measurements errors. In particular, the measurements or precipitate in residual stock-tank oil at 70 mole % of solvent deviated substantially from the other values. Ignoring the latter data point gives an average value for the total amount of precipitate of 7.80 weight %.

With the oil C_{7+} specific gravity and molecular weight given in Table 5.1, application of the characterization method of Li et al. (1985) gave the 10 pseudo components shown in Table 5.3. Note that the heaviest component of the solvent is not part of the original oil. The heaviest component of the oil, C_{31}, is split into two components: C_{31A+} (non-precipitating component) and C_{31B+} (precipitating component). The mole fraction of C_{31B+} is calculated from 7.80 weight % of precipitate:

$$z_{C_{31B+}} = w_{C_{31B+}} \times M_{oil} \div M_{C_{31B+}} = 0.0780 \times 202.4 \div 617.6 = 0.0256 \quad (5.1)$$

Table 5.1
Composition (mole %) and properties of oils and solvent from Burke et al. (1990)

Component and properties	*Oil 1*	*Oil 2*	*Solvent*
N_2	0.57	0.51	3.17
CO_2	2.46	1.42	17.76
C_1	36.37	6.04	30.33
C_2	3.47	7.00	26.92
C_3	4.05	6.86	13.09
iC_4	0.59	0.83	1.26
nC_4	1.34	3.35	4.66
iC_5	0.74	0.70	0.77
nC_5	0.83	3.46	1.26
C_6	1.62	3.16	0.78
C_{7+}	47.96	66.68	
Total	100.00	100.00	100.00
C_{7+} molecular weight	329	281	
C_{7+} specific gravity	0.9594	0.9020	
Live-oil molecular weight	171.4	202.4	
API gravity of stock tank oil	19.0	24.0	
Reservoir temperature, °F	212	218	
Saturation pressure, psia	2950	600	

Table 5.2
Static precipitation test results for Oil 2 with Solvent at 218 °F
(from Burke et al., 1990)

Solvent (mol %)	*Mixture saturation pressure (psia)*	*Test pressure (psia)*	*Precipitates from live oil (wt %)*	*Precipitates in residual stock-tank oil (wt %)*	*Total precipitates (wt %)*
0	600	3014.7	0.14	8.83	8.97
20	1050	3014.7	0.27	7.56	7.83
50	2310	3014.7	1.46	5.50	6.96
70	3750	4214.7	1.65	2.69	4.34
78	4510	5014.7	3.21	4.63	7.84
85	5000	5014.7	1.29	6.73	8.02
90	4250	5014.7	1.10	6.07	7.17

Table 5.3
Modelled composition for Oil 2 and Solvent

No.	Component	Oil 2 (mol %)	Solvent (mol %)
1	CO_2	1.42	17.76
2	N_2 & C_1	6.55	33.50
3	C_2	7.00	26.92
4	C_3	6.86	13.09
5	C_{4G+}	0.00	8.73
6	C_4-C_9	24.66	
7	C_{10}-C_{16}	22.41	
8	C_{17}-C_{30}	19.62	
9	C_{31A+}	8.92	
10	C_{31B+}	2.56	

To estimate f_s^*, the precipitation data at 0 mole % of solvent and p^* = 3014.7 psia and T = 218 °F was used. The amount of precipitate (0.14 weight %) was removed from the feed. The fugacity of $f_{C_{31B+}}$ in the remaining mixture was then calculated with the PR

EOS and equated to f_s^*. The volume shifts for all components are zeros. A value for v_s of 0.9 m^3/kmol was found adequate for use in Equation (4.1) (the molar volume of C_{31B+} calculated with the EOS is 0.776 m^3/kmol).

The interaction coefficients between all hydrocarbon components up to and including C_{31A+} were calculated from Equation (4.6). The interaction coefficients between C_{31B+} and the light hydrocarbon components up to C_5 are assumed to have the same value δ as shown in Equation (4.7). The parameter e in Equation (4.6) and δ in Equation (4.7) affected both the saturation pressures and the amount of precipitates, and had to be adjusted simultaneously.

Matching saturation pressure and precipitation data yields e = 0.5761 and δ = 0.120. The interaction coefficients for C_{31A+} and C_{31B+} are shown in Figure 5.1. Figures 5.2 and 5.3 show the comparison between calculated and experimental saturation pressures and precipitates, respectively. If the precipitation data at 70 mole % solvent was discounted as discussed above, the match was excellent up to 78 mole % solvent. For solvent concentration above 78 mole %, the measurements indicated a substantial drop in the precipitate. For this case, the model does not show a drop in the amount of precipitate. However, it shows that the amount of precipitate levels off at high solvent concentration. Burke et al. (1990) and Chabak (1991) attributed the decrease in the precipitate at high solvent concentration to the switching of the mixture from a bubble-point fluid to a dew-point fluid. The model does not show a decrease in precipitation at high solvent concentration, but does exhibit a change in the precipitation behaviour.

5.3 *Mechanistic Aspect of the Model*

The non-precipitating component can be related to resins, asphaltene/resin micelles that do not dissociate, and heavy paraffins. The precipitating component corresponds to both the asphaltenes that dissociate and the asphaltene/resin micelles that precipitate unaltered. Because of identical critical properties and acentric factors, the non-precipitating and precipitating components behave as a single component in solution. The larger interaction

coefficients between the precipitating and the solvent components cause the precipitation of the former with the addition of solvent.

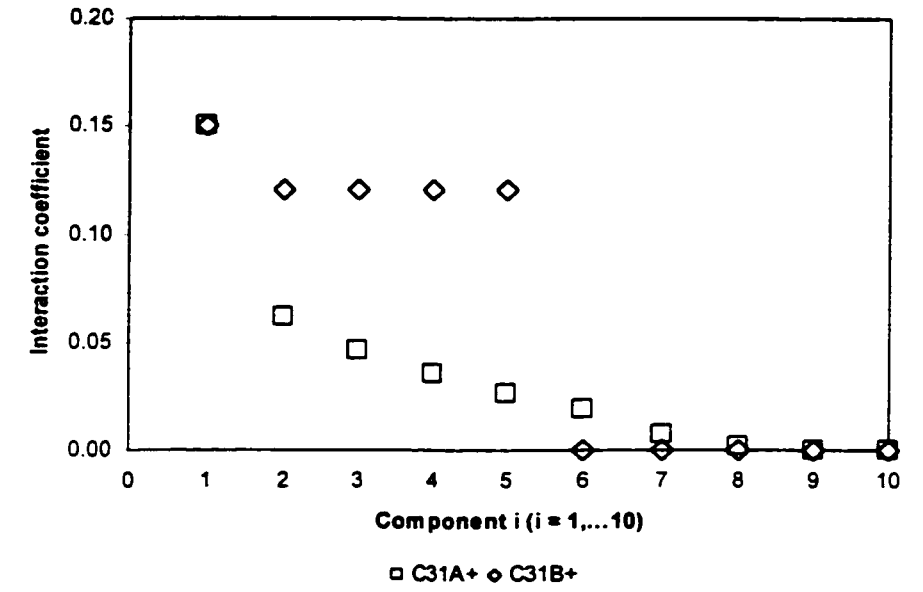

Figure 5.1: Interaction coefficients of C_{31A+} (i=9) and C_{31B+} (i=10) for Oil 2

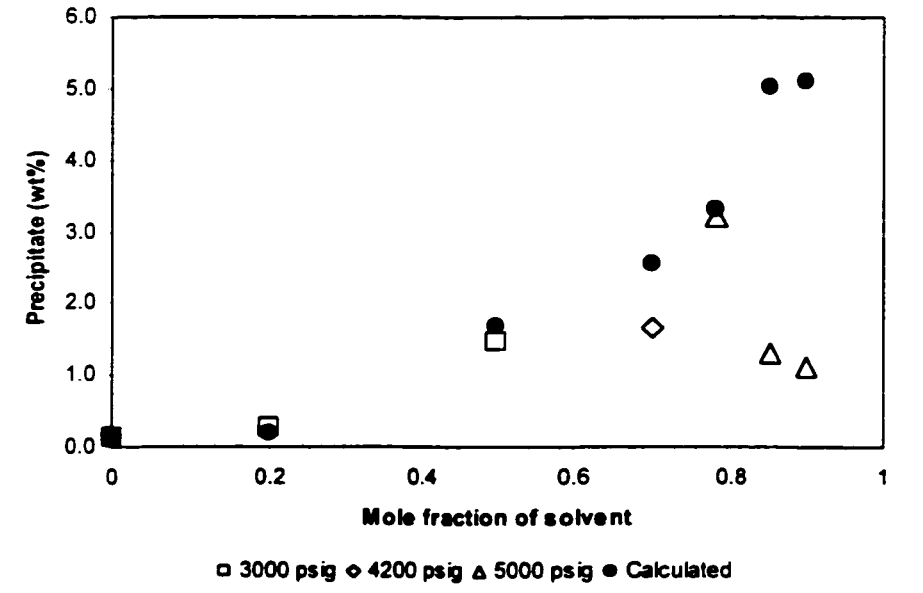

Figure 5.2: Weight % precipitate from Oil 2 with the addition of solvent (Experimental data at 3000 psig, 4200 psig and 5000 psig are shown)

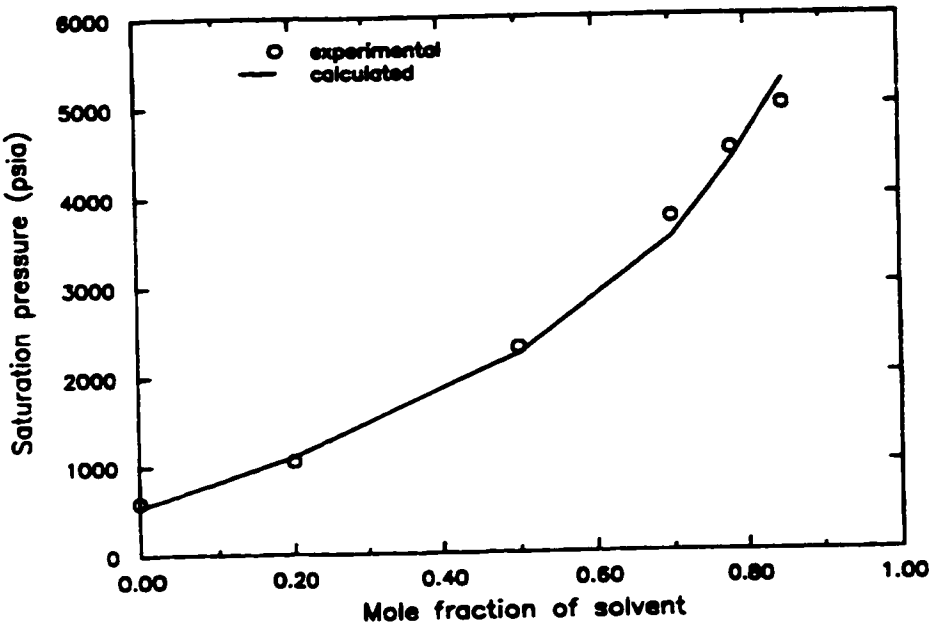

Figure 5.3: Saturation pressures of Oil 2 solvent mixtures

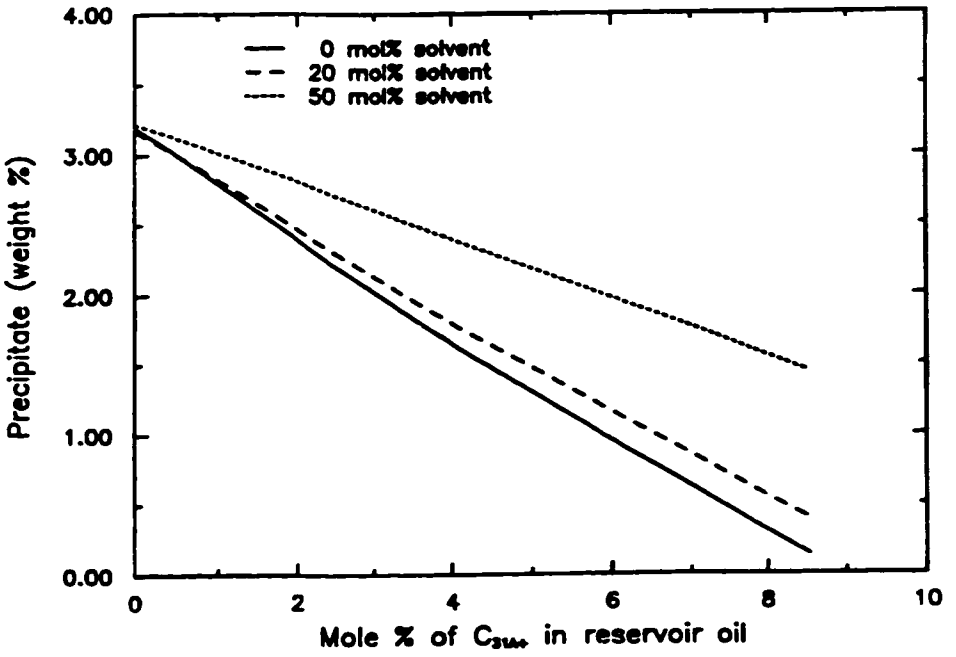

Figure 5.4: Effect of C_{31A+} on precipitate for Oil 2

To illustrate the importance of the amount of C_{31A+} in keeping the asphaltene component in solution, a series of calculations was performed with decreasing amount of C_{31A+} in Oil 2. The results are shown in Figure 5.4 for mixtures of Oil 2 with 0 mole %, 20 mole % and 50 mole % of solvent. The C_{31A+} concentration in the reservoir oil varies from 8.92 mole % (original Oil 2) to 0 mole %. Figure 5.4 shows that the amount of precipitates increases with decreasing amount of C_{31A+} in the reservoir oil. Thus the presence of C_{31A+} enhances to solubility of C_{31B+}. These results substantiate the mechanistic aspect of the thermodynamic model proposed in this dissertation.

5.4 *Burke et al. Oil 1*

Burke et al. (1990) also reported experimental precipitation data for Oil 1 at 212 °F as a function of pressure. Table 5.1 gives the measured oil composition and properties. Table 5.4 shows the precipitation data. Examination of Column 2 of Table 5.4 shows that the amount of precipitate is small and goes through a maximum as the pressure decreases. Column 4 shows the total amount of precipitates that were obtained by summing the values in Column 2 and Column 3. The arithmetic average value for Column 4 is 15.8035 weight %.

Table 5.4
Static precipitation test results for Oil 1 at 212 °F as a function of pressure (from Burke et al, 1990)

Pressure (psia)	*Precipitates from live oil (wt %)*	*Precipitates remaining in residual stock tank oil (wt %)*	*Total precipitates (wt %)*
1014.7	0.403	15.73	16.133
2014.7	1.037	14.98	16.107
3034.7	0.742	15.06	15.802
4014.7	0.402	14.86	15.262

Table 5.5
Modelled fluid composition for Oil 1

No.	*Component*	*mole %*	*MW*
1	CO_2	2.4600	44.010
2	N_2 & C_1	36.9400	16.228
3	C_2	3.4700	30.070
4	C_3	4.0500	44.097
5	C_4	1.9300	58.124
6	C_5	1.5700	72.151
7	C_6-C_7	4.3500	92.667
8	C_8-C_{13}	13.4093	143.321
9	C_{14}-C_{19}	9.4338	227.478
10	C_{20}-C_{24}	5.6864	305.371
11	C_{25}-C_{30}	4.9512	381.763
12	C_{31A+}	7.6812	665.624
13	C_{31B+}	4.0681	665.624
	Total	100.0000	

The C_{7-} fraction of the oil was first split into single carbon number components from C_7 to C_{31-} using the method of Li et al. (1985). All the components are then lumped into 13 components shown in Table 5.5. Also shown are the compositions and the component molecular weights of the components. The heaviest fraction C_{31-} was split into two components: a non-precipitating component, C_{31A-}, and a precipitating component, C_{31B-}. The mole fraction of C_{31B-} is based on the average weight % of 15.8035 discussed above. It is computed as follows:

$$z_{C_{31B-}} = w_{C_{31B-}} \times M_{oil} \div M_{C_{31B-}} = 0.158035 \times 171.343 \div 665.627 = 0.040681 \qquad (5.2)$$

The calculated molecular weight of the oil from the component characterization is 171.343, as compared to the experimentally reported value of 171.4. For a given set of interaction coefficients between C_{31B+} and the other components (discussed later), the saturation pressure is matched by adjusting the power e in Equation (4.6) for interaction coefficients of components from N_2 & C_1 to C_{31A+}.

5.5 *Onset of Precipitation and Reference Solid Fugacity*

The upper APE pressure is obtained by linear extrapolation of the last two pressures in Table 5.4 to zero weight % of precipitate. The value obtained is 5173.4 psia. This pressure was taken as the reference pressure p^* for the solid phase. The fugacity $\ln f_{C_{31B-}}$ in the oil phase was calculated at p^* and at the reservoir temperature, and then equated to the solid fugacity $\ln f_s^*$. The molar volume of the solid phase v_s was set to 1.04 m^3/kmol (the value of pure C_{31B-} at the reference conditions obtained with the Peng-Robinson EOS is 1.02 m^3/kmol).

5.6 *Model Predictions*

Several runs were performed to illustrate:

- the matching of experimental precipitation data,
- the capability of the model to predict the upper and lower APE pressures,
- the sensitivity of the model to the volume shift parameters, interaction coefficients, the amount of precipitating component, and the solid molar volume v_s.

The parameters that are varied in the sensitivity runs are described in the following. The first parameter is the power e in the interaction coefficient Equation (4.6), which is adjusted to match the saturation pressure. The second parameter is the volume shift parameter $s_{C_{31B-}}$. The volume shift parameters for all other components are zero. The third parameter is the value for interaction coefficients between C_{31B-} and the light components up to and including C_5, i.e. components 1 through 6 in Table 5.5. All these interaction coefficients are set to the same value (Equation 4.7). Interaction coefficients between C_{31B-} and components heavier than C_5 are zeros. The fourth parameter is the amount of precipitating component $z_{C_{31B-}}$. Although this amount was estimated from experimental data in Equation (5.2), runs are performed with different amounts to study its effect on the prediction. The fifth parameter is the solid molar volume v_s. Table 5.6 shows the parameters for the different runs. For clarity, values that are different from those in Run 1 are bolded.

The model for asphaltene must satisfy inequality (4.12) for pressures between the upper APE and lower APE pressures, and inequality (4.13) elsewhere. For pressures above the saturation pressure, the above inequalities show the importance of the volume shift parameter $s_{C_{31B^+}}$. Below the bubble point, the composition variation comes into effect, and the interaction coefficients between the asphaltene component and the light components must be such that inequality (4.13) prevails below the lower APE pressure.

The model predicts a maximum precipitation around the saturation pressure, which is consistent with observations reported in the literature (de Boer et al., 1995). Burke et al. data point at 2014.7 psia is questionable as it does not follow the observed trend.

In Run 1, the maximum experimental precipitation at 2014.7 psia was matched. In Run 2, the precipitation data at 4014.7 psia and 3034.7 psia (above the saturation pressure) were matched. Figure 5.5 shows the precipitation results from Runs 1 and 2. The following observations can be made:

- Precipitation starts at 5173.4 psia and increases as the pressure decreases.
- The maximum precipitation data was matched in Run 1.
- The precipitation data above the saturation pressure were matched in Run 2.
- Both runs exhibit a maximum precipitation at the saturation pressure of 2950 psia.
- Asphaltene precipitation decreases as the pressure drops further from the saturation pressure.
- Run 2 shows that the asphaltene precipitation goes to zero at around 1500 psia while the precipitation for Run 1 levels off for pressures below 1500 psia.

Table 5.6
Precipitating-component parameters for the different runs

Run No.	*Dimensionless volume shift parameter for C_{31B+}*	*Interaction coefficients between C_{31B+} and light components (up to C_5)*	*Mole % of C_{31B+}*	*Solid molar volume v_S (m^3/kmol)*
1	0.0129	0.2200	4.0681	1.040
2	**0.0050**	**0.2115**	4.0681	1.040
3	**0.0110**	0.2200	4.0681	1.040
4	**0.0150**	0.2200	4.0681	1.040
5	0.0129	**0.2000**	4.0681	1.040
6	0.0129	**0.2400**	4.0681	1.040
7	0.0129	0.2200	**2.0340**	1.040
8	0.0129	0.2200	**6.1021**	1.040
9	0.0129	0.2200	4.0681	**1.037**
10	0.0129	0.2200	4.0681	**1.043**

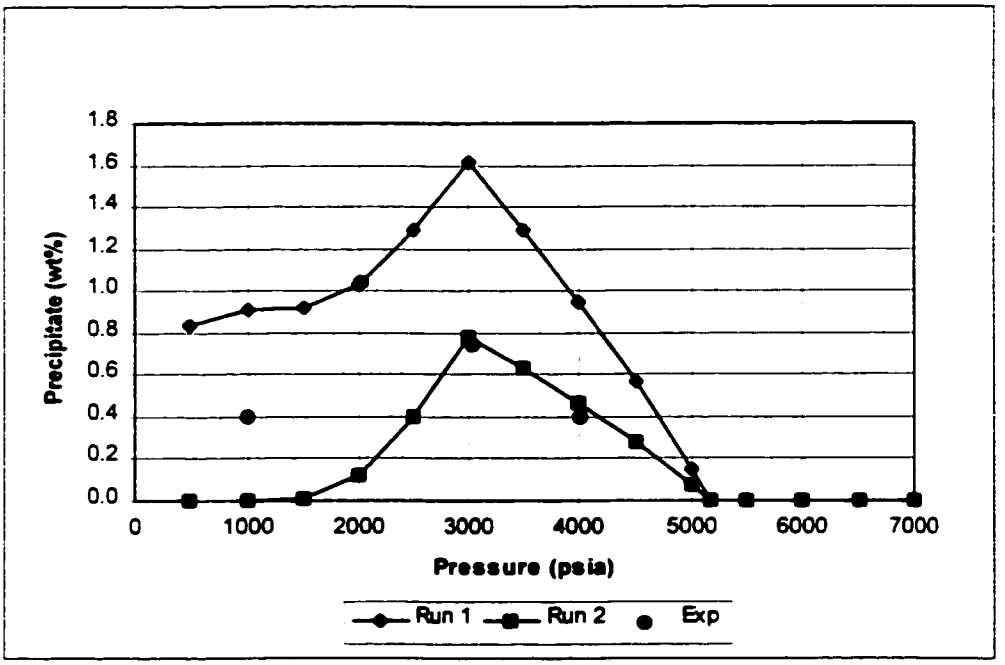

Figure 5.5: Asphaltene precipitation for Runs 1 and 2

Run 2 shows that the model can predict the typical asphaltene precipitation behaviour between the upper and lower onset points on the APE. The precipitation for Run 1 does not go to zero at low pressures. This run was taken as the base case for a sensitivity study of the parameters of the asphaltene component.

5.7 *Effect of Volume Shift Parameter of Asphaltene Component*

In Runs 3 and 4, C_{31B+} interaction coefficients are the same as in Run 1. The volume shift parameters are respectively 0.0110 and 0.0150, as compared to a value of 0.0129 in Run 1. Figure 5.6 shows the comparison between Runs 1, 3, and 4. The results show that the volume shift parameters affect the precipitation both above and below the saturation pressure. A larger volume shift parameter yields more precipitation. Note that the shapes of the precipitation curves are similar when the volume shift parameter varies.

5.8 *Effect of Interaction Coefficients of Asphaltene Component*

In Runs 5 and 6, the volume shift parameter is equal to the value in Run 1. C_{31B-} interaction coefficients in Runs 5 and 6 are respectively 0.2000 and 0.2400, as compared to a value of 0.2200 in Run 1. Figure 5.7 shows the comparison between Runs 1, 5 and 6. Changes in interaction coefficients affect significantly the results below the saturation pressure and only to a small extent the results above the saturation pressure. Run 6 shows that as the interaction coefficients are increased, the asphaltene precipitation goes to zero at lower pressures. Higher interaction coefficients make the C_{31B-} component more incompatible with the light components. As these components come out of solution at lower pressures, the solubility of C_{31B-} in the liquid phase increases. The compositional effect through the interaction coefficients overcomes the pressure effect at a certain pressure and precipitation stops. In Run 5, smaller interaction coefficients were used. This resulted in an increase in precipitation at lower pressures. A plateau in the precipitation behaviour is observed between the saturation pressure and 2000 psia. As the pressure further decreases, the smaller interaction coefficients cannot overcome the pressure effects. This gives rise to an increase in precipitation.

5.9 *Effect of Amount of Precipitating Component*

In Runs 1 through 6, the mole % of C_{31B+} is 4.0681 %, which is the amount estimated in Equation (5.2). In Runs 7 and 8, the volume shift parameter and interaction coefficients are the same as those in Run 1, but the amount of C_{31B-} is varied. In Run 7, the mole % of C_{31B-} is 0.5 times the value in Run 1, and in Run 8 it is 1.5 times. Figure 5.8 shows that the amount of precipitating component has a strong influence on the precipitation. Decreasing this amount induces less precipitation and flattens the peak. Increasing the amount brings about more precipitation and sharpens the peak. Run 7 matches three data points from Burke et al. (1990).

The total amount of precipitate was calculated by adding the amount of precipitate from the live oil to the amount of precipitate remaining in the residual stock tank oil. The latter was obtained by titration with n-heptane (Burke et al., 1990). A different value would have been obtained if n-pentane was used for titration. This titration procedure does not correspond to any in situ process. Therefore the amount of precipitating component calculated from Equation (5.2) is only an estimate, and its adjustment in the matching procedure is justifiable.

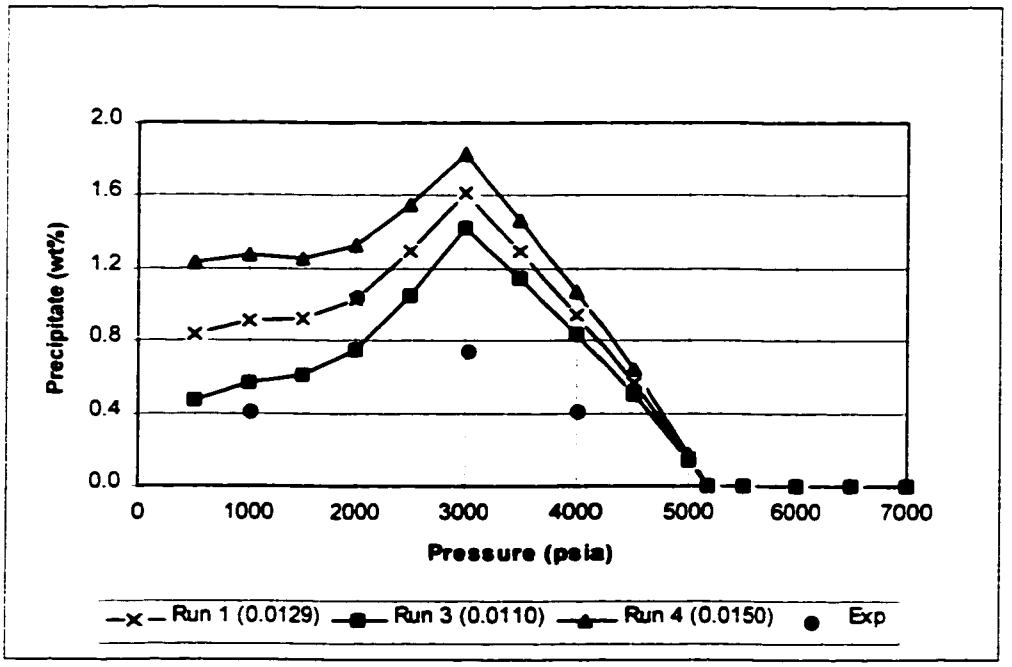

Figure 5.6: Effect of volume shift parameter on asphaltene precipitation

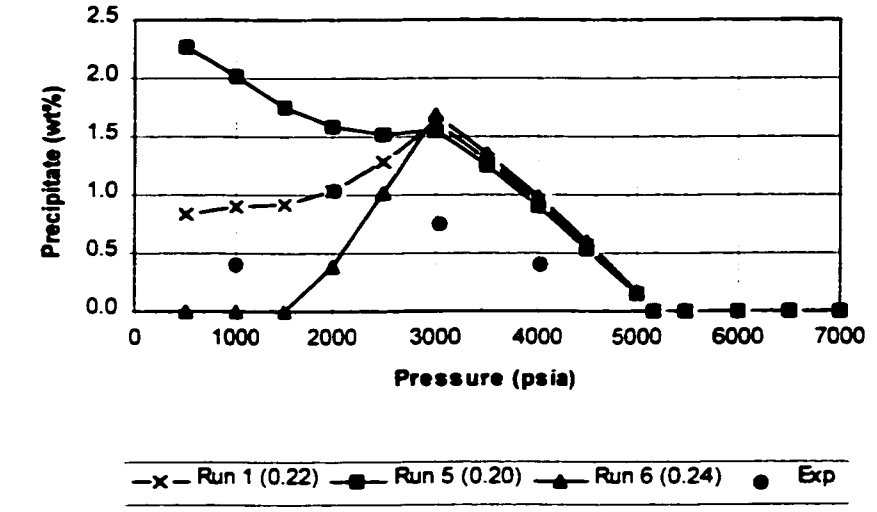

Figure 5.7: Effect of interaction coefficients on asphaltene precipitation

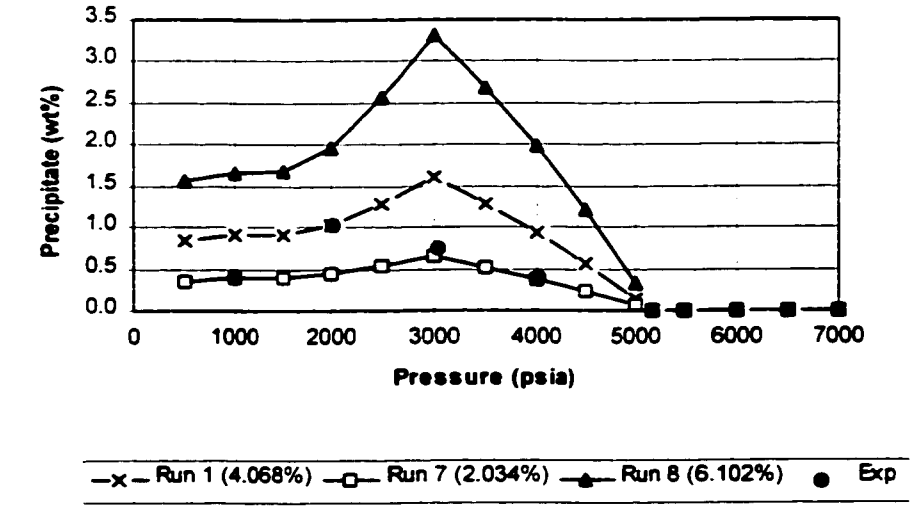

Figure 5.8: Effect of amount of precipitating component on asphaltene precipitation

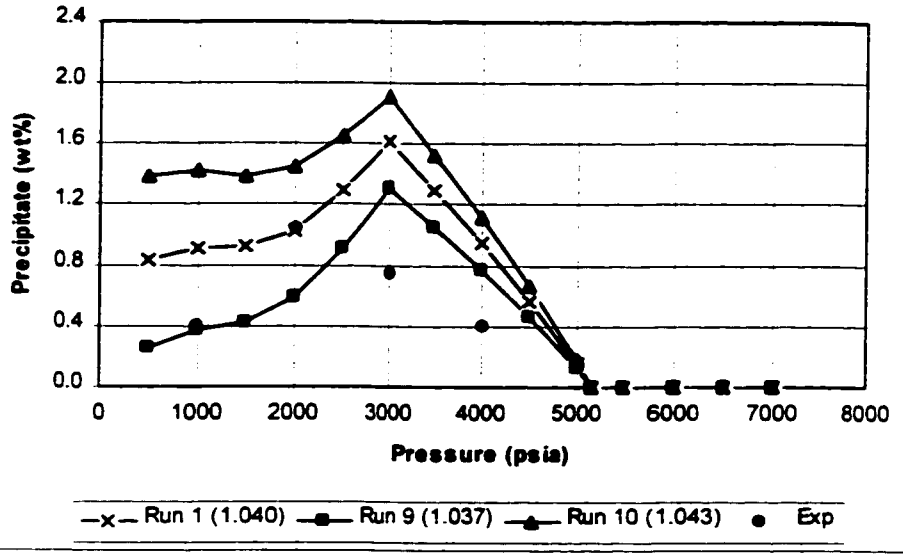

Figure 5.9: Effect of solid molar volume on asphaltene precipitation

5.10 Effect of Solid Molar Volume v_s

The solid molar volume used in Runs 1 through 8 is equal to 1.04 m^3/kmol. The EOS molar volume of C_{31B-} is 1.02 m^3/kmol. The precipitation behaviour of asphaltene is governed by the magnitude of the fugacity of solid phase relative to the fugacity of the asphaltene component in solution, i.e. the difference $(\ln f_{n_c o} - \ln f_s)$. Equations (4.1) and (4.2) show that the volume shift $s_{C_{31B-}}$ and v_s play a similar role in the value of difference $(\ln f_{n_c o} - \ln f_s)$ with changes in pressure. However because of the presence of p^* in Equation (4.1), $(\ln f_{n_c o} - \ln f_s)$ is very sensitive to small changes in v_s when p^* is close to the pressures of interest, which is usually the case. Runs 9 and 10 were performed with v_s = 1.037 m^3/kmol and 1.043 m^3/kmol, respectively. The comparison with the base case in shown in Figure 5.9. Note the similarity between Figure 5.6 and Figure 5.9.

5.11 Fugacity Comparison

As discussed earlier, the difference $(\ln f_{n_c o} - \ln f_s)$ controls the precipitation behaviour of asphaltene. The fugacity difference $(\ln f_{n_c o} - \ln f_s)$ for the Runs 1, 3, 4, 5 and 6 are plotted in Figure 5.10, where $\ln f_{n_c o}$ is the fugacity of the asphaltene component in the liquid phase calculated assuming there is no precipitation. The region where $(\ln f_{n_c l} - \ln f_s) \geq 0$ is where precipitation occurs. Only $(\ln f_{n_c o} - \ln f_s)$ for Run 6 becomes negative at low pressures. The shapes of the $(\ln f_{n_c o} - \ln f_s)$ curves are similar to the precipitation curves and provide the trend of precipitation calculations without actually performing flash calculations.

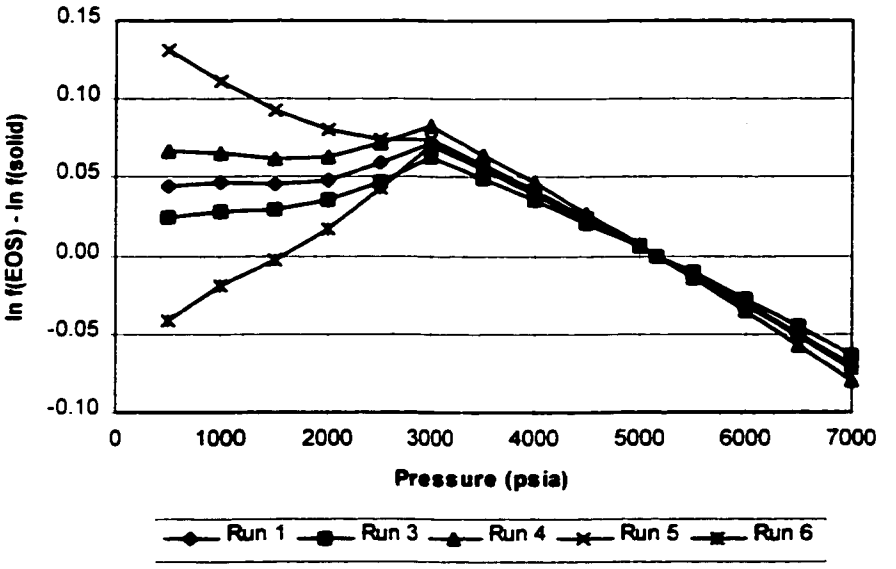

Figure 5.10: Fugacity difference for the different runs

5.12 Pressure-Composition APE Prediction

Experimental APE and saturation pressure curves are available for a North Sea fluid at 90°C. Table 5.7 shows the pseudo-component representation of the reservoir fluid together with separator oil and separator gas compositions. The heaviest fraction C_{32+}, is

split into a non-precipitating component, C_{32A+}, and a precipitating component, C_{32B+} as shown in Table 5.7. The exponents for the interaction coefficients in Equation (4.6) are respectively 0.84 between C_{31A+} and the lighter components, and 1.57 for C_{31B+}. The PR EOS is used to model the oil and gas phases. The experimental saturation pressures and points on the APE for different recombination of dead oil and separator gas are shown in Figure 5.11. The mole % of separator gases for the different mixtures are: 4.53, 5.35, 5.71, 6.10, 6.53 and 6.99%.

The reference fugacity f_s^* was obtained by calculating the fugacity of one point on the APE (recombined oil with 69.9 mole % of separator gas and 600 bar) with the PR EOS, and equating it to f_s^*. A molar volume of v_s of 0.9 m^3/kmol was used.

Figure 5.11 shows a good match of the experimental and calculated APE and saturation pressure curves. The model was able to predict precipitation conditions that are far from the reference conditions. Figure 5.12 presents the precipitation behaviour for different recombined oils. As the pressure decreases, precipitation increases and reaches a maximum value around the saturation pressure. Below the saturation pressure, precipitation decreases with pressure. These results are consistent with observations reported in the literature. The curves in Figure 5.12 were extrapolated to zero weight % precipitate to obtain pressures on the APE in Figure 5.11. The constant line of constant weight % of precipitate (similar to "quality lines" for oil-gas phase diagrams) can also be extracted. These quality lines are also plotted in Figure 5.11.

Table 5.7
Modelled fluid composition for a North Sea reservoir fluid

No.	Component	Dead oil composition (mol %)	Separator gas composition (mol %)	MW
1	N_2 & C_1	8.365	70.216	16.614
2	C_2-C_5	25.273	28.319	41.425
3	C_6-C_9	27.014	1.465	94.626
4	C_{10}-C_{15}	24.625	0.000	167.200
5	C_{21}-C_{31}	9.698	0.000	354.646
6	C_{32A+}	3.654	0.000	591.682
7	C_{32B+}	1.371	0.000	591.682
	Total	100.000	100.000	

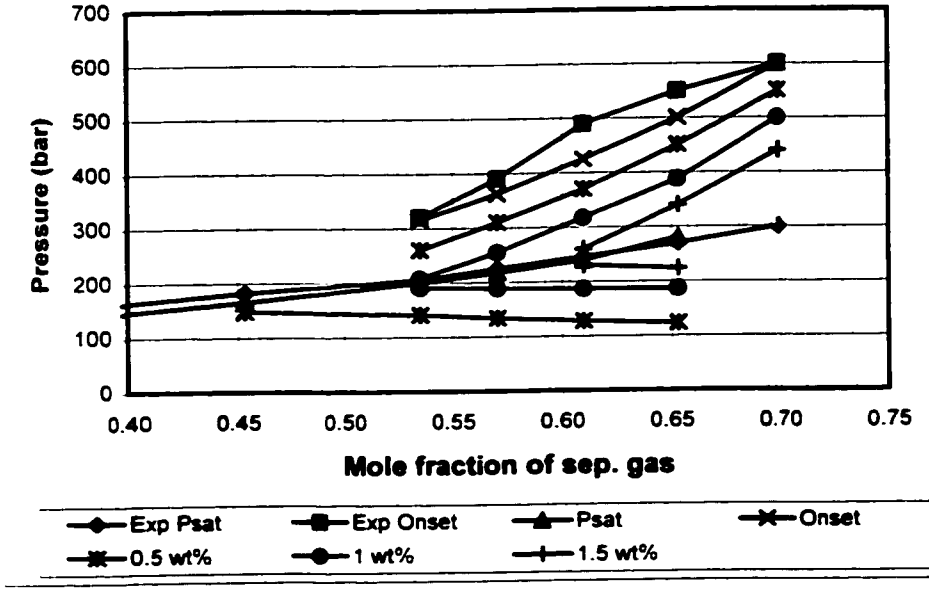

Figure 5.11: Saturation pressure, APE, and precipitation lines for North Sea recombined oils

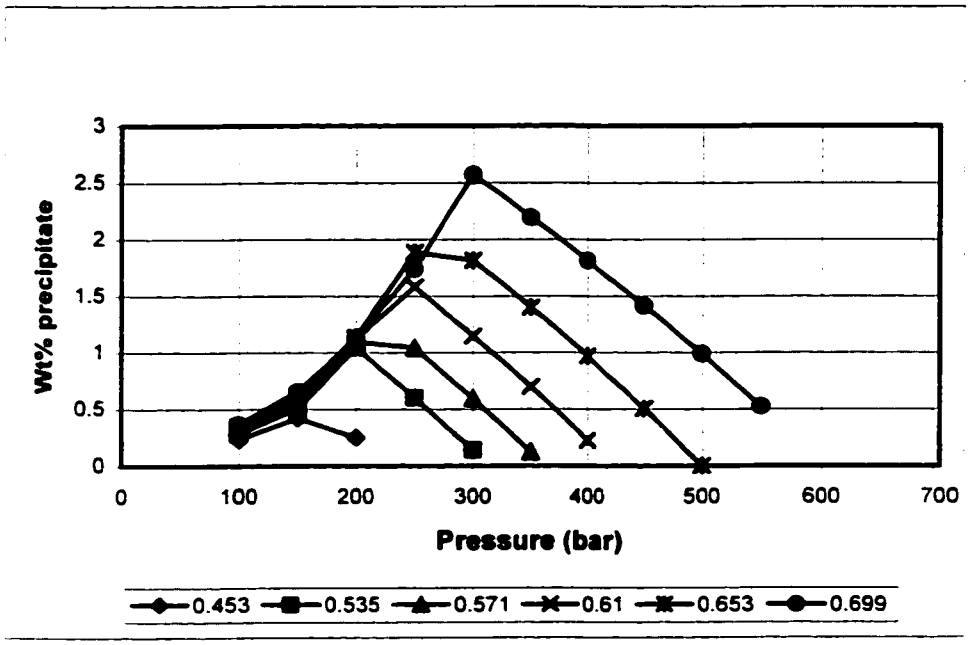

Figure 5.12: Calculated precipitation curves for North Sea recombined oils (legend corresponds to mole fraction of separator gas in recombined oil)

5.13 Pressure-Temperature APE Calculations

The effect of temperature and pressure on the solid model is described in Appendix C. This section presents an example on the application of Equation (C.2) to model the effect of temperature on asphaltene precipitation. Calculations are performed with the North Sea fluid system in Section 5.12. The values for ΔC_{ps} and ΔH_f in Equation (C.2) are 10 cal/mol K and 40000 cal/mol, respectively. Figure 5.13 shows the precipitation curves for the recombined mixture containing 0.535 mole fraction of separator gas at different temperatures. The precipitation lines are extrapolated to zero weight % of precipitate to obtain the temperature on the upper APE. Figure 5.14 shows the upper PT APE for the two recombined North Sea fluids with 0.347 and 0.535 mole fractions of separator gas.

The results show that the amount of precipitation decreases with increasing temperature, which agree with observations made in the literature (Leontaritis, 1996).

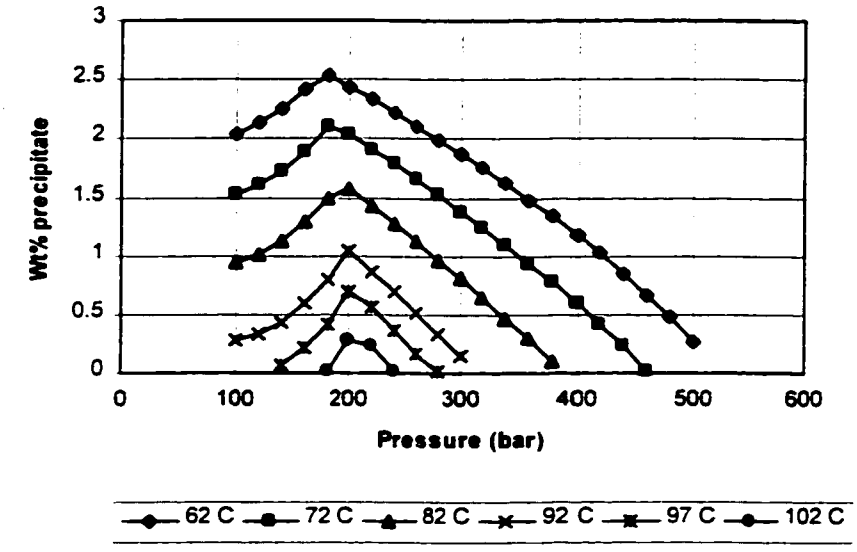

Figure 5.13: Precipitation curve for recombined North Sea fluid (0.535 mole fraction of separator gas) at different temperatures

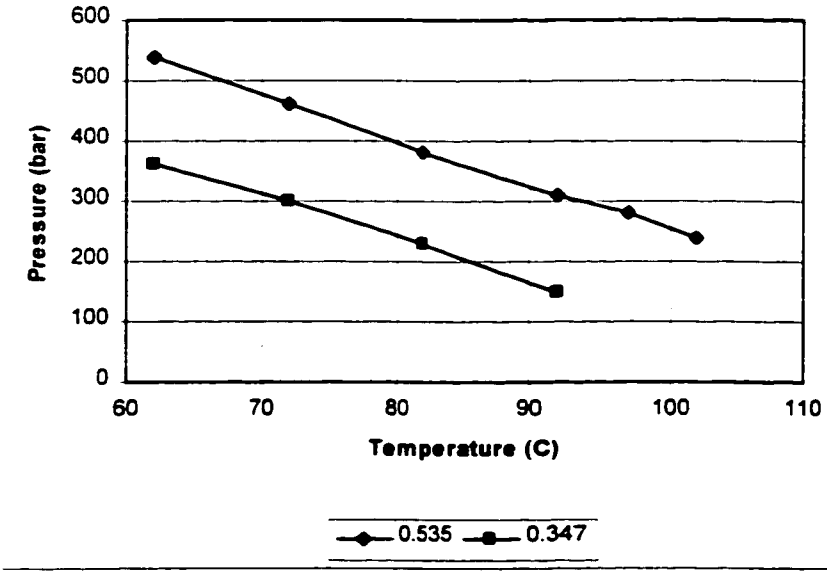

Figure 5.14: PT upper APE for different recombined North Sea fluids (legend indicates the mole fraction of separator gas in recombined mixures)

5.14 Summary

This section summarizes the use and tuning of the proposed improved solid model to match experimental precipitation data.

The important step was the split of the heaviest component into a non-precipitating and precipitating component. Since the asphaltene precipitate consists mainly of C_{30} to C_{60} (Hirschberg et al., 1984), any component in the vicinity of C_{30+} was judged to be adequate. The initial split can be based on the total precipitate from live oil and stock tank oil (as indicated in Equations 5.1 and 5.2). However, some adjustments may be necessary to obtain a good match. This adjustment was justifiable as the precipitate from stock tank oil is normally obtained by titration; as such, it depends on the solvent used (n-pentane or n-heptane) and does not correspond to any in situ process.

The interaction coefficients with the light components (i.e. C_1 to C_5) were also crucial for matching the precipitation behavior. Two approaches were proposed, based on either Equation (4.6) (correlation with critical volumes) or Equation (4.7) (constant). For Burke et al. Oil 2 experiments, the interaction coefficients using Equation (4.7) were equal to 0.12 whereas for Oil 1 experiments, they were around 0.22. Experiments on Oil 2 corresponded to a hydrocarbon gas injection process whereas experiments on Oil 1 corresponded to a pressure depletion process. With the addition of a hydrocarbon gas, additional amounts of light components were available to facilitate the precipitation, and hence the use of smaller interaction coefficients was adequate. For the pressure depletion process, the light components were native to the original oil, and therefore larger interaction coefficients were required to promote precipitation.

The volume shift of the precipitating component was another important parameter in the modelling of pressure effects. It played the same role as the solid molar volume, but was easier to adjust to match experimental data as the model was less sensitive to small changes in the volume shift parameter than to changes in solid molar volume.

The solid model was the simplest model for modelling asphaltene precipitation. The ability of this model to predict precipitation behaviour over a wide range of pressure and

composition was seen to be quite remarkable. This was possible because of the special characterization of the heaviest component proposed in this dissertation. Previous attempts in improving the solid model consisted of adding more empirical parameters to the solid model (Thomas et al., 1992), or using a multicomponent solid system (Thomas et al., 1992; Chung, 1992; MacMillan et al. 1992), which also increased the number of parameters. The approach advanced in this dissertation places the onus on the characterization of the heaviest fraction of the oil, while keeping the solid model unaltered. This approach was successful in matching experimental data.

6. EOS COMPOSITIONAL SIMULATOR WITH ASPHALTENE PRECIPITATION

6.1 Outline

Compositional simulators with EOS flash calculations have been developed to simulate recovery processes with complex oil/gas phase behaviour (Acs et al., 1985; Chien et. al., 1985; Coats, 1980; Collins et al., 1992; Shiralkar et al., 1997; Wang et al., 1999; Watts, 1986; Young and Stephenson, 1983). These processes include hydrocarbon gas injection, CO_2 injection, and the production and cycling of gas condensate reservoirs. The equations in compositional simulators consist of partial differential equations for multiphase multicomponent flow in porous media and correlations for phase behaviour, fluid properties and rock-fluid interactions. Details of these equations can be found in Lake (1989).

This section describes the equations for an EOS compositional simulator with asphaltene precipitation, deposition and plugging.

6.2 Component Flow Equations

Appendix F describes the partial differential equations for multiphase multicomponent flow. These equations are discretized with finite-difference techniques. The resulting discretized equations for the flow of components in the oil and gas phases are:

$$\Psi_i \equiv \Delta T_o^m \left(y_{io} + y_{isf}\right)^m \left(\Delta p^{n+1} - \gamma_o^m \Delta D\right) + \Delta T_g^m \, y_{ig}^m \left(\Delta p^{n+1} + \Delta P_{cog}^m - \gamma_g^m \Delta D\right) + q_i^{n+1} - \frac{V}{\Delta t}\left(N_i^{n+1} - N_i^n\right) = 0, \quad i = 1, \ldots, n_c \tag{6.1}$$

Similarly the discretized equation for the flow of water is:

$$\Psi_w \equiv \Delta T_w^m \left(\Delta p^{n+1} - \Delta P_{cwo}^m - \gamma_w^m \Delta D\right) + q_w^{n+1} - \frac{V}{\Delta t}\left(N_w^{n+1} - N_w^n\right) = 0 \tag{6.2}$$

where,

D = depth [m]

g = gravity acceleration [m/s^2]

N_i = moles of component i per bulk volume [mol]

p = pressure [kPa]

P_{cog} = oil-gas capillary pressure [kPa]

P_{cwo} = water-oil capillary pressure [kPa]

q_i = molar injection/production rate of component i [mol/day]

T_j = transmissibility of phase j [mol/kPa·day]

V = gridblock volume [m^3]

y_{ig} = mole fraction of component i in gas phase

y_{io} = mole fraction of component i in oil phase

y_{isf} = mole fraction of solid in suspension in oil phase

γ_j = $\tilde{\rho}_j g$; gradient of phase j (j = o,g,w) [kPa/m]

$\tilde{\rho}_j$ = mass density of phase j [kg/m^3]

The above equations represent three-dimensional finite-difference flow equations. They are derived from a discretization of material balance equations with fluxes calculated from Darcy's law (Mattax and Dalton, 1990). Viscous, capillary and gravity effects are included in these equations. The difference between Equation (6.1) and the component flow equation in a standard EOS compositional simulator is the presence of the term y_{isf}, which represents the suspended solid in the oil phase. This suspended solid flows with the oil phase. All y_{isf} are zero except for the asphaltene component ($i = n_c$), i.e.

$$y_{isf} = \begin{cases} 0, & \text{if } i \neq n_c \\ N_{sf}/N_o, & \text{if } i = n_c \end{cases} \tag{6.3}$$

where N_o is the moles of oil.

Expansion of the flow term in Equation (6.2) for grid block (I,J,K) gives:

$$
\begin{aligned}
&\Delta T_w^m \left(\Delta p^{n+1} - \Delta P_{cwo}^m - \gamma_w^m \Delta D\right) = \\
&T_{w,I+1/2,J,K}^m \left[p_{I+1,J,K}^{n+1} - p_{I,J,K}^{n+1} - P_{cwo,I+1,J,K}^m + P_{cwo,I,J,K}^m - \gamma_{w,I+1/2,J,K}^m \left(D_{I+1,J,K} - D_{I,J,K}\right)\right] + \\
&T_{w,I-1/2,J,K}^m \left[p_{I-1,J,K}^{n+1} - p_{I,J,K}^{n+1} - P_{cwo,I-1,J,K}^m + P_{cwo,I,J,K}^m - \gamma_{w,I-1/2,J,K}^m \left(D_{I-1,J,K} - D_{I,J,K}\right)\right] + \\
&T_{w,I,J+1/2,K}^m \left[p_{I,J+1,K}^{n+1} - p_{I,J,K}^{n+1} - P_{cwo,I,J+1,K}^m + P_{cwo,I,J,K}^m - \gamma_{w,I,J+1/2,K}^m \left(D_{I,J+1,K} - D_{I,J,K}\right)\right] + \\
&T_{w,I,J-1/2,K}^m \left[p_{I,J-1,K}^{n+1} - p_{I,J,K}^{n+1} - P_{cwo,I,J-1,K}^m + P_{cwo,I,J,K}^m - \gamma_{w,I,J-1/2,K}^m \left(D_{I,J-1,K} - D_{I,J,K}\right)\right] + \\
&T_{w,I,J,K+1/2}^m \left[p_{I,J,K+1}^{n+1} - p_{I,J,K}^{n+1} - P_{cwo,I,J,K+1}^m + P_{cwo,I,J,K}^m - \gamma_{w,I,J,K+1/2}^m \left(D_{I,J,K+1} - D_{I,J,K}\right)\right] + \\
&T_{w,I,J,K-1/2}^m \left[p_{I,J,K-1}^{n+1} - p_{I,J,K}^{n+1} - P_{cwo,I,J,K-1}^m + P_{cwo,I,J,K}^m - \gamma_{w,I,J,K-1/2}^m \left(D_{I,J,K-1} - D_{I,J,K}\right)\right]
\end{aligned}
\tag{6.4}
$$

The above equations are discretized using an adaptive implicit technique (Collins et al., 1992; Grabenstetter et al., 1991). The superscript m corresponds to n for explicit grid blocks and n+1 for implicit grid blocks. The phase transmissibilities T_k^m (k = o, g, w) are calculated from

$$
T_k^m = \frac{A\,k}{\Delta \ell}\left(\frac{k_{rj}\,\rho_j}{\mu_j\,R_f}\right)^m \tag{6.5}
$$

where,

$$
\frac{A}{\Delta \ell} = \begin{cases} \Delta y\,\Delta z / \Delta x \text{ in the x-direction} \\ \Delta z\,\Delta x / \Delta y \text{ in the y-direction} \\ \Delta x\,\Delta y / \Delta z \text{ in the z-direction} \end{cases} \tag{6.6}
$$

k	=	permeability [μm^2]
k_{rj}	=	relative permeability of phase j (j = o,g,w)
R_f	=	permeability reduction factor
μ_j	=	viscosity of phase j [mPa·sec]
ρ_j	=	molar density of phase j (j = o,g,w) [kmol/m^3]

The permeability reduction factor, R_f, models the plugging process, and is discussed later.

6.3 *Volume and Saturation Equations*

The volume constraint equation expresses the equality of the volume of all fluid phases plus the solid phase to the pore volume:

$$\Psi_v \equiv \sum_k \frac{N_k}{\rho_k} + \frac{N_s}{\rho_s} - \phi = 0; \quad k = o, g, w \tag{6.7}$$

where the N_k's and N_s are repectively the moles of phase k (k = o,g,w) and the moles of solids per bulk volume.

The saturations S_j are calculated from:

$$S_j = \frac{N_j / \rho_j}{\sum_m (N_m / \rho_m)}, \quad k = o, g, w; \quad m = o, g, w \tag{6.8}$$

6.4 Phase Equilibrium Equations

The phase equilibrium equations for the components are:

$$\Psi_{eq.i} \equiv \ln f_{ig} - \ln f_{io}; \quad i = 1,...,n_c \tag{6.9a}$$

$$\Psi_{eq.n_c+1} \equiv \ln f_{n_co} - \ln f_s \tag{6.9b}$$

Given N_i, the above equations can be solved for the moles of component i in the gas phase N_{ig} and the moles of solid N_s. The moles of component i in the oil phase, N_{io}, can be determined from the following equations:

$$N_i = N_{io} + N_{ig}, \quad i = 1,...,n_c - 1 \tag{6.10a}$$

$$N_{n_c} = N_{n_co} + N_{n_cg} + N_s \tag{6.10b}$$

Alternatively, the equilibrium equations can also be solved for K_{ig} (i = 1,...,n_c), K_{n_cs}, F_g and F_s as discussed in Section 4.7.

6.5 Deposition Equations

As discussed in Section 3, the precipitated solid is comprised of three parts:

- N_{sa}, moles of solid that deposit onto the rock surface through adsorption;
- N_{se}, moles of solid that deposit through mechanical entrapment;
- N_{sf}, moles of solid that remain as a suspended solid in the oil phase.

From a material balance, the following equation can be written:

$$N_s = N_{sa} + N_{se} + N_{sf} \tag{6.11}$$

The adsorption follows a Langmuir isotherm:

$$w_{sa} = \frac{w_{sa,max}\, K_a\, C_{sf}}{K_a\, C_{sf} + 1} \tag{6.12}$$

where,

C_{sf} = concentration of solid in the oil phase [ppm (μg/g)]

w_{sa} = mass of adsorbed asphaltene per mass of rock [mg/g]

$w_{sa,max}$ = maximum adsorbed mass fraction [mg/g]

K_a = ration of rate constants of the adsorption/desorption reactions

The suspended concentration of solid C_{sf} in the oil phase can be determined from

$$C_{sf} = \frac{N_{sf}\, M_s}{N_o\, M_o} \cdot 10^6 \tag{6.13}$$

where,

M_o = molecular weight of oil

M_s = molecular weight of solid

The mass of adsorbed asphaltene is related to the adsorbed moles per bulk volume, N_{sa}, through the equation:

$$N_{sa} = \frac{(1-\phi)\,\tilde{\rho}_R\, w_{sa}}{M_s} \tag{6.14}$$

where $\tilde{\rho}_R$ is the mass density of rock [kg/m^3].

The moles of solid deposited through mechanical entrapment follow the ordinary differential equation (3.2). Discretization of this equation gives:

$$\eta^{n+1} = \eta^n + \Delta t \left[(\alpha_0 + \alpha_1\, \eta) |u_o|\, \hat{C}_{sf} \right]^n \tag{6.15}$$

with η, the volume of asphaltene deposited per unit initial pore volume, given by:

$$\eta = \frac{N_{se}\, v_s}{\phi^0} \tag{6.16}$$

and $\hat{C}_{sf}$, the volume concentration of precipitated asphaltene in oil phase, given by:

$$\hat{C}_{sf} = \frac{N_{sf}\, v_s}{(N_o / \rho_o)} \tag{6.17}$$

Given N_s, Equations (6.11), (6.14), and (6.15) with the auxiliary Equations (6.13), (6.16), and (6.17), can be solved for N_{sa}, N_{se}, and N_{sf}.

6.6 *Plugging Equations*

As discussed in Section 3.3, a generalized form of Equation (3.4) is used to model the plugging process:

$$\frac{1}{R_f} = \frac{k}{k^0} = \left(\frac{\hat{\phi}}{\phi^0}\right)^a \left(\frac{1-\phi^0}{1-\hat{\phi}}\right)^b \tag{6.18}$$

where R_f is the permeability reduction factor in Equation (6.5), and a and b are parameters. The porosity $\hat{\phi}$ in Equation (6.18) is equal to the pore volume that is not occupied by the volume of deposited asphaltene, i.e.

$$\hat{\phi} = \phi - (N_{sa} + N_{se}) \cdot v_s \tag{6.19}$$

In Section 8.2, the following alternative correlation for permeability reduction is proposed:

$$R_f = \begin{cases} 1 + (R_{f,max} - 1) \cdot \dfrac{w_{sd}}{w_{sd,max}}, & w_{sd} \le w_{sd,max} \\ R_{f,max}, & w_{sd} > w_{sd,max} \end{cases} \tag{6.20}$$

where

w_{sd} = the weight % of solid deposited through adsorption and mechanical entrapment

$R_{f,max}$ = permeability reduction factor at deposition $w_{sd,max}$

Equation (6.20) corresponds to a linear relationship between R_f and w_{sd}, with a plateau at $R_{f,max}$.

7. SOLUTION METHOD

7.1 Primary and Secondary Variables

The $(2n_c + 3)$ primary unknowns per grid block are: $(p, N_1, \ldots, N_{n_c}, N_w, N_{1g}, \ldots, N_{n_cg}, N_s)^{n+1}$. These can be obtained by solving simultaneously the system of Equations (6.7), (6.1), (6.2), (6.9a), (6.9b) with Newton's method. Those are the primary equations and unknowns. The remaining equations are secondary equations for calculating properties from the primary variables.

Let Ψ_b be the vector of values of the left-hand sides of the equations (residual values) and let ξ_b be the vector of variables for Gridblock b. The elements of Ψ_b are:

$$\Psi_b = \left(\psi_v, \psi_1, \ldots, \psi_{n_c}, \psi_w, \Psi_{eq.1}, \ldots, \Psi_{eq.n_c}, \Psi_{eq.n_c+1}\right)_b ; \quad b = 1, \ldots, n_b \tag{7.1}$$

The $(2n_c+3)$ primary variables for each gridblock are:

$$\xi_b = \left(p^{n+1}, N_1^{n+1}, \ldots, N_{n_c}^{n+1}, N_w^{n+1}, N_{1g}^{n+1}, \ldots, N_{n_cg}^{n+1}, N_s^{n+1}\right)_b \tag{7.2}$$

The well constraint equations and flowing bottom hole pressures are also included in Ψ and ξ, after the reservoir variables as discussed in Behie et al. (1985) and Nghiem and Rozon (1988). The whole system of equations is solved with Newton's method, i.e.:

$$\xi^{(k+1)} = \xi^{(k)} - \left[\left(\frac{\partial \Psi}{\partial \xi}\right)^{(k)}\right]^{-1} \Psi^{(k)} \tag{7.3}$$

7.2 Jacobian Structure and Matrix Preprocessing

As the adaptive method is used, some gridblocks will be Implicit Pressure, Explicit Compositions and Saturations (IMPECS) and some will be implicit. To illustrate the Jacobian structure, a one-dimensional four-gridblock three-component system is selected. For clarity, water is assumed not to be present and ψ_w and N_w are removed from the equation and variable set, respectively. Let the first and second gridblock be IMPECS and the third and fourth gridblock be implicit. The Jacobian structure for the resulting system is shown in Figure 7.1. For clarity, the block diagonal matrices are shaded.

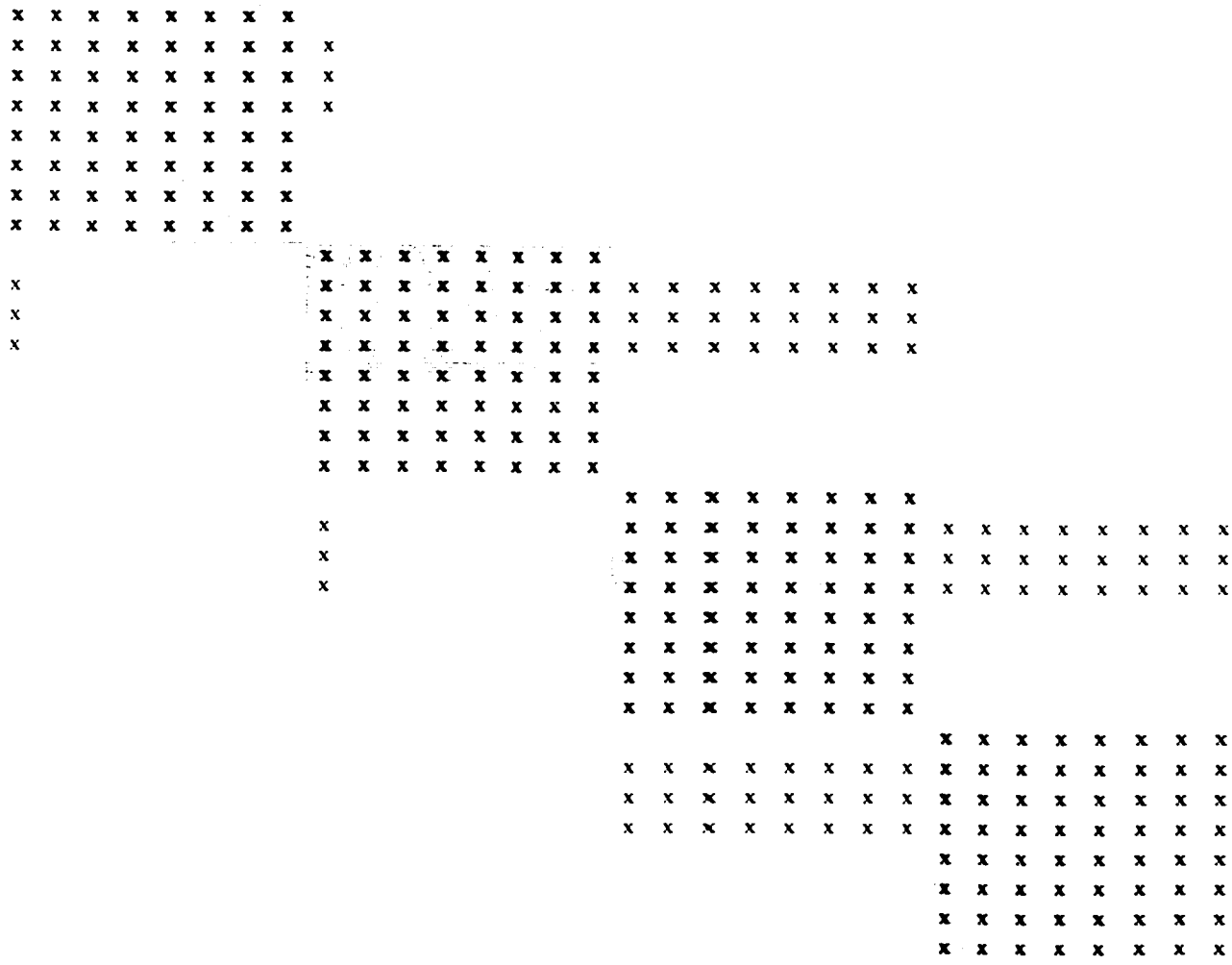

Figure 7.1: Jacobian structure for a 3-component 4-gridblock system

Note that because the volume constraint equation (6.7) and the equilibrium equations (6.9) do not involve variables from adjacent gridblocks, the corresponding rows of the Jacobian matrix do not contain off-diagonal elements. Before the matrix shown in Figure 7.1 is fed to a sparse solver, some processing can be done to simplify the matrix.

7.2.1 Processing of the Equilibrium Variables

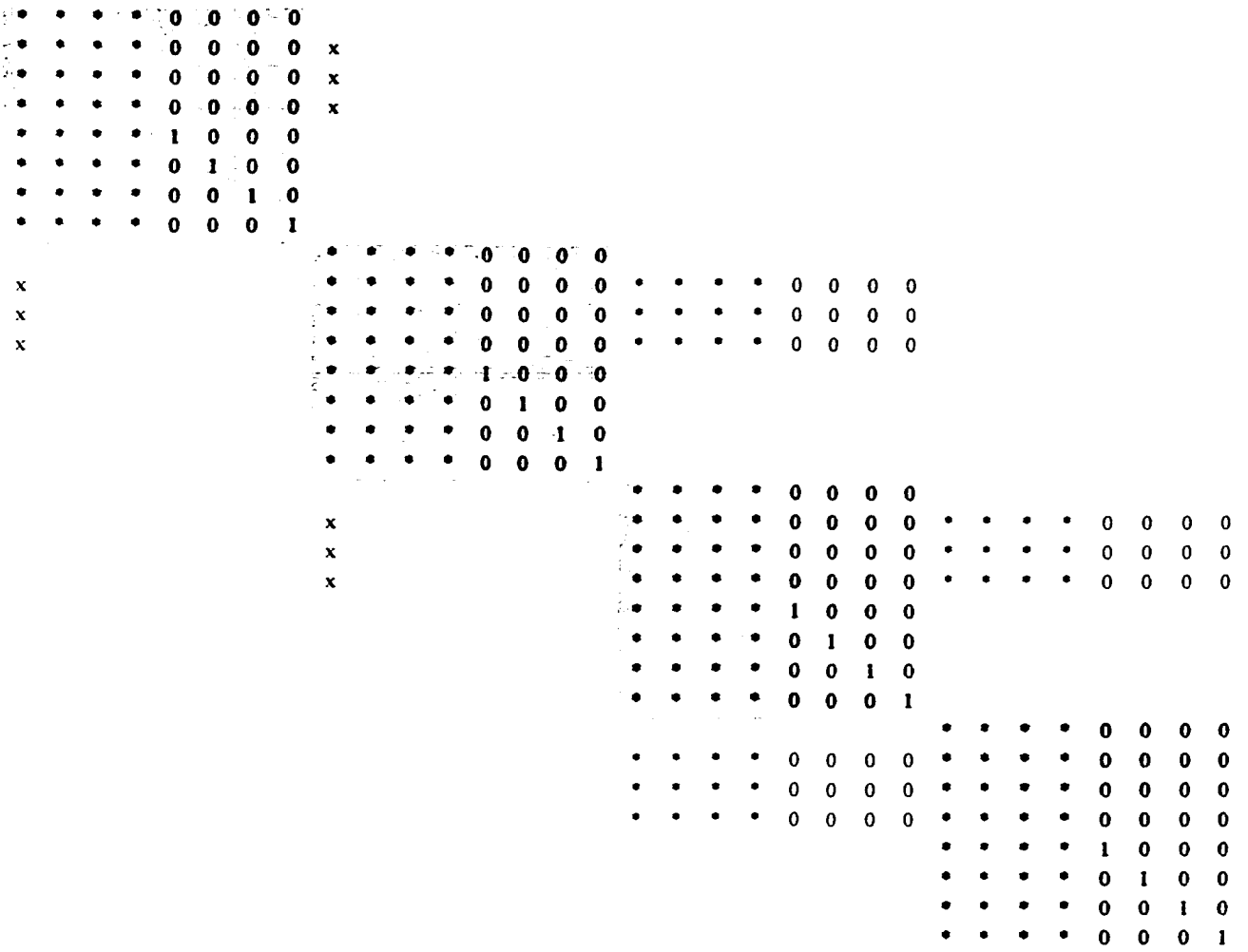

Figure 7.2: Jacobian structure for a 3-component 4-gridblock system after processing of the equilibrium variables

The equilibrium equations can be preprocessed through a partial Gaussian elimination giving the matrix shown in Figure 7.2. Note that the diagonal matrices corresponding to the equilibrium variables have been diagonalized. The elements of the Jacobian that were affected in these processing steps are represented by the symbol *. This partial Gaussian elimination decouples the phase-equilibrium variables $\left(N_{lg}^{n+1}, ..., N_{n_c g}^{n+1}, N_s^{n+1}\right)$ from the flow variables. These variables are now dependent on $\left(p^{n+1}, N_l^{n+1}, ..., N_{n_c}^{n+1}\right)$, but the latter are not functions of the equilibrium variables any more. Thus the system can be solved for

$\left(p^{n+1}, N_1^{n+1}, ..., N_{n_c}^{n+1}\right)$ first, and then back substitution can be applied to obtain the remaining $\left(N_{1g}^{n+1}, ..., \ln N_{n_cg}^{n+1}, N_s^{n+1}\right)$.

7.2.3 Processing of the explicit variables

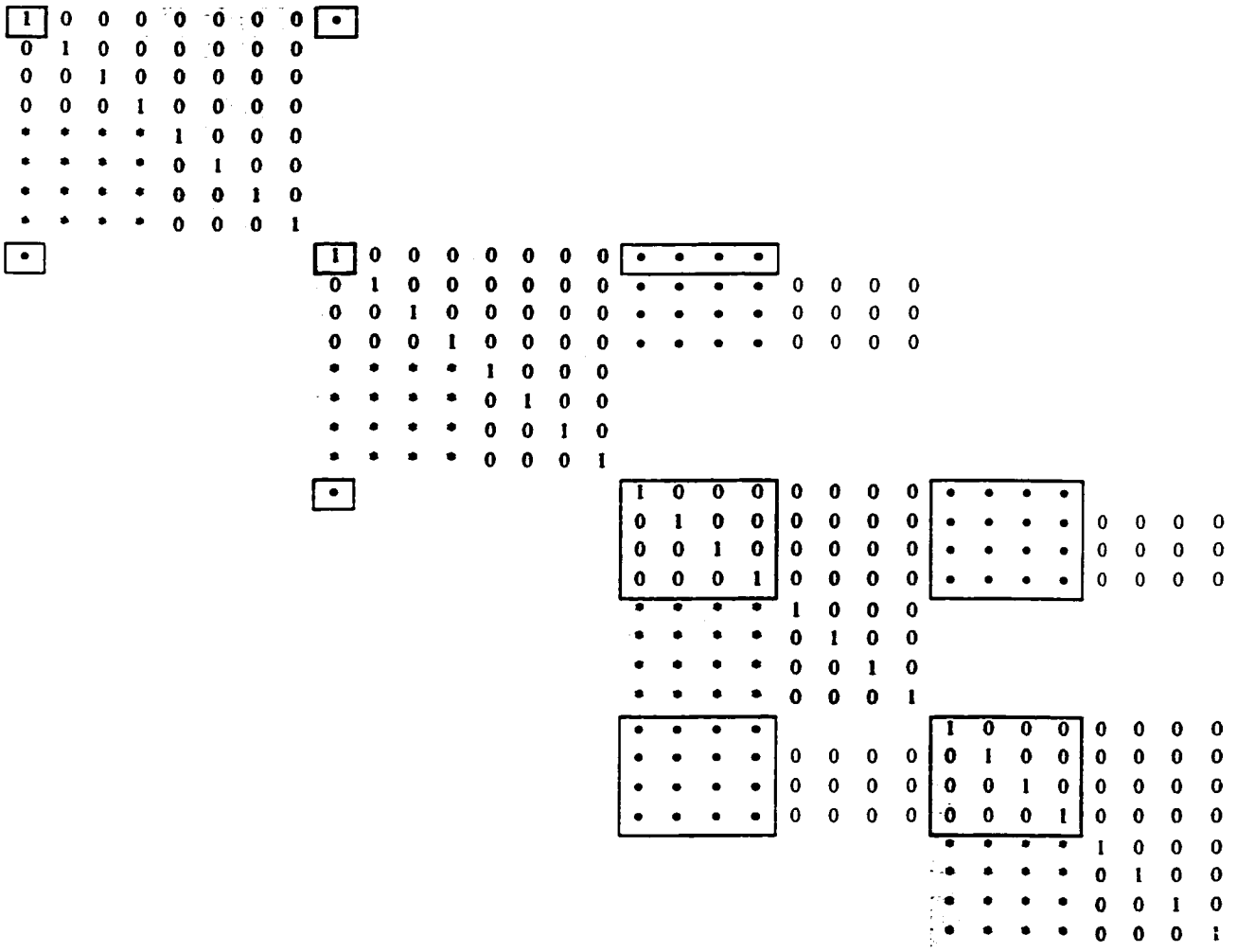

Figure 7.3: Jacobian structure for a 3-component 4-gridblock system after processing of the explicit variables

The first and second gridblocks are IMPECS, while the third and fourth gridblock are implicit. For IMPECS gridblocks, only the pressure at time n+1 is used to calculate the flow while the other variables are explicit. This relationship gives rise to more zeros in the off-diagonal submatrices corresponding to IMPECS gridblocks, as shown in Figure 7.2. Another partial Gaussian elimination can be applied to decouple $\left(N_1^{n+1}, ..., N_{n_c}^{n+1}\right)$ for

Gridblock 1 and 2. The resulting matrix is shown in Figure 7.3, where denotes the off-diagonal elements that have been changed in the process. Matrix elements with a border around correspond to the variables that are still coupled and have to be solved simultaneously. The remaining variables can be obtained by back substitution.

7.3 Sparse Solution Method

The elements in the bordered regions in Figure 7.3 are solved by a preconditioned incomplete LU factorization (ILU) followed by the GMRES iterative solution method (Saad and Schultz, 1986).

Gaussian elimination is too time-consuming for most reservoir-simulation problems, and one usually resorts to an incomplete Gaussian elimination (or ILU factorization) followed by an iterative method. To solve the linear sparse matrix equation

$$\mathbf{A}\,\mathbf{x} = \mathbf{b}, \tag{7.4}$$

let **M** be an ILU factorization of the matrix **A**, i.e.

$$\mathbf{M} = \tilde{\mathbf{L}}\,\tilde{\mathbf{U}} \tag{7.5}$$

where $\tilde{\mathbf{L}}$ and $\tilde{\mathbf{U}}$ are respectively the approximate lower and upper triangular factors produced by the ILU factorization. The residual $\mathbf{r}^{(i)}$ at the i-th iteration is defined as:

$$\mathbf{r}^{(i)} = \mathbf{b} - \mathbf{A}\,\mathbf{x}^{(i)} \tag{7.6}$$

where $\mathbf{x}^{(i)}$ is the i-th iterate approximate solution vector. The iteration is initialized with:

$$\mathbf{x}^{(0)} = \mathbf{0} \tag{7.7}$$

$$\mathbf{r}^{(0)} = \mathbf{b} \tag{7.8}$$

The i-th iterated solution $\mathbf{x}^{(i)}$ is defined as the linear combination

$$\mathbf{x}^{(i)} = \mathbf{x}^{(0)} + \sum_{j=1}^{i} c_j\,\mathbf{v}_j \tag{7.9}$$

where $\mathbf{v}_j$ are certain basis vectors. The coefficients c_j are chosen to minimize the norm $\left\|\mathbf{r}^{(i)}\right\|_2$, which is a linear least squares problem. In GMRES, the basis is generated as follows:

$$\mathbf{v}_1 = \mathbf{r}^{(0)} / \left\|\mathbf{r}^{(0)}\right\|_2 \tag{7.10}$$

$$\mathbf{w}_1 = \left(\mathbf{A}\,\mathbf{M}^{-1}\right)\mathbf{v}_1 \tag{7.11}$$

The second basis vector $\mathbf{v}_2$ is obtained through Gram-Schmidt orthogonalization

$$\mathbf{v}_2 = \left(\mathbf{w}_1 - \left(\mathbf{v}_1 \cdot \mathbf{w}_1\right)\mathbf{v}_1\right) / \left\|\left(\mathbf{w}_1 - \left(\mathbf{v}_1 \cdot \mathbf{w}_1\right)\mathbf{v}_1\right)\right\|_2 \tag{7.12}$$

and so on. Convergence is tested by examining the reduction in residual norm. If $\left\|\mathbf{r}^{(i)}\right\|_2 / \left\|\mathbf{r}^{(0)}\right\|_2$ is less than a chosen tolerance the iteration is assumed to have converged.

Different orderings can be used to calculate the ILU factors. The most common orderings are natural and red-black orderings. More details on sparse solution methods for reservoir simulation can be found in Nghiem and Rozon (1989).

8. COMPOSITIONAL SIMULATION OF ASPHALTENE DEPOSITION AND PLUGGING

8.1 Outline

This section describes example on compositional simulation of asphaltene deposition and plugging. The dynamic aspect of asphaltene deposition is an area of active research and at this time, complete experimental data on the deposition and plugging process are not available. The experiments on the deposition and plugging process mentioned in Section 3 (Piro et al., 1996; Minssieux, 1997; Ali and Islam, 1998) used preformed mixtures of oil and asphaltene precipitates. They did not include the effect of in-situ asphaltene precipitation and redissolution that normally occur in reservoirs.

In the following, simulation of a typical core gas-injection experiment and of a single-well primary depletion case is carried out. The results obtained are discussed and compared qualitatively with observations reported in the literature.

8.2 Gas Injection Simulation

Simulation of a typical gas core displacement was performed with the North Sea reservoir fluid described in Section 5.12. Table 8.1 shows the relevant data.

Figures 8.1 and 8.2 show the gas saturation profile, the amounts of precipitated and deposited asphaltene (through both adsorption and entrapment), and the gas-oil interfacial tension (IFT) profile along the core at 0.5 PV injected. The same information at 0.7 PV injected is shown in Figures 8.3 and 8.4. The IFT is calculated from the Macleod-Sugden correlation (Reid et al., 1977, p. 614).

The following results can be observed:

- All the precipitated asphaltene deposits except at the leading edge of the flood front. The deposition process through adsorption is instantaneous, while the deposition through mechanical entrapment follows an ordinary differential equation (Equation 6.15) and builds up with time. At the leading edge of the flood front the deposition is mainly due to the adsorption of asphaltene onto the rock surface. The plateau at the

leading edge of the flood front in Figure 8.3 corresponds to the maximum amount of adsorbed asphaltene. Behind this region, there is the additional effect of mechanical entrapment. For the values of the mechanical-entrapment parameters used, all the precipitated asphaltene will deposit eventually. These results agree with the experimental observations of Minssieux (1997) and Piro et al. (1996).

- Asphaltene precipitation occurs in the low IFT region, which corresponds to the development of miscibility. These results agree with the experimental observations for solvent injection by Bryant and Monger (1988) and Monger and Trujillo (1991), who reported extensive solid phase precipitation in the development of miscibility by CO_2 and rich-gas flooding.
- The asphaltene precipitation region moves with the flood front and occupies a sizable portion of the core. This gives rise to asphaltene precipitation at the producer at gas breakthrough as illustrated in Figure 8.5, which shows the produced gas-oil ratio and suspended asphaltene versus pore volume injected. These results agree with the field observations reported in Pittaway et al. (1987), Nagel et al. (1990) and Novosad and Costain (1990).
- Simulation runs were also performed with adsorption but without mechanical entrapment. The gas saturation and asphaltene profiles at 0.7 PV injected are shown in Figure 8.6. The results show that adsorption is at its maximum value in most of the precipitation region.

Table 8.1
Core displacement data

Length	0.6858 m (2.25 ft)
Diameter	0.0508 m (2.0 in)
Permeability	500 md
Porosity	30 %
Water saturation	0.0
Pressure	25000 kPa (3626 psia)
Temperature	92 °C (197.6 °F)
Separator gas in recombined oil	35 mole %
Injection gas	Separator gas
Rate	0.6858 m/D (2.25 ft/D)
$w_{sa,max}$	0.5 mg/g of rock
Rock density	2650 kg/m^3
$R_{f,max}$	5
α_0 (Equation 6.15)	1000 m^{-1}
α_1 (Equation 6.15)	20 m^{-1}
No. of gridblocks	30

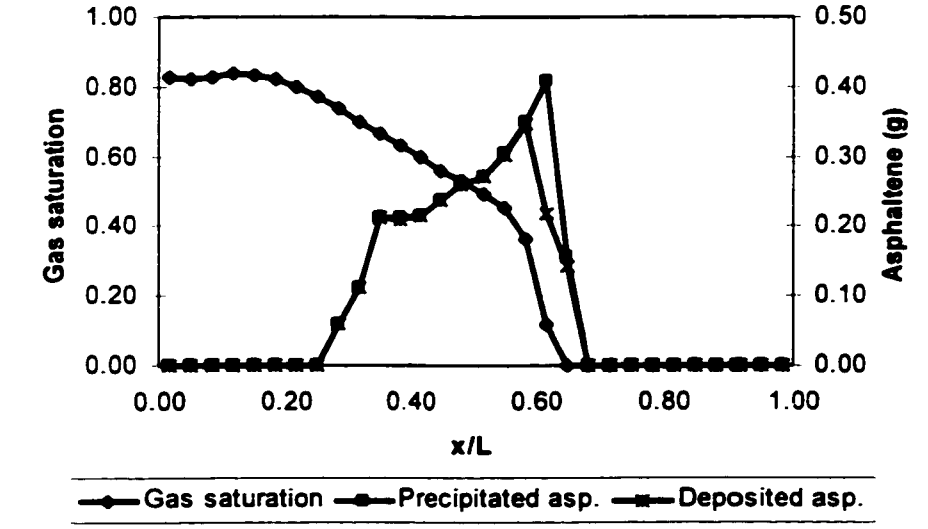

Figure 8.1: Gas saturation and asphaltene profiles at 0.5 PV injected

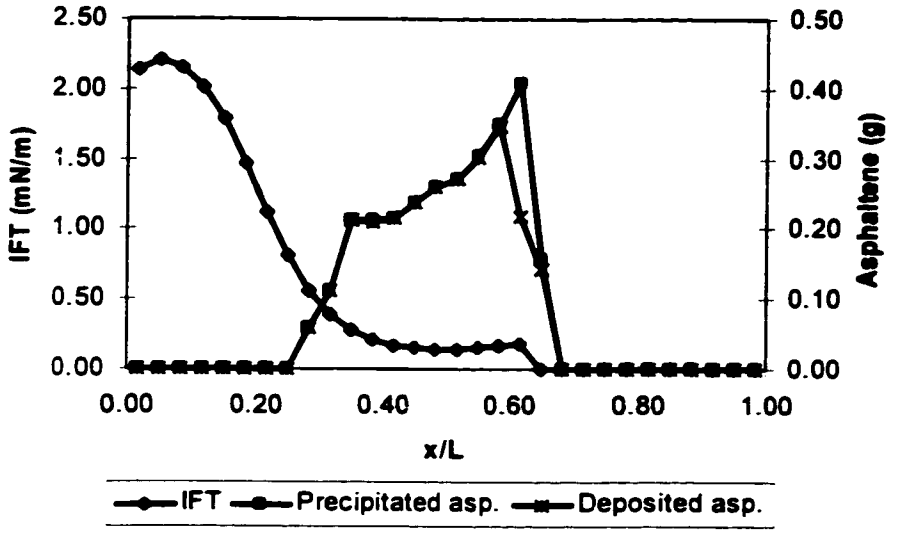

Figure 8.2: IFT and asphaltene profiles at 0.5 PV injected

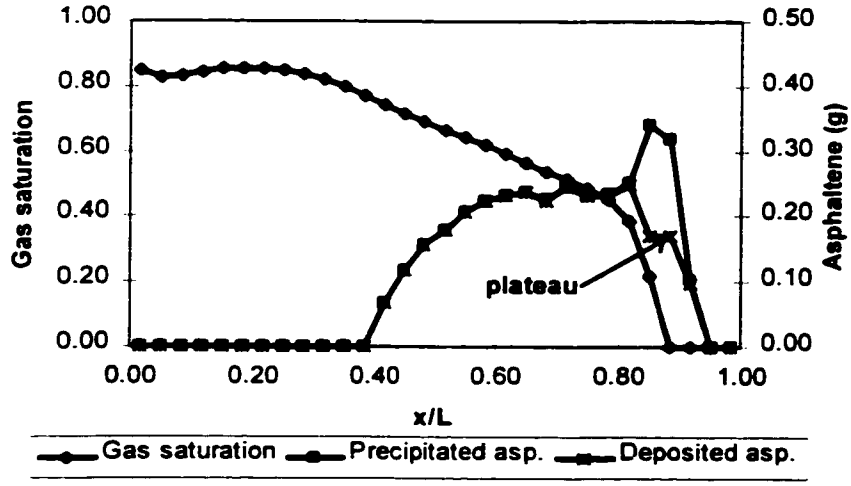

Figure 8.3: Gas saturation and asphaltene profiles at 0.7 PV injected

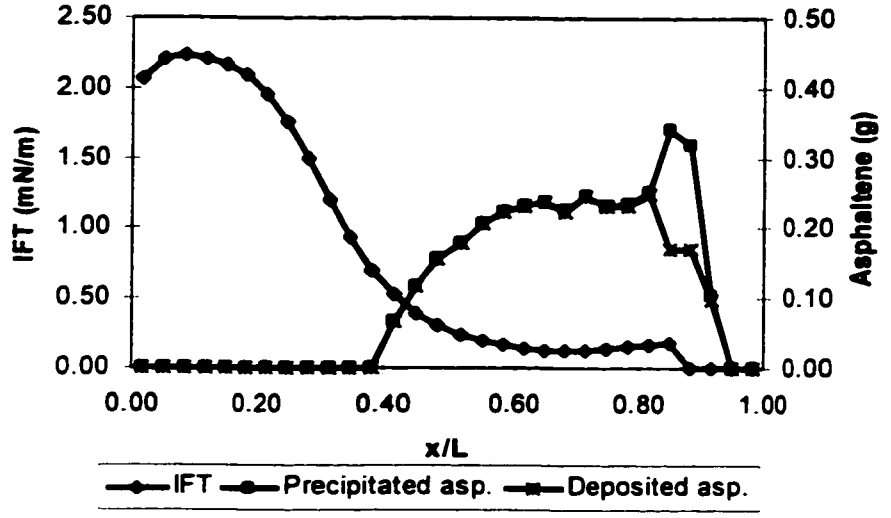

Figure 8.4: IFT and asphaltene profiles at 0.7 PV injected

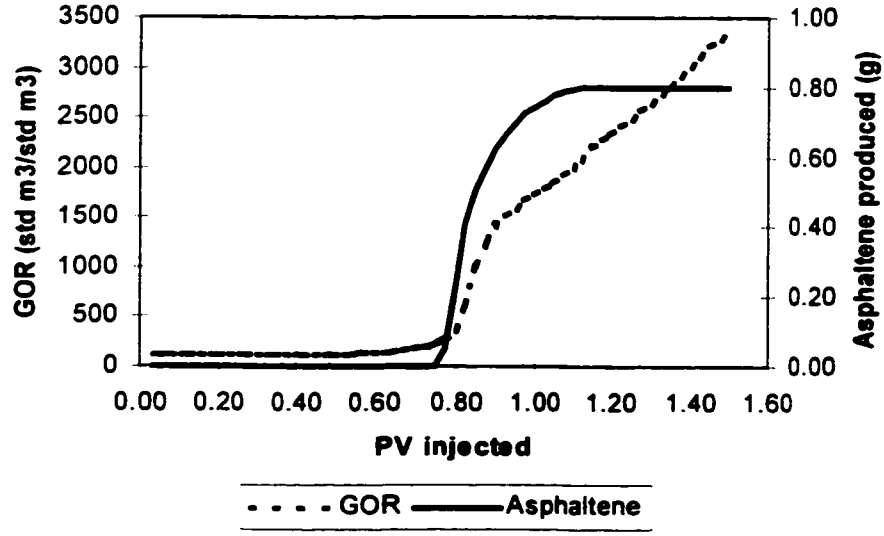

Figure 8.5: Produced GOR and asphaltene for core displacement

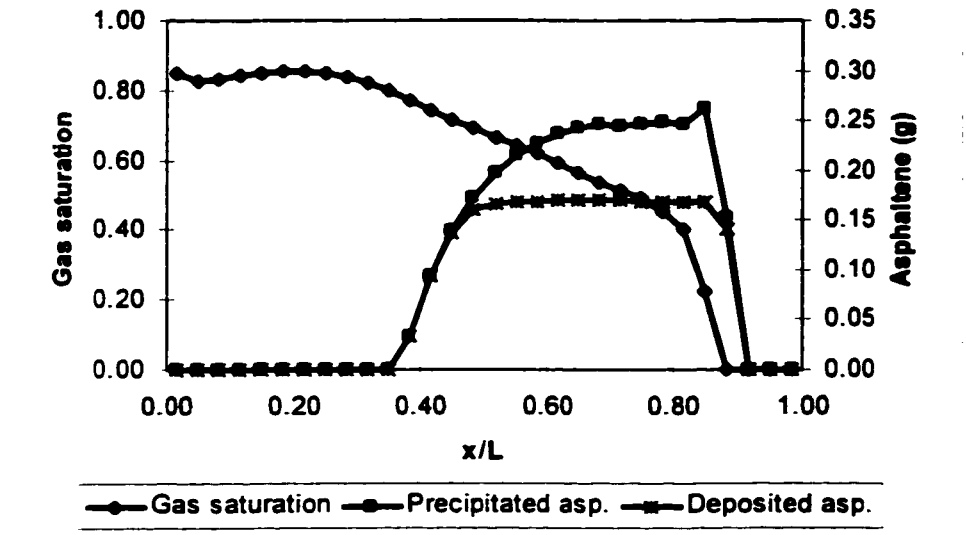

Figure 8.6: Gas saturation and asphaltene profiles at 0.7 PV injected with adsorption and without mechanical entrapment

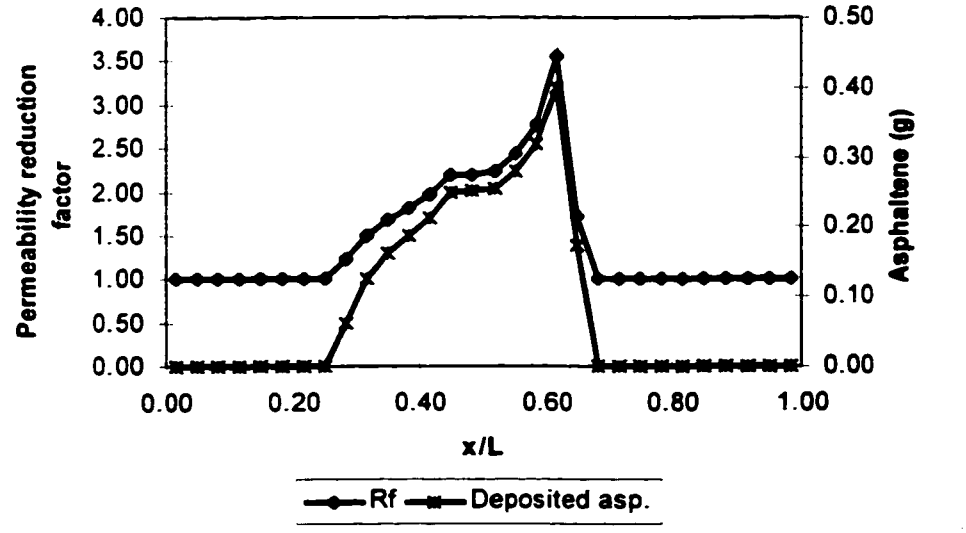

Figure 8.7: Permeability reduction factor and asphaltene profiles at 0.5 PV injected for a = 90 and b = 60

- The permeability reduction factor calculated with a = 3 and b= 2 in Equation (6.25) is very close to unity (i.e. very little permeability reduction). These values correspond to those in the Kozeny-Carman equation (3.3). To obtain permeability reduction factor in the order of 3.0, typical values of a and b are 90 and 60 respectively. The derivation of the Kozeny-Carman equation was based on an idealized representation of the porous media as a bundle of capillary tubes (Bear, 1972, pp. 165-166), which may be very different that the actual pore geometry and connectivity of the reservoir. Therefore large variations in a and b may be necessary to obtain the proper permeability reduction factor. Figure 8.7 shows the profile of asphaltene deposited and permeability reduction factor R_f at 0.5 PV injected for a = 90 and b = 60. The profile of R_f is very similar to the profile of the deposited asphaltene. This suggests that a linear relationship between R_f and the amount of deposited asphaltene as in Equation (6.20) would yield similar results.

8.3 Single-Well Depletion Simulation

To illustrate the asphaltene precipitation and plugging effect in a primary depletion process, a two-dimensional radial simulation was performed. The relevant data are shown in Table 8.2. Equation (6.20) was used for the permeability reduction. Four simulation runs were made with different values of $R_{f,max}$ (1, 2, 7, and 10). Figure 8.8 depicts the BHP behaviour for different values of $R_{f,max}$. Increasing $R_{f,max}$ increases the plugging, and the BHP reaches the minimum value sooner. Figures 8.9 and 8.10 shows the pressure profiles after two years of production for $R_{f,max}$ of 1 and 10 respectively. The profiles illustrate the effect of permeability impairment caused by plugging. The permeability impairment is sufficient to change the nature of the profiles, from primarily a gravity-dominated system to essentially a viscous-dominated (vertically uniform pressure) system.

8.4 Summary

This chapter presents simulation runs on a gas injection process and a pressure depletion process. The simulation results agree qualitatively with important field and laboratory observations related to asphaltene precipitation.

This dissertation is the first work to make the solid model functional through the characterization of the heaviest fraction of the oil, and to integrate it subsequently into a compositional simulator together with the additional modelling of adsorption, mechanical entrapment and plugging.

The success of the use of the solid model for the precipitate allows an effective implementation of asphaltene precipitation behavior modelling in a compositional simulator. Any other more complicated models or any models that do not use the EOS components such as activity-coefficients models would create many conceptual and computational difficulties.

Table 8.2
Reservoir data for single-well depletion case

Horizontal permeability	30 md
Vertical permeability	15 md
Porosity	20 %
Reservoir Thickness	40 m (131.2 ft)
Radial extent	289 m (948.2 ft)
Gas in recombined oil	61 mole %
Average initial pressure	41,910 kPa (6,078.5 psia)
Saturation pressure	24,500 kPa (3553.4 psia)
Temperature	92 °C (197.6 °F)
Oil production rate	120 std m^3/D (754.8 STB/D)
No. of gridblocks	7 x 8
Rock density	2650 kg/m^3
$w_{sa,max}$	0.1 mg/g of rock
$R_{f,max}$	1, 2, 7, 10
Minimum BHP	700 kPa (101.5 psia)

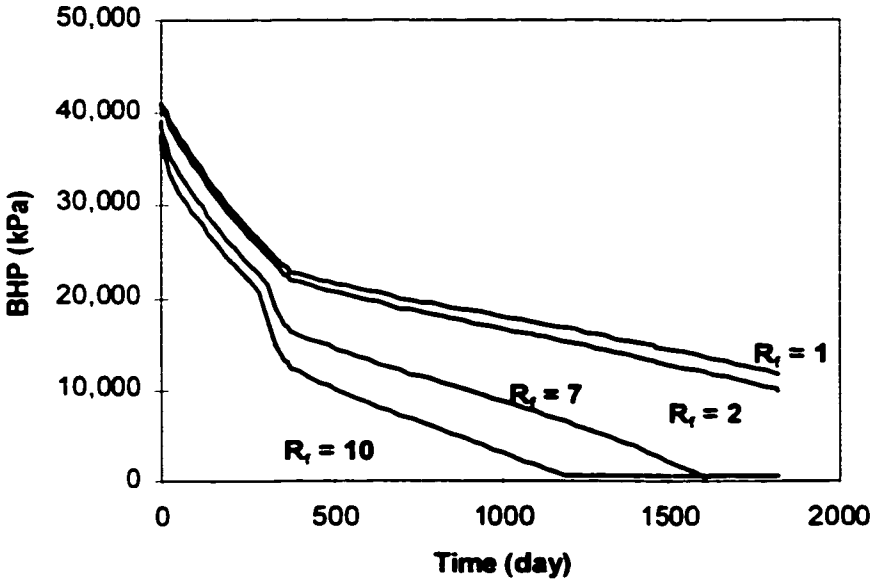

Figure 8.8: Effect of $R_{f,max}$ on BHP

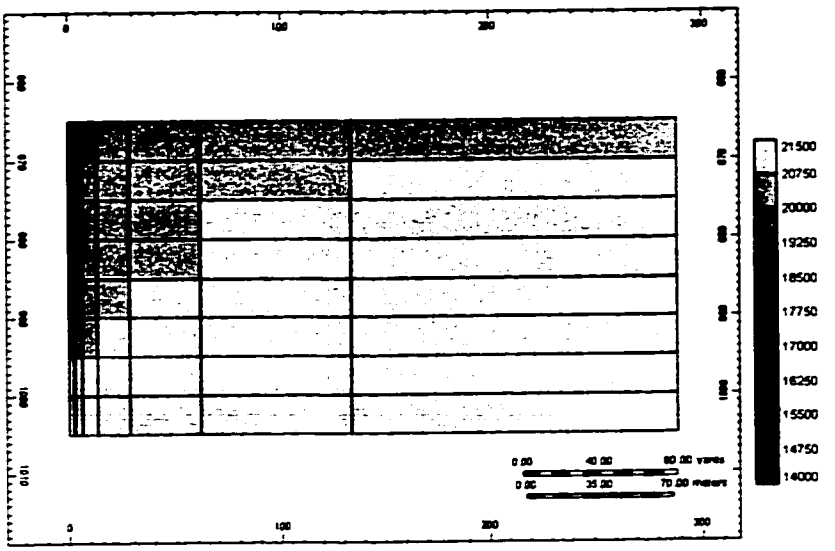

Figure 8.9: Pressure profile (in kPa) for $R_{f,max} = 1$

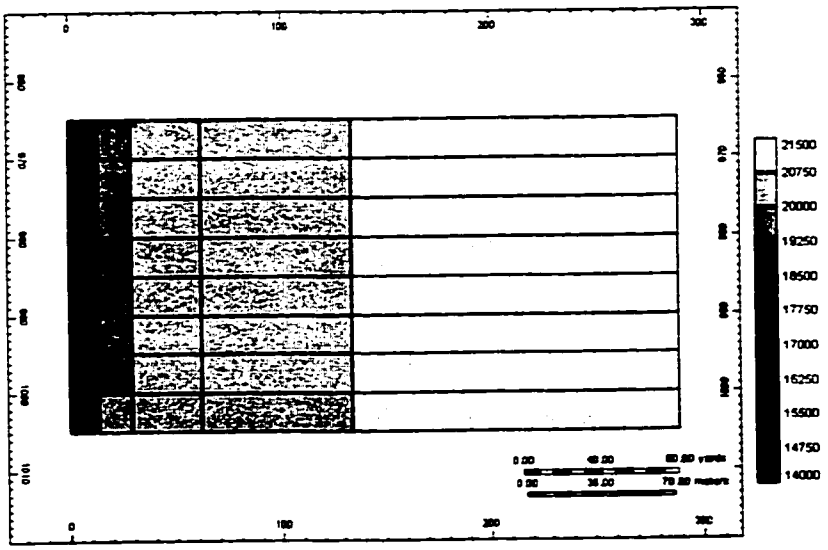

Figure 8.10: Pressure profile (in kPa) for $R_{f,max} = 10$

9. CONCLUSIONS

This dissertation addresses both the modelling of the phase behaviour of asphaltene precipitation and the modelling of the dynamic aspects of asphaltene precipitation in reservoirs. The following conclusions can be drawn from the work performed and the results obtained:

- It is shown that the solid model provides an effective thermodynamic approach for modelling asphaltene precipitation phase behaviour. The key to the success is the split of the heaviest component into a non-precipitating and precipitating component together with a proper selection of interaction coefficients and volume shift parameters. Good matches of laboratory precipitation data related to a gas injection process, a pressure depletion process, and of a North Sea APE were obtained with the model. A robust three-phase oil/gas/solid flash-calculation algorithm is also described.
- The thermodynamic model for asphaltene precipitation has been successfully incorporated in a compositional simulator together with the equations for multiphase multicomponent flow, the equations for solid deposition and entrapment, and the equations for permeability reduction. Numerical techniques for solving all these equations simultaneously are described.
- Simulation of a gas injection process and a primary depletion process shows results that agree with field observations: asphaltene precipitation in producers at gas breakthrough, precipitation in the low IFT region, plugging of wellbore.
- The combined modelling of the phase behaviour and dynamics of asphaltene precipitation provides insights into asphaltene deposition phenomena that would assist engineers in applying appropriate strategies to optimize recovery. Such strategies may involve changing the injected gas composition, operating pressures, well rates to minimize the negative impact of asphaltene deposition. This is particularly important in offshore developments with subsea wells, as the cleaning of plugged wells is very expensive.

10. RECOMMENDATIONS FOR FURTHER STUDIES

Based on the work performed and the results obtained, the following recommendations are offered:

- The solid model should be tested for non isothermal conditions. A matching of an experimental pressure-temperature APE is desirable. Studies of the sensitivity of the model with respect to changes in the heat capacity of fusion, ΔC_{pf}, and melting-point enthalpy of fusion, ΔH_f, are also recommended.
- It is important that laboratory core displacements of gas injection processes that involve in situ asphaltene precipitation be performed to obtain data for asphaltene deposition and plugging. The asphaltene dynamics models proposed in this dissertation could then be used to match these data.
- The effects of asphaltene deposition on wettability alteration (Section 3.4), and the effect of wettability changes on displacement processes should be modelled and incorporated in a compositional simulator. As the formation wettability changes from water-wet to oil-wet upon asphaltene deposition, the effect of asphaltene deposition on WAG processes could be significant.

11. REFERENCES

Acs, G., Doleschal, S. and Farkas, E.: "General Purpose Compositional Model," *Soc. Petrol. Eng. J.* (August 1985) 727-742.

Ali, M.A. and Islam, M.R.: "The Effect of Asphaltene Precipitation on Carbonate-Rock Permeability: An Experimental and Numerical Approach," *SPE Production & Facilities*, Vol. 13 (August 1998) 178-183.

Andersen, S.I. and Speight, J.G.: "Thermodynamic Models for Asphaltene Solubility and Precipitation," *J. Petroleum Science and Engineering*, Vol. 22 (1999) 53-66.

Bear, J.: *Dynamics of Fluids in Porous Media*, American Elsevier, New York, 1972.

Behie, A., Collins, D., Forsyth Jr., P.A., and Sammon, P.H.: "Fully Coupled Multiblock Wells in Oil Simulation," ," *Soc. Petrol. Eng. J.* (August 1985) 535-542.

Broyden, C.G.: "A Class of Method for Solving Nonlinear Simultaneous Equations," *Math. Comp.*, Vol. 19 (1965) 577-593.

Bryant, D.W. and Monger, T.G.: "Multiple-Contact Phase Behavior Measurement and Application With Mixtures of CO_2 and Highly Asphaltic Crude," *SPE Reservoir Engineering*, Vol. 3 (May 1988) 701-710.

Buckley, J.S., Liu, Y., Xie, X. and Morrow, N.R.: "Asphaltenes and Crude Oil Wetting – The Effect of Oil Composition," ," *Soc. Petrol. Eng. J.* (June 1997) 107-119.

Burke, N.E., Hobbs, R.E. and Kashou, S.F.: "Measurement and Modeling of Asphaltene Precipitation," *J. Petrol. Technol.* (November 1990) 1440-1456.

Butler, R.M. and Mokrys, I.J.: "Recovery of Heavy Oils Using Vapourized Hydrocarbon Solvents: Further Development of the Vapex Process," *J. Can. Petrol. Technol.*, Vol. 32 (June 1993) 56-62.

Cavett, R.H.: "Physical Data for Distillation Calculations – Vapor/Liquid Equilibrium," *Proceedings* 27th Annual Meeting, API, 1962, Dallas, Texas.

Chaback, J.J.: "Discussion of Measurement and Modeling of Asphaltene Precipitation," *J. Petrol. Technol.*, Vol. 43 (December 1991) 1519-1520.

Chang, F.F. and Civan, F.: "Practical Model for Chemically Induced Formation Damage," *J. Petroleum Science and Engineering*, Vol. 17 (1997) 123-137.

Chien, M.C.H., Lee, S.T. and Chen, W.H.: "A New Fully Implicit Compositional Simulator," Paper SPE 13385, *Proceedings* SPE Reservoir Simulation Symposium, Dallas, Texas, February 10-13, 1985.

Chueh, P.L. and Prausnitz, J.M.: "Vapor-Liquid Equilibria at High Pressures: Calculation of Partial Molar Volumes in Nonpolar Liquid Mixtures," *AIChE J.*, Vol. 13 (November 1967) 1099-1107.

Chung, T.-H.: "Thermodynamic Modeling for Organic Solid Precipitation," Paper SPE 24851, *Proceedings* 67th Annual Technical Conference and Exhibition, Washington, DC, October 4-7, 1992.

Civan, F.: "Evaluation and Comparison of the Formation Damage Models," Paper SPE 23787, *Proceedings* International Symposium on Formation Damage Control, Lafayette, Louisiana, February 26-27, 1992.

Civan, F.: "A Muti-Purpose Formation Damage Model," Paper SPE 31101, *Proceedings* Formation Damage Control Symposium, Lafayette, Louisiana, 14-15 February 1996.

Clementz, D.M.: "Alteration of Rock Properties by Adsorption of Petroleum Heavy Ends: Implications for Enhanced Oil Recovery," Paper SPE/DOE 10683, *Proceedings* 1982 SPE/DOE Third Joint Symposium on Enhanced Oil Recovery, Tulsa, Oklahoma, April 4-7, 1982.

Coats, K.H.: "An Equation of State Compositional Model," *Soc. Petrol. Eng. J.* (October 1980) 363-386.

Collins, D.A., Nghiem, L.X., Li, Y.-K. and Grabenstetter, J.E.: "An Efficient Approach to Adaptive-Implicit Compositional Simulation With an Equation of State," *SPE Reservoir Engineering* (May 1992) 259-264.

Collins, S.H. and Melrose, J.C.: "Adsorption of Asphaltenes and Water on Reservoir Rock Minerals," Paper SPE 11800, *Proceedings* International Symposium on Oilfield and Geothermal Chemistry, Denver, Colorado, June 1-3, 1983.

Crocker, M.E. and Marchin, L.M.: "Wettability and Adsorption Characteristics of Crude-Oil Asphaltene and Polar Fractions," *J. Petrol. Technol.* (April 1988) 470-474.

Danesh, A.: *PVT and Phase Behaviour of Petroleum Reservoir Fluids*, Elsevier, Amsterdam, The Netherlands, 1998.

de Boer R.B., Leerlooyer, K., Eigner, M.R.P. and van Bergen, A.R.D.: "Screening of Crude Oils for Asphalt Precipitation: Theory, Practice, and the Selection of Inhibitors," *SPE Production & Facilities*, Vol. 10 (February 1995) 55-61.

Dubey, S.T. and Waxman, M.H.: "Asphaltene Adsorption and Deposition From Mineral Surfaces," *SPE Reservoir Engineering*, Vol. 6 (August 1991) 389-395.

Escobedo, J. and Mansoori, G.A.: "Viscometric Determination of the Onset of Asphaltene Flocculation: A Novel Method" *SPE Production & Facilities*, Vol. 10 (May 1995), 115-118.

Firoozabadi, A: *Thermodynamics of Hydrocarbon Reservoirs*, McGraw-Hill, New York, 1999.

González, G. and Travalloni-Louvisse, A.M.: "Adsorption of Asphaltenes and Its Effect on Oil Production," *SPE Production & Facilities* (May 1973) 91-96.

Grabenstetter, J., Li, Y.-K., Collins, D. and Nghiem, L., "Stability-Based Switching Criterion for Adaptive-Implicit Compositional Reservoir Simulation," Paper SPE 21225, *Proceedings* SPE Symposium on Reservoir Simulation, Anaheim, California, February 17-20, 1991.

Gruesbeck, C. and Collins, R.E.: "Entrainment and Deposition of Fine Particles in Porous Media," *Soc. Petrol. Eng. J.* (December 1982) 847-856.

Gupta, A.K.: *A Model for Asphaltene Flocculation Using an Equation of State*, M.Sc. Thesis, Department of Chemical and Petroleum Engineering, The University of Calgary, June 1986.

Hammani, A. and Raines, M.: "Paraffin Deposition From Crude Oils: Comparison of Laboratory Results to Field Data," *Soc. Petrol. Eng. J.*, Vol. 4 (March 1999) 9-18.

Hammami, A., Phelps, C.H., Monger-McClure, T., and Little, T.M.: "Asphaltene Precipitation from Live Oils: An Experimental Investigation of the Onset Conditions and Reversibility," *Proceedings* AIChE 1999 Spring National Meeting, Houston, Texas, March 14-18.

Heidemann, R.A.: "Computation of High Pressure Phase Equilibria," *Fluid Phase Equilibria*, Vol. 14 (1983) 55-78.

Hirschberg, A., deJong, L.N.J., Schipper, B.A. and Meijer, J.G.: "Influence of Temperature and Pressure on Asphaltene Flocculation," *Soc. Petrol. Eng. J.* (June 1984) 283-293.

Huang, E.T.S. and Holm, L.W.: "Effect of WAG Injection and Rock Wettability on Oil Recovery During Carbon Dioxide Flooding," *SPE Reservoir Engineering* (February 1988), 119-129.

Jhaveri, B.S. and Youngren, G.K.: "Three-Parameter Modification to the Peng-Robinson Equation of State to Improve Volumetric Predictions," *SPE Reservoir Engineering*, Vol. 3 (August 1988) 1033-1040.

Katz, D.L. and Firoozabadi, A.: "Predicting Phase Behavior of Condensate/Crude-Oil Systems Using Methane Interaction Coefficients," *J. Petrol. Technol.*, Vol. 30 (November 1978) 1649-1655.

Kamath, V.A., Yang, J. and Sharma, G.D.: "Effect of Asphaltene Deposition on Dynamic Displacements of Oil by Water," Paper SPE 26046, *Proceedings* 1993 SPE Western Regional Meeting, Anchorage, Alaska, May 26-28.

Kawanaka, S., Park, S.J. and Mansoori, G.A.: "Organic Deposition From Reservoir Fluids: A Thermodynamic Predictive Technique," *SPE Reservoir Engineering*, Vol. 6 (May 1991) 185-192.

Kesler, M.G. and Lee, B.I.: "Improved Predictions of Enthalpy of Fractions," *Hydrocarbon Processing*, Vol. 55 (1977) 153-158.

Kokal, S.L., Najman, J., Sayegh, S.G. and George, A.E.: "Measurement and Correlation of Asphaltene Precipitation From Heavy Oils by Gas Injection," *J. Can. Petrol. Technol.*, Vol. 31 (April 1992) 24-30.

Kumar, T. and Todd, A.C.: "A New Approach for Mathematical Modelling of Formation Damage to Invasion of Solid Suspensions," Paper SPE 18203, *Proceedings* 63rd Annual Technical Conference and Exhibition, Houston, Texas, October 2-5, 1988.

Lake, L.W.: *Enhanced Oil Recovery*, Prentice Hall, Englewood Cliffs, New Jersey, 1989.

Lee, B.I. and Kesler, M.G.: "A Generalized Thermodynamic Correlation Based on Three-Parameter Corresponding States," *AIChE J.*, Vol. 21 (May 1975) 510-526.

Leontaritis, K.J.: "The Asphaltene and Wax Deposition Envelopes," *Fuel Science and Technology Int'l*, Vol. 14 (1996) 13-19.

Leontaritis, K.J., Amaefule, J.O. and Charles, R.E.: "A Systematic Approach for the Prevention and Treatment of Formation Damage Caused by Asphaltene Deposition," *SPE Production & Facilities* (August 1994) 157-164.

Leontaritis, K.J. and Mansoori, G.A: "Asphaltene Flocculation During Oil Production and Processing: A Thermodynamic Colloidal Model," Paper SPE 16258, *Proceedings* SPE International Symposium on Oil Field Chemistry, San Antonio, Texas, February 4-6, 1987.

Leontaritis, K.J. and Mansoori, G.A.: "Asphaltene Deposition: A Survey of Field Experiences and Research Approaches," *J. Petroleum Science and Engineering*, Vol. 1 (1988) 229-239.

Li, Y.-K., Nghiem, L.X. and Siu, A.: "Phase Behaviour Computations for Reservoir Fluids: Effect of Pseudo Components on Phase Diagrams and Simulation Results," *J. Can. Petrol. Technol.*, Vol. 24 (November-December 1985) 29-36.

Lin, E.C. and Huang, E.T.S.: "The Effect of Rock Wettability on Water Blocking During Miscible Displacement," *SPE Reservoir Engineering* (May 1990), 205-212.

MacMillan, D.J., Tackett, J.E. Jr., Jessee, M.A. and Monger-McClure, T.G.: "A Unified Approach to Asphaltene Precipitation: Laboratory Measurement and Modeling," *J. Petrol. Technol.* (September 1995) 788-793.

McCain, Jr. W.D.: *The Properties of Petroleum Fluids*, Second Edition, PennWell Publishing Company, Tulsa, Oklahoma (1990).

Mattax, C.C. and Dalton, R.L.: *Reservoir Simulation*, SPE Monograph, Society of Petroleum Engineers, Dallas, Texas, 1990, 133-139.

Mehra, R.K.: *The Computation of Multi-Phase Equilibrium in Compositional Reservoir Studies*, Ph.D. dissertation, The University of Calgary, 1981.

Michelsen, M.L.: "The Isothermal Flash Problem. I. Stability," *Fluid Phase Equilibria*, Vol. 9 (1982a) 1-19.

Michelsen, M.L.: "The Isothermal Flash Problem. II. Phase Split Calculation," *Fluid Phase Equilibria*, Vol. 9 (1982b) 21-40.

Minssieux, L.: "Core Damage From Crude Asphaltene Deposition," Paper SPE 37250, *Proceedings* SPE International Symposium on Oilfield Chemistry, Houston, Texas, 18-21 February 1997.

Monger, T.G. and Trujillo, D.E.: "Organic Deposition During CO_2 and Rich-Gas Flooding," *SPE Reservoir Engineering* (February 1991) 17-24.

Montel, F. and Gouel, P.: "A New Lumping Scheme of Analytical Data for Compositional Studies," Paper SPE 13119, *Proceedings* 59th SPE Annual Technical Conference and Exhibition, Houston, Texas, September 16-19, 1984.

Morrow, N.: "Wettability and Its Effect on Oil Recovery," *J. Petrol. Technol.* (December 1990) 1476-1484.

Nagel, R.G., Hunter, B.E., Peggs, J.K., Fong, D.K. and Mazzocchi, E.: "Tertiary Application of a Hydrocarbon Miscible Flood: Rainbow Keg River "B" Pool", *SPE Reservoir Engineering* (August 1990) 301-308.

Nghiem, L.X.: "A New Approach to Quasi-Newton Methods With Application to Compositional Modeling," *Proceedings* Seventh SPE Reservoir Simulation Symposium, San Francisco, California, November 16-18, 1983.

Nghiem, L.X. and Li, Y.-K.: "Computation of Multiphase Equilibrium Phenomena With an Equation of State," *Fluid Phase Equilibria*, Vol. 17 (1984) 77-95.

Nghiem, L.X.: "An Integral Approach to Discretizing the Reservoir Flow Equations," *SPE Reservoir Engineering*, Vol. 3 (May 1988) 685-690.

Nghiem, L., and Rozon, B.: "A Unified and Flexible Approach for Handling and Solving Large Systems of Equations in Reservoir Simulation," *Proceedings* First and Second International Forum on Reservoir Simulation, Alpbach, Austria, September 1988 and 1989.

Novosad, Z. and Costain, T.G.: "Experimental and Modeling Studies of Asphaltene Equilibria For a Reservoir Under CO_2 Injection," Paper SPE 20530, *Proceedings* 1990 SPE Annual Technical Conference and Exhibition, New Orleans, Louisiana, September 23-26, 1990.

Nutakki, R., Hamoodi, A.N., Li, Y.-K. and Nghiem, L.X.: "Experimental Analysis, Modelling, and Interpretation of Recovery Mechanisms in Enriched-Gas Processes," Paper SPE 22634, *Proceedings* SPE Annual Technical Conference and Exhibition, Dallas, Texas, October 6-9, 1991.

Oellrich, L., Plocker, U., Prausnitz, J.M. and Knapp, H.: "Equation-of State Methods for Computing Phase Equilibria and Enthalpies," *Int. Chem. Eng.*, Vol. 21 (January 1981) 1-15.

Pan, H. and Firoozabadi, A.: "A Thermodynamic Micellization Model for Asphaltene Aggregation and Precipitation in Petroleum Fluids," *SPE Production & Facilities*, Vol. 13 (May 1998) 118-127.

Pedersen, K.S., Thomassen, P. and Fredenslund, Aa.: "Thermodynamics of Petroleum Mixtures Containing Heavy Hydrocarbons," 1. Phase Envelope Calculations by Use of the Soave-Redlich-Kwong Equation of State," *Ind. Eng. Chem. Process Des. Dev.*, Vol. 23 (1984) 163-170.

Pedersen, K.S., Fredenslund, Aa. and Thomassen, P: *Properties of Oils and Natural Gases*, Gulf Publishing Company, Houston, Texas (1989).

Penéloux, A., Rauzy, E. and Frèze, R.: "A Consistent Correction For Redlich-Kwong-Soave Volumes," *Fluid Phase Equilibria*, Vol. 8 (1982) 7-23.

Peng, D.-Y. and Robinson, D.B.: "A New Two-Constant Equation of State," *Ind. Eng. Chem. Fundam.*, Vol. 15 (1976) 59-64.

Piro, G., Canonico, L.B., Galbariggi, G., Bertero, L. and Carniani, C.: "Asphaltene Adsorption Onto Formation Rock: An Approach to Asphaltene Formation Damage Prevention," *SPE Production & Facilities*, Vol. 11 (August 1996) 156-160.

Pittaway, K.R., Albright, J.C., Hoover, J.W. and Moore, J.S.: "The Maljamar CO_2 Pilot: Review and Results," *J. Petrol. Technol.* (October 1987) 1256-1260.

Prausnitz, J.M., Lichtenthaler, R.N. and de Azevedo, E.G.: *Molecular Thermodynamics of Fluid-Phase Equilibria*, Second Edition, Prentice-Hall, Englewood Cliffs, New Jersey (1986) 306-316.

Reid, R.C., Prausnitz, J.M. and Sherwood, T.K.: *The Properties of Gases and Liquids*, Third Edition, McGraw-Hill, New York, 1977.

Riazi, M.R. and Daubert, T.E.: "Simplified Property Predictions," *Hydrocarbon Processing*, Vol. 59 (1980) 115-116.

Saad, Y. and Schultz, M.H.: "GMRES: A Generalized Minimal Residual Algorithm for Solving Nonsymmetric Linear Systems," *SIAM J. Sci. Stat. Comp.*, Vol 7 (1986) 856-869.

Shiralkar, G.S., Stephenson, R.E., Joubert, W., Lubeck, O. and van Bloemen Waanders, B.: "Falcon: A Production Quality Distributed Memory Reservoir Simulator," Paper SPE 37975, *Proceedings* SPE Reservoir Simulation Symposium, Dallas, Texas, June 8-11, 1997.

Sivaraman, A., Thomas, F.B. and Bennion, D.B.: "Advanced Acoustic Approach for Reservoir Solids Problems/Effects of Inhibitors on Solids Onset and EOS Modeling," Paper 99-64, *Proceedings* CSPG and Petroleum Society Joint Convention, Calgary, Alberta, June 14-18, 1999.

Soave, G.: "Equilibrium Constants from a Modified Redlich-Kwong Equation of State," *Chem. Eng. Sci.*, Vol. 27 (1972) 1197-1203.

Srivastava, R.K., Huang, S.S., Dyer, S.B. and Mourits, F.M.: "Quantification of Asphaltene Flocculation During Miscible CO_2 Flooding in the Weyburn Reservoir," *J. Can. Petrol Technol.*, Vol. 34 (October 1995) 31-42.

Thomas, F.B., Bennion, D.B., Bennion, D.W. and Hunter, B.E.: "Experimental and Theoretical Studies of Solids Precipitation From Reservoir Fluid," *J. Can. Petrol. Technol.*, Vol. 31 (January 1992) 22-31.

Turta, A.T., Najman, J., Singhal, A., Leggitt, S. and Fisher, D.: "Permeability Impairment due to Asphaltenes During Gas Miscible Flooding and Its Mitigation," Paper SPE 37287, *Proceedings* International Symposium on Oilfield Chemistry, Houston, Texas, 18-21 February, 1997.

Turta, A., Najman, J., Fisher D. and Singhal, A.: "Viscometric Determination of the Onset of Asphaltene Flocculation," Paper 97-81, *Proceedings* 48th Annual Meeting of the Petroleum Society of CIM, Calgary, Alberta, June 8-11, 1997.

Twu, C.H.: "An Internally Consistent Correlation for Predicting the Critical Properties and Molecular Weights of Petroleum and Coal-Tar Liquids," *Fluid Phase Equilibria*, Vol. 16 (1984) 137-150.

Wang, P., Balay S., Sepehrnoori, K., Wheeler, J., Abate J., Smith B., Pope, G.A.: "A Fully Implicit Parallel EOS Compositional Simulator for Large Scale Reservoir Simulation," Paper SPE 51885, *Proceedings* SPE Reservoir Simulation Symposium, Houston, Texas, 14-17 February 1999.

Watts, J.W.: "A Compositional Formulation of the Pressure and Saturation Equations," *SPE Reservoir Engineering* (May 1986) 243-252.

Whitson, C.H.: "Characterizing Hydrocarbon Plus Fractions," *Soc. Petrol. Eng. J.*, Vol. 23 (August 1983) 683-694.

Whitson, C.H.: "Effect of C_{7+} Properties on Equation-of-State Predictions," *Soc. Petrol. Eng. J.*, Vol. 24 (December 1984) 685-696.

Won, K.W.: "Thermodynamics for Solid-Liquid-Vapor Equilibria: Wax Phase Formation From Heavy Hydrocarbon Mixtures," *Fluid Phase Equilibria*, Vol. 30 (1986) 265-279.

Yeh, S.W., Ehrlich, R. and Emanuel, A.S.: "Miscible-Gasflood-Induced Wettability Alteration: Experimental Observations and Oil Recovery Implications," *SPE Formation Evaluation* (June 1992), 167-172.

Young, L.C. and Stephenson, R.E.: "A Generalized Compositional Approach for Reservoir Simulation," *Soc. Petrol. Eng. J.*, Vol. 23 (October 1983) 727-742.

APPENDIX A: CUBIC EQUATIONS OF STATE

A.1 General Cubic Equations of State

Cubic EOS's have received wide acceptance in the industry because of their simplicity ant their ability to predict accurately the phase behavior of oil/gas systems. There are many EOS's available in the literature (Danesh, 1998); most of them can be represented by the equation:

$$p = \frac{R\,T}{v-b} - \frac{a}{(v+\delta_1\,b)\,(v+\delta_2\,b)} \tag{A.1}$$

where a is the attraction parameter, b is the repulsion parameter. For mixtures, the parameters a and b are given by the mixing rules:

$$a = \sum_{i=1}^{n_c}\sum_{k=1}^{n_c} y_i\,y_k\,a_{ik} \tag{A.2}$$

$$b = \sum_{i=1}^{n_c} y_i\,b_i \tag{A.3}$$

The values a_{ik} are obtained from:

$$a_{ik} = \sqrt{a_i}\,\sqrt{a_k}\,(1-d_{ik}) \tag{A.4}$$

where d_{ik} are interaction coefficients between components i and k. The pure component a_{ii} and b_i are expressed in terms of the critical properties p_c and T_c, and the acentric factor ω:

$$a_{ii} = \frac{\Omega_a\,R^2\,T_{ci}^2}{p_{ci}}\left[1+m_i\left(1-\sqrt{\frac{T}{T_{ci}}}\right)\right]^2 \tag{A.5}$$

$$b_i = \frac{\Omega_b\,R\,T_{ci}}{p_{ci}} \tag{A.6}$$

where the constants Ω_a and Ω_b are determined from the critical conditions of the pure component.

For the Peng-Robinson (PR) (Peng and Robinson, 1976) and the Soave-Redlich-Kwong (SRK) (Soave, 1972) EOS, the constants are:

EOS	δ_1	δ_2	Ω_a	Ω_b	m_i
SRK	1	0	0.42748	0.08664	$0.480 + 1.574\ \omega_i - 0.176\ \omega_i^2$
PR	$1 + \sqrt{2}$	$1 - \sqrt{2}$	0.45724	0.07780	$0.37464 + 1.54226\ \omega_i - 0.26992\ \omega_i^2$

The interaction coefficients between hydrocarbon and hydrocarbon components are calculated from:

$$d_{ij} = \left(\frac{2\, v_{ci}^{1/6}\, v_{cj}^{1/6}}{v_{ci}^{1/3} + v_{cj}^{1/3}} \right)^e \tag{A.7}$$

where v_{ci} is the critical volume of component i, and e is an adjustable parameter. A value of e = 1.2 was shown to give a good match of the paraffin-paraffin interaction coefficients of Oellrich et al. (1981). The interaction coefficients between hydrocarbon and non-hydrocarbon components entered by the users.

The EOS can be expressed as a cubic equation in terms of the compressibility factor Z ≡ pv/RT as follows:

$$\begin{aligned} &Z^3 - (\delta_1\delta_2 B + 1)Z^2 + \left[A - (\delta_1 + \delta_2)B - (1 - 2\delta_1\delta_2)B^2\right]Z \\ &- \left[AB + \delta_1\delta_2\left(B^3 + B^2\right)\right] = 0 \end{aligned} \tag{A.8}$$

where

$$A \equiv \frac{ap}{(RT)^2} \tag{A.9}$$

$$B \equiv \frac{bp}{RT} \tag{A.10}$$

A.2 Fugacities

The molar Gibbs free energy of a homogeneous mixture of n_c components at a pressure p and temperature T is given by

$$G = RT\sum_{i=1}^{n_c} y_i \ln f_i + G_0(p,T) \tag{A.11}$$

where

f_i = fugacity of component i

G = Gibbs molar free energy

G_0 = reference Gibbs free energy

R = universal gas constant

y_i = mole fraction of component i

It is common to work with the dimensionless Gibbs free energy defined as:

$$G^* = \frac{G}{RT} = \sum_{i=1}^{n_c} y_i \ln f_i + G_0^*(p,T) \tag{A.12}$$

The fugacity f_i can be calculated from an EOS with the following integral:

$$\ln \varphi_i = \frac{1}{RT}\int\left[\left(\frac{\partial p}{\partial N_i}\right)_{T,v,N_k} - \frac{RT}{v}\right]dv - \ln Z \tag{A.13}$$

$$\varphi_i = \frac{f_i}{y_i\, p} \tag{A.14}$$

where φ_i is the fugacity coefficient of component i. The SRK and PR EOS gives the following expression for the fugacity coefficient:

$$\ln \varphi_i = \frac{b_i}{b}(Z-1) - \ln(Z-B) - \frac{1}{\delta_1-\delta_2}\frac{A}{B}\left(\frac{2\sum_{k=1}^{n_c} y_i\, a_{ik}}{a} - \frac{b_i}{b}\right)\ln\left(\frac{Z+\delta_2 B}{Z+\delta_1 B}\right) \tag{A.15}$$

The cubic equation (A.8) has either one or three real roots for the compressibility factor Z. When the equation has three real roots, the intermediate root is discarded and the root that yields the lowest Gibbs free energy among the remaining two is selected. Let Z_a and Z_b be these two real roots with respective dimensionless Gibbs free energy G_a^* and G_b^*. It can easily be shown from Equations (A.12), (A.14) and (A.15) that

$$G_a^* - G_b^* = \ln\left(\frac{Z_b - B}{Z_a - B}\right) + \frac{1}{\delta_2 - \delta_1}\frac{A}{B}\ln\left(\frac{Z_b + \delta_2 B}{Z_a + \delta_2 B}\cdot\frac{Z_b + \delta_1 B}{Z_a + \delta_1 B}\right) - (Z_b - Z_a) \qquad (A.16)$$

If $G_a^* - G_b^* > 0$, Z_b is selected to be the compressibility factor Z for the mixture. Otherwise, Z_a is selected.

A.3 Volume Shifts

The above EOS provides good predictions of phase equilibrium conditions. However, volumetric predictions, especially for liquids, are known not to be as accurate. Penéloux et al. (1982) and Jhaveri and Youngren (1988) discussed the use of volume shift parameters to improve volume and density predictions. The corrected volume for phase k is given by:

$$v_k^s = v_k - \sum_{i=1}^{n_c} y_{ik}\, s_i\, b_i \qquad (A.17)$$

where

b_i = repulsion parameter for component i given in Equation (4.3)

s_i = volume shift parameter for component i

v_k = molar volume for phase k from EOS

v_k^s = corrected molar volume for phase k

With the volume shifts, the fugacity coefficients become:

$$\ln \varphi_{ik}^s = \ln \varphi_{ik} - \frac{s_i\, p}{R\, T} \qquad (A.18)$$

where φ_{ik}^s is the fugacity coefficient for component i in phase k when volume shifts are used. For oil-gas equilibrium calculations where both the oil and gas phases are calculated with the EOS, the volume shift coefficients do not affect the phase compositions as the correction terms for oil and gas cancel out (see Equation A.18. For oil-gas-solid equilibrium calculations, the volume shift does affect the equilibrium conditions as the fugacity for solid does not contain a volume shift correction. The

volume shift parameters can be estimated as described in Jhaveri and Youngren (1988) or obtained from regression.

APPENDIX B: CHARACTERIZATION OF PSEUDO COMPONENTS

B.1 Approach

In phase behavior modelling, it is necessary to represent the heavy fractions of the oil or gas by pseudo components. The heavy fraction of a reservoir fluid are normally reported as a lumped fraction (e.g. C_6^+) with a given molecular weight ($M_{C_6^+}$), and specific gravity ($\gamma_{C_6^+}$). A partial single-carbon-number (SCN) distribution of the C_6^+ fraction from chromatographic measurements up to C_{20}^+ is also usually available (Pedersen et al., 1989). Whitson (1983) and Pedersen et al. (1989) proposed a procedure for characterizing the heavy fraction of reservoir fluids. The procedure consists of three steps:

1. Splitting of the heaviest fraction into SCN's with mole fractions, molecular weights and specific gravities that match measured the measured properties.
2. Estimation of critical properties and acentricities of all SCN's.
3. Regrouping (lumping) the SCN's into pseudo components for EOS modelling.

The three steps with some variations to the original approach are described in the following. The first step is not required if the SCN distribution from chromatographic analysis up to C_{20}^+ is sufficient.

B.2 Splitting the Heaviest Fraction into SCN's

In the modelling of asphaltene precipitation, it is desirable to have SCN molar distribution up to the C_{30}^+ range. The chromatographic analysis normally gives SCN's up to C_{20}^+. Correlations are available to extend the plus fraction C_{20}^+ into heavier SCN's. Pedersen et al. (1989) assume a logarithmic distribution of the molar fraction z_i versus the carbon number C_N:

$$\ln z_i = A + B \times C_N \tag{B.1}$$

where A and B are constant parameters determined from the measured mole fraction and molecular weight of the plus-fraction. Whitson (1983) proposed a gamma function where the component distribution with respect to molecular weight, M, is represented by:

$$z_i = P(M_i) - P(M_{i-1}) \tag{B.2}$$

$$P(M) = \frac{(M - M_0)^{\alpha-1} \exp[(M - M_0)/\beta]}{\beta^{\alpha}\,\Gamma(\alpha)} \tag{B.3}$$

where α, β and M_0 are parameters determined for the available analytical information.

B.3 Estimation of Critical Properties and Acentricities of SCN's

Whitson (1984) provides a review of correlations for estimating critical properties and acentricities of SCN's from their specific gravities and normal boiling points. Correlations frequently used are due tog Cavett (1962), Kesler and Lee (1977), Katz and Firoozabadi (1978), Riazi and Daubert (1980), and Twu (1984) to name only a few.

B.4 Lumping SCN's Into Pseudo Components

For modelling purposes the C_6^+ fractions are normally represented by 3 to 5 pseudo components. Once the number of plus pseudo components have been selected, the SCN's are lumped into pseudo components according to certain criteria. Whitson (1983) proposed a lumping procedure whereby each pseudo will have the same range in ln (M). Pedersen et al. (1984) based their lumping procedure on equal weight fraction for each pseudo component. The procedure used in Section 5 is due to Li et al. (1985) who proposed the lumping on constant intervals in the ln (K_i) of the SCN's. These K_i's are evaluated at the saturation pressure of the reservoir oil. In this lumping scheme, SCN's with similar K_i's or oil-gas mole fraction ratios are grouped together. Montel and Gouel (1984) used a clustering algorithm to group SCN's according to the similarities of some properties.

The last step in the characterization of pseudo components is the estimation of their critical properties, acentricities and molecular weights. This is achieved through mixing rules. For example, Lee and Kesler (1975) proposed the following mixing rules:

$$\overline{\omega} = \sum_i y_i \omega_i \tag{B.4}$$

$$\overline{v}_c = \frac{1}{8}\sum_i \sum_k y_i y_k \left(v_{ci}^{1/3} + v_{ck}^{1/3}\right)^3 \tag{B.5}$$

$$\overline{T}_c = \frac{1}{8\,\overline{v}_c}\sum_i \sum_k y_i y_k \left(v_{ci}^{1/3} + v_{ck}^{1/3}\right)^3 \left(T_{ci}\, T_{ck}\right)^{1/2} \tag{B.6}$$

$$\overline{Z}_c = 0.2905 - 0.085\,\overline{\omega} \tag{B.7}$$

$$\overline{p}_c = \frac{\overline{Z}_c\, R\, \overline{T}_c}{\overline{v}_c} \tag{B.8}$$

The above lumping procedure is applicable for a oil and its solution gas. In IOR gas injection process, the injected gas may be quite different than the solution gas. In this case the lumping of the plus fraction of the injection gas should be different than that for the oil (Nutakki et al., 1991). This will yield different pseudo component for oil and injection gas. The pseudo components in Table 5.3 were obtained with this method. Nutakki et al. (1991) discussed additional cases where this approach is necessary.

APPENDIX C: EFFECT OF PRESSURE AND TEMPERATURE ON SOLID MODEL

The general equation that relates the solid fugacity to liquid fugacity of a pure component is (see for example Firoozabadi, 1999, 298-299):

$$\ln f_s(p,T) = \ln f_\ell(p,T) - \frac{\Delta H_f}{R}\left(\frac{1}{T} - \frac{1}{T_f}\right) - \frac{\Delta C_p}{R}\left[\ln\left(\frac{T_f}{T}\right) - \left(1 - \frac{T_f}{T}\right)\right] + \frac{1}{RT}\int_{p_f}^{p}(v_s - v_\ell)\,dP \tag{C.1}$$

where

f_s = solid fugacity

f_ℓ = liquid fugacity

p_f = pressure at the melting-point temperature T_f

T_f = melting-point temperature

v_ℓ = liquid molar volume

v_s = solid molar volume

ΔC_p = heat capacity of fusion [cal/mol K]

ΔH_f = melting-point enthalpy of fusion [cal/mol]

From Equation (C.1), the solid fugacity at (p_1,T_1) is related to the solid fugacity at (p_0,T_0) through the equation:

$$\ln f_s(p_1,T_1) - \ln f_s(p_0,T_0) = \ln f_\ell(p_1,T_1) - \ln f_\ell(p_0,T_0) - \frac{\Delta H_f}{R}\left(\frac{1}{T_1} - \frac{1}{T_0}\right) - \frac{\Delta C_p}{R}\left[\ln\left(\frac{T_0}{T_1}\right) + T_f\left(\frac{1}{T_1} - \frac{1}{T_0}\right)\right] + \frac{1}{RT_1}\int_{p_f}^{p_1}(v_s - v_\ell)_{T_1}\,dP - \frac{1}{RT_0}\int_{p_f}^{p_0}(v_s - v_\ell)_{T_0}\,dP \tag{C.2}$$

The melting point enthalpy of fusion, ΔH_f, and the heat capacity of fusion, ΔC_p, are taken as adjustable parameters. The fugacity of pure liquid asphaltene, f_ℓ, and the liquid molar volume, v_ℓ can be calculated from an EOS. The melting point temperature in K can be estimated form the following correlation due to Won (1986):

$$T_f = 374.5 + 0.02617\,M_s - 20172/M_s \qquad (C.3)$$

where M_s is the molecular weight of the asphaltene component. The pressure p_f corresponds to the atmospheric pressure.

As pointed out in Section 5.10, the solid molar volume v_s is chosen to be close to the liquid molar volume v_ℓ. When temperature changes, it is assumed that the difference $v_s - v_\ell$ remain constant.

With the above assumptions, Equation (C.2) allows the calculations of f_s at (p_1,T_1) from f_s at (p_0,T_0).

If the temperature is fixed at T (isothermal condition), Equation (C.2) becomes:

$$\ln f_s(p_1,T) - \ln f_s(p_0,T) = \ln f_\ell(p_1,T) - \ln f_\ell(p_0,T) + \frac{1}{RT}\int_{p_0}^{p_1} v_s\,dP - \frac{1}{RT}\int_{p_0}^{p_1} v_\ell\,dP \qquad (C.4)$$

From thermodynamics, the following equality holds:

$$\ln f_\ell(p_1,T) - \ln f_\ell(p_0,T) = \frac{1}{RT}\int_{p_0}^{p_1} v_\ell\,dP \qquad (C.5)$$

Sustituting Equation (C.5) into Equation (C.4) and assuming that v_s does not vary with pressure give:

$$\ln f_s(p_1,T) = \ln f_s(p_0,T) + \frac{v_s(p_1 - p_0)}{RT} \qquad (C.6)$$

which is Equation (4.1).

APPENDIX D: STABILITY OF MULTICOMPONENT MIXTURES

D.1. Tangent Plane Criterion for Stability

The stability analysis and algorithm in this section follows the paper by Nghiem and Li (1984). A system a given temperature and pressure is said to be stable if there is no accessible state with lower Gibbs free energy. The stability of multicomponent mixtures can be stated in terms of the tangent plane criterion. A mixture of composition **x** at p and T is stable if and only if the tangent plane to the Gibbs free energy surface a **x** is everywhere below th Gibbs free energy surface.

The dimensionless molar Gibbs free energy of a single-phase system of composition **y** is:

$$G^*(\mathbf{y}) = \sum_{i=1}^{n_c} y_i \ln f_i(\mathbf{y}) + G_0^*(p,T) \tag{D.1}$$

The equation of the tangent plane $P_x^*(\mathbf{y})$ that is tangent to the G^* surface at **x** is:

$$P_x^*(\mathbf{y}) = \sum_{i=1}^{n_c} y_i \ln f_i(\mathbf{x}) + G_0^*(p,T) \tag{D.2}$$

The dimensionless distance $D_x^*(\mathbf{y})$ between the G^* surface and the tangent plane at **x** is:

$$D_x^*(\mathbf{y}) = G^*(\mathbf{y}) - P_x^*(\mathbf{y}) = \sum_{i=1}^{n_c} y_i \ln\left[\frac{f_i(\mathbf{y})}{f_i(\mathbf{x})}\right] \tag{D.3}$$

The tangent plane criterion for stability can be mathematically expressed as follows. A mixture with composition **x** is stable at a specified p and T if and only if

$$D_x^*(\mathbf{y}) \geq 0 \text{ for all } \mathbf{y}. \tag{D.4}$$

Equation (D.4) must be satisfied for all **y**. In particular, $D_x^*(\mathbf{y})$ must be positive for the pure component, i.e.

$$\ln\left[\frac{f_i^0}{f_i(\mathbf{x})}\right] \geq 0; \quad i = 1,...,n_c \tag{D.5}$$

where f_i^0 is the fugacity of pure component i at p and T. Equation (D.5) shows that the fugacity of component i in solution must be less that the fugacity of component i in the pure state.

D.2. Stability Test Algorithm

Testing $D_x^*(\mathbf{y})$ for all for all **y** is not physically possible. Fortunately, it is sufficient to test the stability at all **stationary points** of $D_x^*(\mathbf{y})$. The stationary points of $D_x^*(\mathbf{y})$ satisfy

$$\left(\frac{\partial D_x^*}{\partial y_i}\right)_{y_j;\, j\neq i,r} = \ln\left[\frac{f_i(\mathbf{y})}{f_i(\mathbf{x})}\right] - \ln\left[\frac{f_r(\mathbf{y})}{f_r(\mathbf{x})}\right] = 0;\quad i=1,\ldots,n_c;\ i\neq r \tag{D.6}$$

In Equation (D.6), the derivatives are taken with respect to the mole fractions y_i with y_r being the dependent variable, i.e.

$$y_r = 1 - \sum_{\substack{j=1 \\ j\neq r}}^{n_c} y_j \tag{D.7}$$

Equation (D.6) is equivalent to

$$\ln\left[\frac{f_i(\mathbf{y})}{f_i(\mathbf{x})}\right] = \zeta;\quad i=1,\ldots,n_c \tag{D.8}$$

where ζ is a constant that is independent of the component index. Substituting Equation (D.8) into Equation (D.3) yields

$$D_x^* = \zeta \tag{D.9}$$

at the stationary point. Figure D.1 shows the stationary condition of $D_x^*(\mathbf{y})$ for a binary system. P_A is the tangent plane at Point A. The stationary point of $D_x^*(\mathbf{y})$ denoted by $D^*(\tilde{\mathbf{x}})$ in Figure D.1 corresponds to the composition of the point of tangency B of the plane $\tilde{P}$ that is parallel to P_A. Clearly the mixture A is unstable because $D^*(\tilde{\mathbf{x}}) < 0$.

The stationary condition (D.8) can be written as follows:

$$g_i \equiv \ln Y_i + \ln\varphi_i(\mathbf{y}) - \ln x_i - \ln\varphi_i(\mathbf{x}) = 0;\quad i = 1,\ldots,n_c \tag{D.10}$$

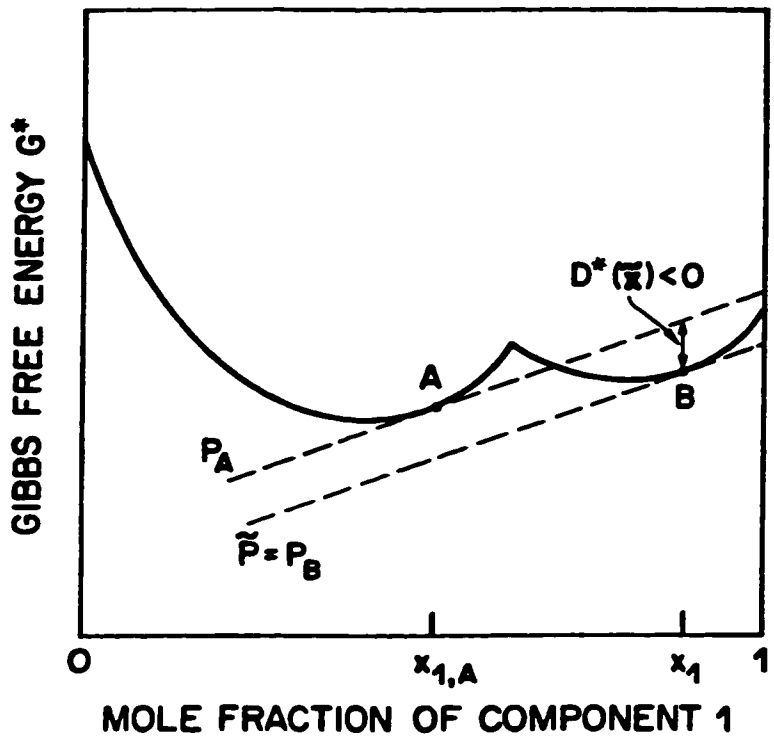

Figure D.1: Stationary point for stability test based on the tangent plane criterion

with

$$y_i = \frac{Y_i}{\sum_{i=1}^{n_c} Y_j}; \quad i = 1,\ldots,n_c \tag{D.11}$$

and

$$-\ln\left(\sum_{j=1}^{n_c} Y_j\right) = \zeta \tag{D.12}$$

For stability it is required that

$$-\ln\left(\sum_{j=1}^{n_c} Y_j\right) \geq 0 \tag{D.13}$$

or

$$\sum_{j=1}^{n_c} Y_j \leq 1. \qquad \text{(D.14)}$$

Therefore, if Equation (D.10) is solved for Y_i at a given p and T, and a solution is found such that

$$\sum_{j=1}^{n_c} Y_j > 1 \qquad \text{(D.15)}$$

The mixture **x** is unstable at p and T.

Equation (D.10) can be solved with Newton's method or with the QNSS method (Nghiem and Li, 1984). With the QNSS method, let the K-values be defined as

$$K_i = \frac{Y_i}{x_i}: \quad i = 1,\ldots,n_c \qquad \text{(D.16).}$$

and Equation (D.10) can be rewritten as

$$g_i \equiv \ln K_i + \ln \varphi_i(\mathbf{y}) - \ln \varphi_i(\mathbf{x}) = 0; \quad i = 1,\ldots,n_c \qquad \text{(D.17)}$$

Let α be the vector with elements $\ln K_i$, and let $\alpha^{(k)}$ be the k-th iteration value for the vector α. The QNSS iteration is:

$$\Delta \boldsymbol{\alpha}^{(k)} = \boldsymbol{\alpha}^{(k-1)} - \boldsymbol{\alpha}^{(k)} \qquad \text{(D.18)}$$

$$\boldsymbol{\alpha}^{(k-1)} = \boldsymbol{\alpha}^{(k)} - \xi^{(k)}\, \mathbf{g}^{(k)} \qquad \text{(D.19)}$$

$$\xi^{(k)} = -\left(\frac{\Delta \boldsymbol{\alpha}^{(k-1)} \cdot \mathbf{g}^{(k-1)}}{\Delta \boldsymbol{\alpha}^{(k-1)} \cdot \Delta \mathbf{g}^{(k-1)}} \right) \xi^{(k-1)} \qquad \text{(D.20)}$$

$$\xi^{(0)} = 1 \qquad \text{(D.21)}$$

The following initial guesses for the above procedure are found adequate for oil/gas mixtures:

- $K_i^{(0)} = \widetilde{K}_i$ if **x** is vapour-like (D.22)
- $K_i^{(0)} = \frac{1}{\widetilde{K}_i}$ if **x** is liquid-like (D.22)

where $\tilde{K}_i$ are the K-values due to Wilson (Heidemann, 1983), i.e.

$$\ln \tilde{K}_i = \ln\left(\frac{p}{p_{ci}}\right) + 5.373\,(1+\omega_i)\left(1-\frac{T_{ci}}{T}\right). \tag{D.23}$$

At convergence, the single-phase system **x** is unstable if

$$\sum_{j=1}^{n_c} K_j\, x_j > 1. \tag{D.24}$$

Two-phase flash calculations can then be initiated with the converged K_i's as initial guesses. Thus this procedure not only tests the stability of single-phase mixtures, but provides also initial guesses for two-phase flash calculations in the event the single-phase mixture is unstable. To test the stability of a two-phase system, stability test is performed on one of the phases as described above. If one of the phases is unstable, both phases are unstable, and the system may have to split into three phases for stability.

APPENDIX E: QUASI-NEWTON SUCCESSIVE SUBSTITUTION METHODS

A class of quasi-Newton methods for solving nonlinear equations, termed quasi-Newton successive substitution (QNSS), is derived in the following. Additional details can be found in Nghiem (1983).

Consider a system of nonlinear equations:

$$\mathbf{f}(\mathbf{x}) = \mathbf{0} \tag{E.1}$$

and let

$$\Delta\mathbf{x}^{(k)} = \mathbf{x}^{(k+1)} - \mathbf{x}^{(k)} \tag{E.2}$$

$$\Delta\mathbf{f}^{(k)} = \mathbf{f}^{(k+1)} - \mathbf{f}^{(k)} \tag{E.3}$$

where the superscript (k) denotes the iteration level.

Broyden (1965) introduced a quasi Newton (QN) iterative procedure for solving Equation (E.1) as follows:

$$\mathbf{J}^{(k)}\,\Delta\mathbf{x}^{(k)} = -\mathbf{f}^{(k)} \tag{E.4}$$

where $\mathbf{J}^{(k)}$ is an approximation to the Jacobian $(\partial\mathbf{f}/\partial\mathbf{x})^{(k)}$ and is modified at each iteration as follows:

$$\mathbf{J}^{(k)} = \mathbf{J}^{(k-1)} + \Delta\mathbf{J}^{(k)} \tag{E.5}$$

Since $\Delta\mathbf{J}^{(k)}$ is of rank one, the inverse $\mathbf{H}^{(k)}$ of $\mathbf{J}^{(k)}$ can also be obtained with rank-one updates:

$$\mathbf{H}^{(k)} = \left[\mathbf{J}^{(k)}\right]^{-1} = \mathbf{H}^{(k-1)} + \Delta\mathbf{H}^{(k)} \tag{E.6}$$

Equation (E.4) becomes:

$$\Delta\mathbf{x}^{(k)} = -\mathbf{H}^{(k)}\,\mathbf{f}^{(k)} \tag{E.7}$$

By working with $\mathbf{H}^{(k)}$, the inversion of $\mathbf{J}^{(k)}$ at each iteration is avoided. The updates $\Delta\mathbf{H}^{(k)}$ are of the form:

$$\Delta \mathbf{H}^{(k)} = \frac{\left[\Delta \mathbf{x}^{(k-1)} - \mathbf{H}^{(k-1)}\, \Delta \mathbf{f}^{(k-1)}\right] \mathbf{w}^{(k-1)^T}}{\mathbf{w}^{(k-1)^T}\, \Delta \mathbf{f}^{(k-1)}} \tag{E.8}$$

where the vector $\mathbf{w}^{(k)}$ can be either

Scheme 1: $\mathbf{w}^{(k)} = \Delta \mathbf{f}^{(k-1)}$ or (E.9)

Scheme 2: $\mathbf{w}^{(k)} = \Delta \mathbf{x}^{(k-1)}$. (E.10)

The superscript T in Equation (E.8) denotes the transpose.

Other rank-one QN updates are also available. Insertion of Equations (E.6) and (E.8) into Equation (E.7) yields:

$$\Delta \mathbf{x}^{(k)} = -\mathbf{H}^{(k-1)}\, \mathbf{f}^{(k)} - \frac{\left[\Delta \mathbf{x}^{(k-1)} - \mathbf{H}^{(k-1)}\, \Delta \mathbf{f}^{(k-1)}\right] \mathbf{w}^{(k-1)^T} \mathbf{f}^{(k)}}{\mathbf{w}^{(k-1)^T}\, \Delta \mathbf{f}^{(k-1)}} \tag{E.11}$$

Substituting $\Delta \mathbf{f}^{(k-1)} = \mathbf{f}^{(k)} - \mathbf{f}^{(k-1)}$ and $\Delta \mathbf{x}^{(k-1)} = -\mathbf{H}^{(k-1)}\, \mathbf{f}^{(k-1)}$ in the numerator yields:

$$\Delta \mathbf{x}^{(k)} = -\mathbf{H}^{(k-1)}\, \mathbf{f}^{(k)} + \frac{\mathbf{H}^{(k-1)}\, \mathbf{f}^{(k)}\, \mathbf{w}^{(k-1)^T}\, \mathbf{f}^{(k)}}{\mathbf{w}^{(k-1)^T}\, \Delta \mathbf{f}^{(k-1)}} \tag{E.12}$$

or

$$\Delta \mathbf{x}^{(k)} = -\left[1 - \frac{\mathbf{w}^{(k-1)^T}\, \mathbf{f}^{(k)}}{\mathbf{w}^{(k-1)^T}\, \Delta \mathbf{f}^{(k-1)}}\right] \mathbf{H}^{(k-1)}\, \mathbf{f}^{(k)} \tag{E.13}$$

Again, substituting Equation (E.3) into Equation (E.13) gives:

$$\Delta \mathbf{x}^{(k)} = -\left[-\frac{\mathbf{w}^{(k-1)^T}\, \mathbf{f}^{(k-1)}}{\mathbf{w}^{(k-1)^T}\, \Delta \mathbf{f}^{(k-1)}}\right] \mathbf{H}^{(k-1)}\, \mathbf{f}^{(k)} \tag{E.14}$$

which is of the form

$$\Delta \mathbf{x}^{(k)} = -\xi^{(k)}\, \mathbf{H}^{(k-1)}\, \mathbf{f}^{(k)} \tag{E.15}$$

with

$$\xi^{(k)} = -\frac{\mathbf{w}^{(k-1)^T}\, \mathbf{f}^{(k-1)}}{\mathbf{w}^{(k-1)^T}\, \Delta \mathbf{f}^{(k-1)}} \tag{E.16}$$

Equations (E.15) and (E.16) point out a very interesting result. Although $\mathbf{H}^{(k)}$ computed from Equations (E.6) and (E.8) is obviously different from $\xi^{(k)}\,\mathbf{H}^{(k-1)}$, the product $\mathbf{H}^{(k)}\,\mathbf{f}^{(k)}$ is equal to $\xi^{(k)}\,\mathbf{H}^{(k-1)}\,\mathbf{f}^{(k)}$. This feature suggests a very convenient approach to QN updates. If after every iteration, the approximate inverse $\mathbf{H}^{(k)}$ of the Jacobian is replaced by $\xi^{(k)}\,\mathbf{H}^{(k-1)}$, the following recursive formula can be derived:

$$\Delta\mathbf{x}^{(k)} = -\sigma^{(k)}\,\mathbf{H}^{(0)}\,\mathbf{f}^{(k)} \tag{E.17}$$

with

$$\sigma^{(k)} = -\frac{\mathbf{w}^{(k-1)^T}\,\mathbf{f}^{(k-1)}}{\mathbf{w}^{(k-1)^T}\,\Delta\mathbf{f}^{(k-1)}}\,\sigma^{(k-1)} = \xi^{(k)}\,\sigma^{(k-1)} \tag{E.18a}$$

$$\sigma^{(0)} = 1 \tag{E.18b}$$

where $\mathbf{H}^{(0)}$ is the initial approximate inverse of the Jacobian. There is a subtle difference between the conventional QN method and the QN procedure in Equations (E.17) and (E.18). The conventional QN method continuously updates $\mathbf{H}^{(k)}$ at every iteration, whereas the proposed method replaces $\mathbf{H}^{(k)}$ by $\sigma^{(k)}\,\mathbf{H}^{(0)}$ after every iteration and then applies the QN update. This method is call Quasi Newton Successive Substitution. The QNSS procedure for flash calculations described in Section 4.6.2 and for stability test described in Appendix D corresponds to using $\mathbf{H}^{(0)} = \mathbf{I}$, the identity matrix, and Equation (E.10) for $\mathbf{w}^{(k)}$.

APPENDIX F: MULTIPHASE MULTICOMPONENT FLOW IN POROUS MEDIA

This Appendix describes the partial differential equation for multiphase multicomponent flow in porous media.

For a component i present in the oil, gas and water phases, the conservation equation is:

$$-\nabla \sum_{j} \rho_j \, y_{ij} \, \mathbf{u}_j + \hat{q}_i - \frac{\partial N_i}{\partial t} = 0, \quad i = 1,\ldots,n_t, \; j = o,g,w \tag{F.1}$$

where,

N_i = moles of component i per bulk volume [kmol/m^3]

n_t = total number of components including water component

$\mathbf{u}_j$ = velocity of Phase j [m/day]

y_{ij} = mole fraction of Component i in Phase j

$\hat{q}_i$ = well source/sink term [kmol/m^3 day]

ρ_j = molar density of phase j [kmol/m^3]

In porous media, the phase velocity $\mathbf{u}_j$ corresponds to the Darcy velocity:

$$\mathbf{u}_j = -\frac{\mathbf{k}\, k_{rj}}{\mu_j} \nabla \Phi_j \tag{F.2}$$

with

$$\nabla \Phi_o = \nabla p_o - \gamma_o \nabla D \tag{F.3}$$

$$\nabla \Phi_g = \nabla p_o + \nabla P_{cog} - \gamma_g \nabla D \tag{F.4}$$

$$\nabla \Phi_w = \nabla p_o - \nabla P_{cwo} - \gamma_j \nabla D \tag{F.5}$$

$$\gamma_j = \tilde{\rho}_j \, g, \quad j = o,g,w \tag{F.6}$$

where,

D = depth [m]

g	=	gravity acceleration [m/s^2]
$\mathbf{k}$	=	permeability [md]
k_{rj}	=	relative permeability of phase j
p_o	=	oil-phase pressure [kPa]
P_{cog}	=	oil-gas capillary pressure [kPa]
P_{cwo}	=	water-oil capillary pressure [kPa]
γ_j	=	gradient of phase j [kPa/m]
Φ_j	=	potential of phase j (j = o,g,w) [kPa]
μ_j	=	viscosity of phase j [mPa s]
$\tilde{\rho}_j$	=	mass density of phase j [kg/m^3]

Substituting Equation (F.2) into Equation (F.1) yields:

$$\nabla\left[\sum_j \rho_j\, y_{ij}\, \nabla \Phi_j\right] + \hat{q}_i - \frac{\partial N_i}{\partial t} = 0, \quad i = 1,\ldots,n_t,\ j = o,g,w \tag{F.7}$$

It is assumed that water is not present in the oil and gas phases and that hydrocarbon solubility in the water phase is negligible. Let n_c be the number of components in the oil and gas phases, with n_c being the index of the precipitating component. The suspended solid concentration in the oil phase defined as:

$$y_{n_c sf} = N_{sf} / N_o \tag{F.8}$$

where,

N_o	=	total moles in oil phase
N_{sf}	=	moles of solid suspended in oil phase
$y_{n_c sf}$	=	suspended solid concentration in oil phase

With the above assumption and definition, the following conservation equations can be derived from Equation (F.6):

$$\nabla\left[\rho_o\, y_{io}\, \nabla \Phi_o\right] + \nabla\left[\rho_g\, y_{ig}\, \nabla \Phi_g\right] + \hat{q}_i - \frac{\partial N_i}{\partial t} = 0, \quad i = 1,\ldots,n_c - 1 \tag{F.9}$$

$$\nabla \left[\rho_o \left(y_{n_c o} + y_{n_c sf}\right) \nabla \Phi_o\right] + \nabla \left[\rho_g \; y_{n_c g} \; \nabla \Phi_g\right] + \hat{q}_{n_c} - \frac{\partial N_{n_c}}{\partial t} = 0 \qquad \text{(F.10)}$$

$$\nabla \left[\rho_w \; y_{iw} \; \nabla \Phi_w\right] + \hat{q}_w - \frac{\partial N_w}{\partial t} = 0 \qquad \text{(F.11)}$$

Equations (F.9), (F.10) and (F.11) are discretized using finite-difference techniques (Nghiem, 1988) and solved as described in Section (6.2).